NASA Contractor Report 178348

Low Speed Wind Tunnel Test of a Propulsive Wing/Canard Concept in the STOL Configuration

Volume I: Test Description and Discussion of Results

V. R. Stewart

ROCKWELL INTERNATIONAL CORPORATION
Columbus, Ohio 43216

NASA Contractor Report 178348

Low Speed Wind Tunnel Test of a Propulsive Wing/Canard Concept in the STOL Configuration

Volume I: Test Description and Discussion of Results

V. R. Stewart

ROCKWELL INTERNATIONAL CORPORATION

Columbus, Ohio 43216

NASA

National Aeronautics and
Space Administration

Langley Research Center
Hampton, Virginia 23665-5225

ABSTRACT

A propulsive wing/canard model has been tested at STOL operating conditions in the NASA Langley Research Center 4 x 7 meter wind tunnel. Longitudinal and lateral/directional aerodynamic characteristics were measured for various flap deflections, angles of attack and sideslip, and blowing coefficients. Testing was conducted for several model heights to determine ground proximity effects on the aerodynamic characteristics. Flow field surveys of local flow angles and velocities were performed behind both the canard and the wing.

This report consists of two volumes. Volume I (NASA CR-178348) describes the model, instrumentation, and test procedures; and includes an analysis of the data. Volume II (NASA CR-178349) contains all of the test data in three appendices. Appendix A presents tabulated six component force and moment data, Appendix B presents tabulated wing pressure coefficients, and Appendix C presents the flow field data.

TABLE OF CONTENTS

LIST OF FIGURES

LIST OF FIGURES (Cont'd)

LIST OF FIGURES (Cont'd)

LIST OF TABLES

ix

LIST OF SYMBOLS

COMPUTER PLOTS	SYMBOL	DEFINITION
	A	Aspect Ratio $\sim b^2/S$
	AF	Aft Force - balance
	$b_{exposed}$	Exposed Span
	b_f	Flap Span
BN/B	b_j	Jet Span/Exposed Span
	BP	Butt Plane (B.P. = 0 at wing root)
MAC	$\bar{c}$	Mean Aerodynamic Chord
CD	C_D	Drag Coefficient $\sim \dfrac{Drag}{qS}$
CDTR	$C_{D_{TR}}$	Thrust Removed Drag Coefficient
CL	C_L	Lift Coefficient $\sim \dfrac{Lift}{qS}$
CLTR	$C_{L_{TR}}$	Thrust Removed Lift Coefficient
CM	C_M	Pitching Moment Coefficient $\sim \dfrac{Pitching\ Moment}{qS\ \bar{c}}$
CMTR	$C_{M_{TR}}$	Thrust Removed Pitching Moment Coefficient
	C_p	Pressure Coefficient
CMU	C_μ	Blowing Coefficient $\sim \dfrac{\dot{m}\ V_j}{qS}$
CN	C_n	Yawing Moment Coefficient
CROLL	C_ℓ	Rolling Moment Coefficient
CY	C_Y	Side Force Coefficient
	FRL	Fuselage Reference Line
	H	Height of FRL above Ground

LIST OF SYMBOLS (Cont'd)

COMPUTER PLOTS	SYMBOL	DEFINITION
	M	Mach Number
	$\dot{m}$	Nozzle Mass Flow
	NF	Normal Force - Balance
	P_L	Local Static Pressure
	P_∞	Ambient Pressure
	q	Dynamic Pressure $\sim \frac{1}{2}\rho V^2$
	S	Reference Area
V	V_∞	Freestream Velocity
	V_j	Jet Velocity
	Y	Spanwise Measurement
	α	Angle of Attack of Fuselage
	ρ	Density of Air
DELC	δ_C	Canard Deflection
DELF	δ_F	Flap Deflection
	ϵ	Downwash Angle

Subscripts

	c	Canard
	N	Nozzle
	w	Wing
	TR	Thrust Removed

SECTION 1.0

INTRODUCTION

Design specifications for future fighters may be expected to include STOL requirements. The aircraft will undoubtedly have a low aspect ratio wing, operate at high maneuvering load factors, and utilize less runway length for take-off and landing as compared to contemporary fighters. Reduced operating field lengths are desired because of potential field battle damage or to provide the flexibility for forward basing of the fighter vehicle. Very high thrust to weight ratios will be required to achieve the desired maneuvering load factors and reduced field lengths. If the thrust system can also be used to augment lift, then a significant level of STOL capability may be generated.

A propulsive wing concept offers the potential for producing large circulation lift coefficients and also improving high speed flight characteristics. The propulsive wing has been the subject of numerous studies and the capabilities and limitations of propulsive lift systems have been discussed. The addition of large amounts of blowing to the wing is known to develop high circulation lift coefficients which are accompanied by significant leading edge down moments. A possible solution to the nose down moment is to combine the propulsive wing with a propulsive canard. The propulsive wing/canard concept provides the capability to attain large aerodynamic lift coefficients as well as the means to trim the configuration at these high lift coefficients.

References 1, 2 and 3 report on recent investigations of propulsive wing/canard concepts at STOL speeds, and References 4 and 5 describe the transonic characteristics of jet flaps. The test program reported in Reference 1 investigated the effects of relative wing/canard placement and flap nozzle span on the longitudinal characteristics of a propulsive wing/canard fighter configuration. The tests described in this report have continued the Reference 1 investigation to extend the propulsive wing/canard data base by measuring lateral/directional characteristics and ground proximity effects. Wing surface pressures were recorded and local flow characteristics were surveyed behind both the wing and canard.

The earlier model had a box-shaped fuselage to provide flat sides for the surface interaction study. The flat sides permitted the relative position between the wing and canard to be easily changed, but it was felt that the unrealistic shape might have an adverse influence on lateral/directional and ground effects data. A revised fuselage representative of a high thrust fighter configuration was fabricated to be compatible with the existing wing and canard surfaces. A high canard/low wing placement was selected as the preferred configuration based upon results of the previous STOL and transonic tests.

1

The revised model has been tested in the NASA 4 x 7 meter tunnel and the results are compared with those from the earlier model. The basic longitudinal characteristics were relatively unchanged by the modification. The major objectives of the test with the revised fuselage were:

(1) Compare longitudinal axis data with previous results

(2) Obtain lateral/directional characteristics

(3) Measure ground effects

(4) Conduct flow field surveys

SECTION 2.0

MODEL DESCRIPTION AND TEST PROCEDURE

2.1   Model Description

The propulsive wing/canard model is a generic fighter model with a low
aspect ratio wing and a canard to provide nose up trim moments. The wing
and the canard each have blown trailing edge flaps. The flaps are simple
hinged and can be deflected from zero to sixty degrees with blowing at all
deflections. The blowing jet nozzle is a slot nozzle located at the unswept
flap hinge line (the 80 percent local chord position). The wing twist, five
degrees of leading edge down twist at the wing tip, also occurs about the
hinge line. The twist line was selected for fabrication purposes and was
not expected to have an aerodynamic effect. The model fuselage was designed
such that the canard could be tested in three positions and the wing in two
positions, see Figure 1. Figures 1 and 2 present the model layout with
major dimensional data. Table 1 presents a tabulation of the model geometry.

The wing and canard of the model are supercritical airfoils with a thickness
of 6 percent of the local chord. The wing has a twist of -5 degrees about
the flap hinge line and the canard is untwisted, but is fabricated to allow
variable incidence. The airfoils are designed for a lift coefficient of
approximately 0.6. The airfoil coordinates are presented in Table 2. The
wing and the canard panels are attached to the fuselage by an air plug
located at the fifty-percent root chord of each surface. The plug
arrangement allows for mounting, positioning, and variation of canard
incidence; and provides the means for introducing high pressure air to the
wing and canard for the blowing nozzles. The plug and mounting are shown in
Figure 3.

Air was supplied to the model through the NASA air sting and into the
fuselage center plenum at high pressure, approximately 400 PSIA. Inside
the model the air is ducted at high pressure to the individual nozzles by
the tubing arrangement shown in Figure 4. The model, shown in Figure 4, was
fabricated to provide a total of six separate nozzles. In addition to the
four lifting surfaces (two wings and two canards) two bottom fuselage
nozzles are also available. The fuselage nozzles provide the capability to
simulate a thrust reverser and a RALS nozzle, but they were not installed
for the current tests. Air flow to each nozzle is regulated by a remotely
controlled barrel valve located in each nozzle supply tube. The thrust
and/or pressure ratios of the four jets are adjustable by means of the
barrel valves. The high pressure air then flows from the center plenum
through the control valves and into the wing or canard through the mounting
plugs. Inside the surface the spanwise distribution to each nozzle is
controlled by a series of supply holes from the high pressure plenum. The
nozzle plenum is in turn screened to better distribute the flow out the
nozzle. Variations in hole spacing and screening are utilized to control
nozzle distribution for each nozzle span configuration. Figure 5 shows the
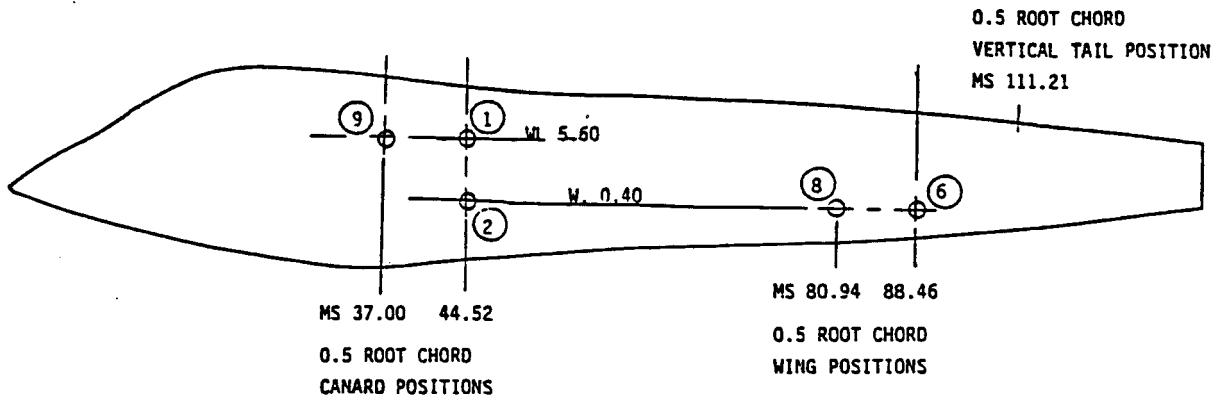internal air flow path of the model.

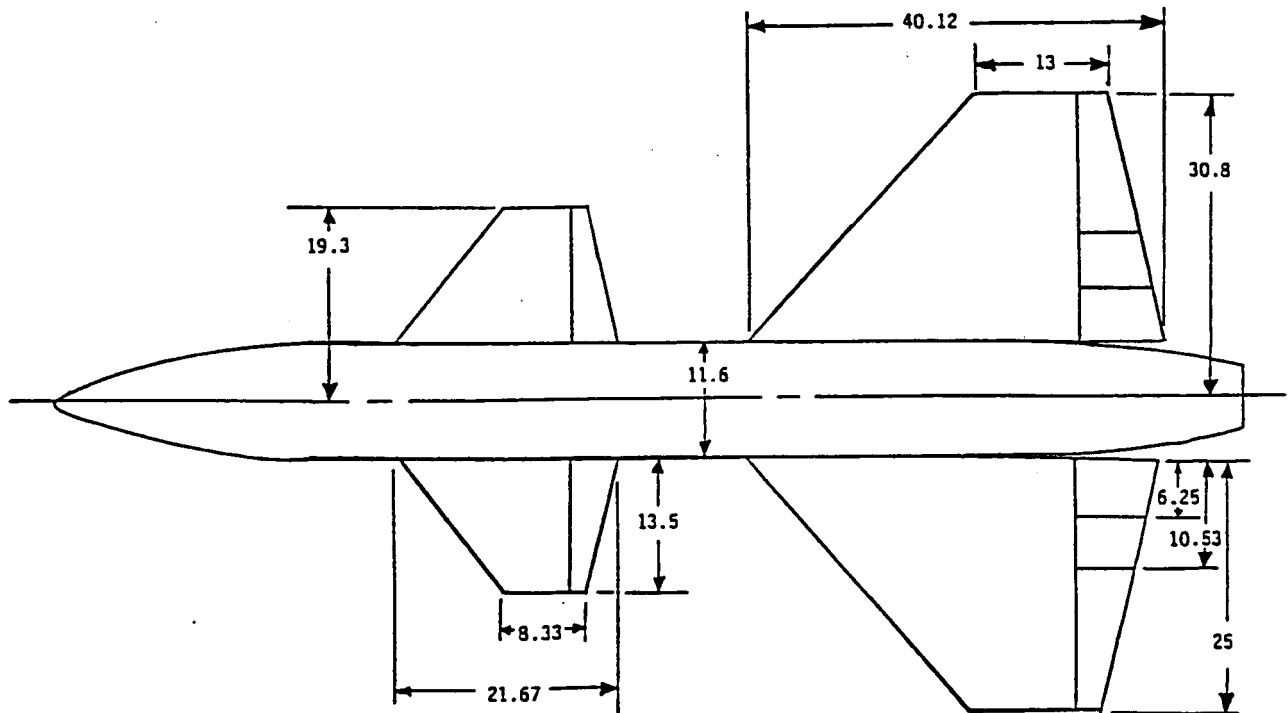Figure 1   Fuselage Side View with Surface Locations

Figure 2   Model Plan View with Dimensions

TABLE 1   MODEL GEOMETRY

ITEM	WING	CANARD	BODY	VERTICAL TAIL
Tip Chord	13 In.	8.3 In.	-	4.25 In.
Root Chord Exposed	40.12 In.	21.67 In.	-	19.50 In.
Root Chord BP=0	46.41 In.	-	-	-
Span Total	61.60 In.	-	-	-
Span Exposed	50.00 In.	27.00 In.	-	15.20 In.
Area Total	12.71 Ft^2	-	-	-
Area Exposed	-	2.812 Ft^2	-	1.253 Ft^2
Aspect Ratio Exposed	-	1.80	-	2.56
Aspect Ratio Total	2.074	-	-	-
MAC Exposed	-	16.0 In.	-	13.5 In.
MAC Total	32.83 In.	-	-	-
Body Length	-	-	116.52 In.	-
Body Width	-	-	11.60 In.	-
Body Height	-	-	20.00 In.	-
Sweep Leading Edge	41 Deg.	38.3 Deg.	-	45 Deg.
Taper Ratio	.28	.38	-	.22

TABLE 2   AIRFOIL COORDINATES

X/C	WING NO DROOP Y/C_U	WING NO DROOP Y/C_L	WING DROOP Y/C_U	WING DROOP Y/C_L	CANARD NO DROOP Y/C_U	CANARD NO DROOP Y/C_L	CANARD DROOP Y/C_U	CANARD DROOP Y/C_L
0	0	0	-.035	-.035	0	0	-.025	-.025
.002	.0046	-.0044	-.0299	-.0395	.0046	-.0044	-.0195	-.0295
.005	.0068	-.00605	-.0263	-.04095	.0068	-.00605	-.0154	-.0311
.01	.0093	-.0077	-.0217	-.0411	.0093	-.0077	-.01035	-.0308
.02	.0126	-.0100	-.0150	-.0398	.0126	-.0100	-.003	-.029
.03	.0153	-.0120	-.0097	-.0383	.0153	-.0120	.0024	-.0278
.04	.0175	-.0133	-.0051	-.0370	.0175	-.0133	.007	-.0266
.06	.0212	-.0157	.0034	-.0346	.0212	-.0157	.0142	-.0249
.08	.0242	-.0176	.0107	-.0324	.0242	-.0176	.01955	-.0235
.10	.0264	-.0192	.0165	-.0303	.0264	-.0192	.0235	-.0226
.125	.0287	-.0208	.02235	-.0279	.0287	-.0208	.0273	-.0220
.15	.0305	-.0222	.0267	-.0258	.0305	-.0222	.030	-.0224
.20	.0329	-.0241	.0321	-.0246	.0329	-.0241	.0329	-.0241
.25	.0342	-.0254	.0342	-.0254	.0342	-.0254	.0342	-.0254
.30	.0350	-.0256	.0350	-.0256	.0350	-.0256	.0350	-.0256
.35	.03548	-.02545	.03548	-.02545	.0354	-.02545	.0354	-.02545
.40	.0357	-.0249	.0357	-.0249	.0357	-.0249	.0357	-.0249
.45	.03575	-.0241	.03575	-.0241	.0358	-.0241	.0358	-.0241
.50	.03565	-.0230	.03565	-.0230	.0358	-.0230	.0358	-.0230
.55	.03535	-.02175	.03535	-.02175	.0358	-.02175	.0358	-.02175
.060	.03488	-.01945	.03488	-.01945	.0356	-.01945	.0356	-.01945
.65	.0342	-.0165	.0342	-.0165	.03535	-.0165	.03535	-.0165
.70	.0332	-.0126	.0332	-.0126	.0348	-.0126	.0348	-.0126
.75	.03165	-.0081	.03165	-.0081	.0340	-.0081	.0340	-.0081
.80	.029	-.0028	.0290	-.0028	.0325	-.0028	.0325	-.0028
.85	.02325	.002	.02325	+.002	.02325	+.002	.02325	+.002
.90	.0173	+.003	.0173	+.003	.0176	+.003	.0176	+.003
.95	.00935	+.0008	.00935	+.0008	.0112	+.0008	.0112	+.0008
1.00	0	.004	0	-.004	.004	-.004	.004	-.004

FLAP { .85 .90 .95 1.00

L.E. RADIUS = .012

WING ROOT INCIDENCE 0.0°

WING TIP INCIDENCE -5.0°

TWIST ALONG X/C = 0.80

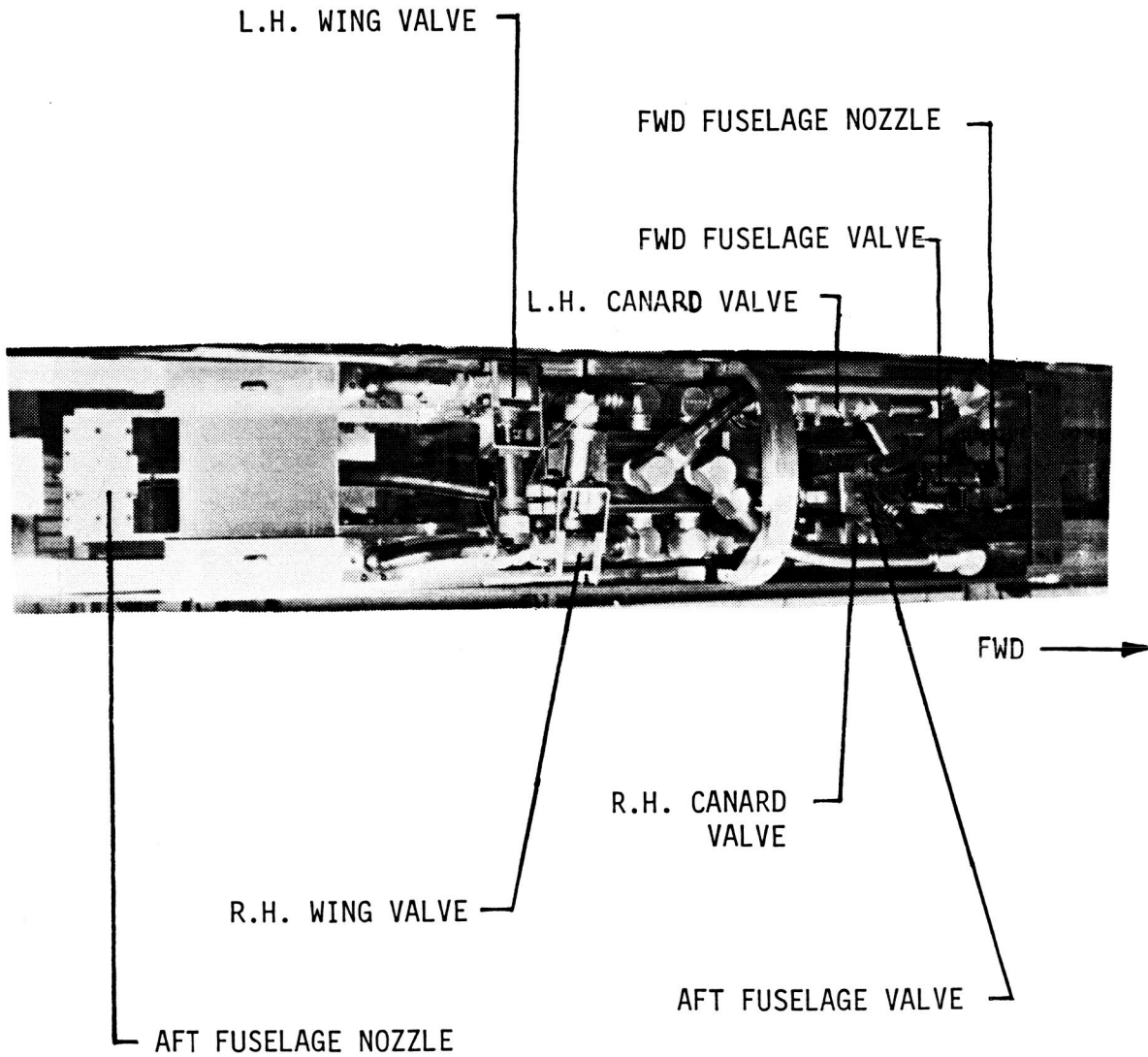6
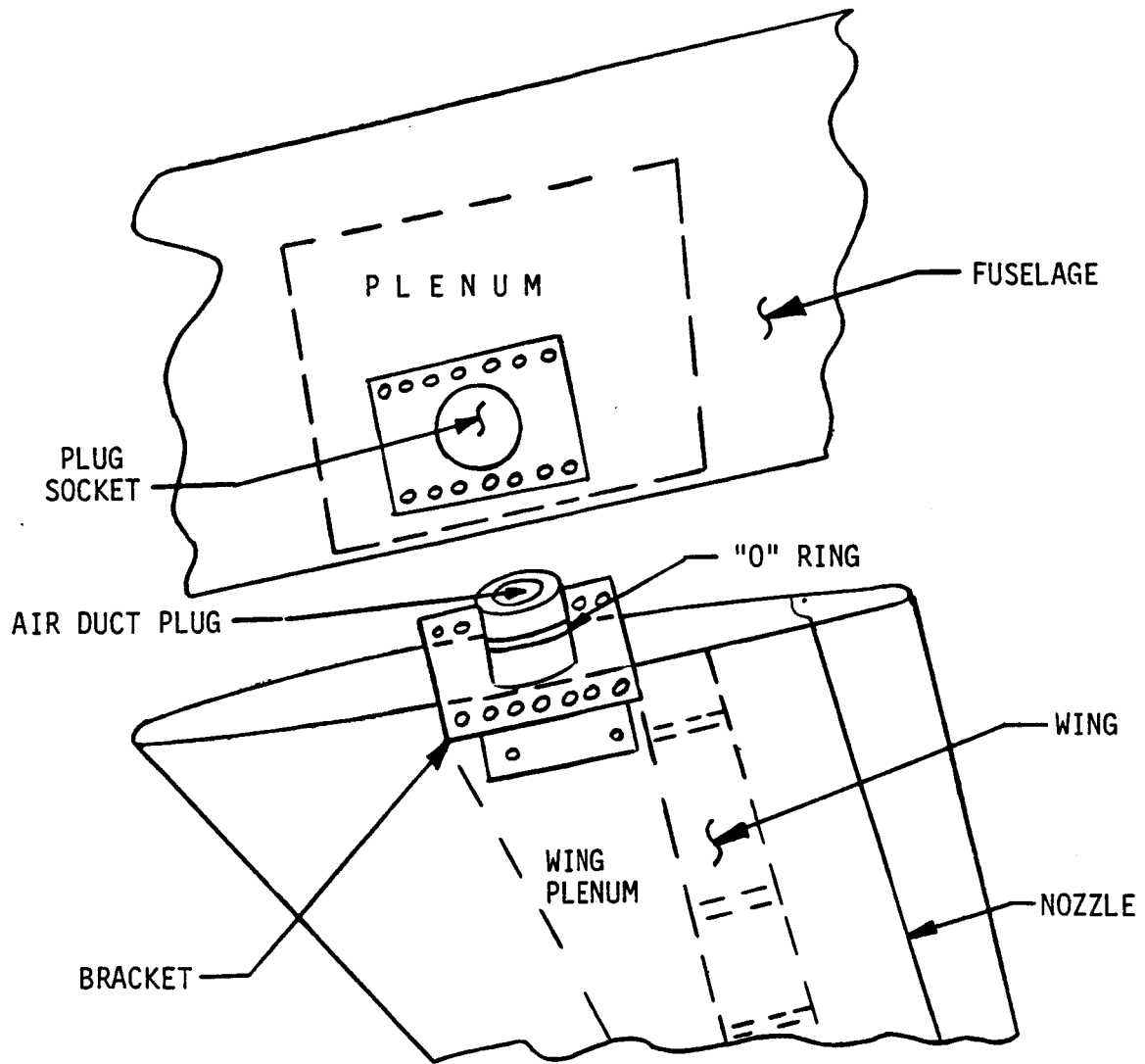
Figure 3 Mounting Bracket and Air Inlet into Wing

Figure 4 Model Internal Air Ducting

8

MODEL STATION
37.00 (.5 C$_R$)
POSITION 9

40.12

13

30.8

19.3

13.5

8.33

21.67

25

WING AND
CANARD
VALVES

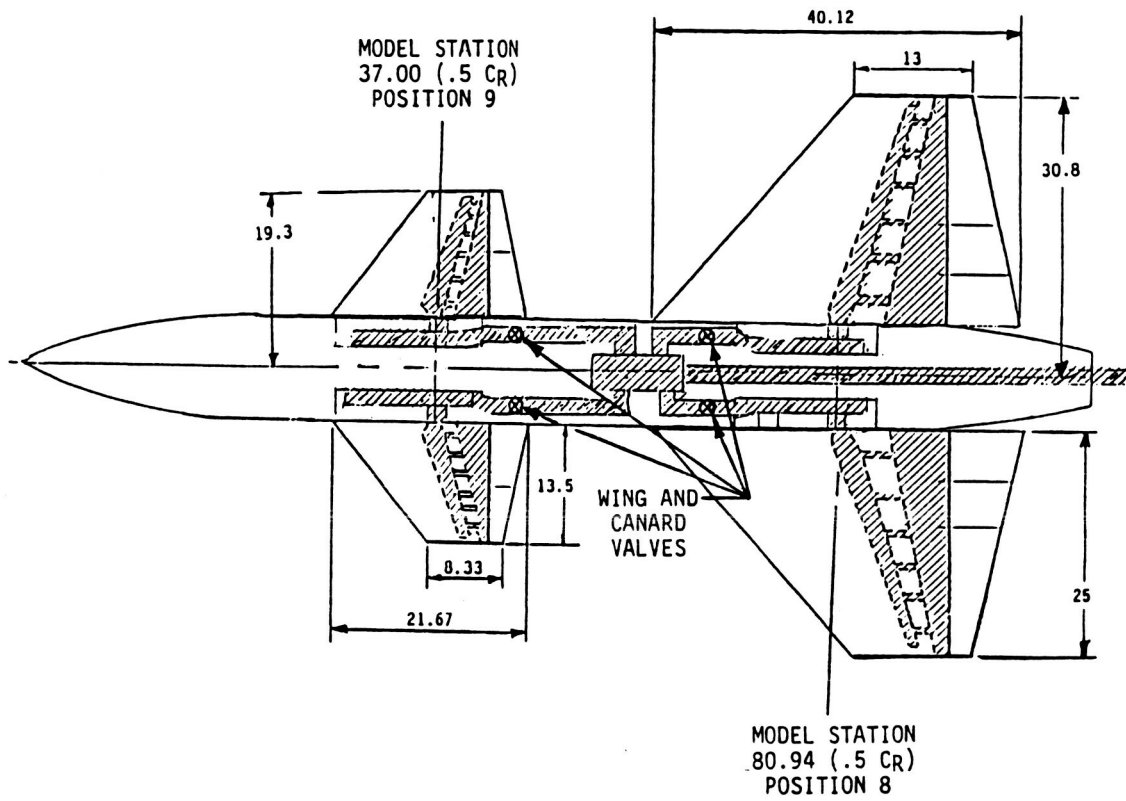MODEL STATION
80.94 (.5 C$_R$)
POSITION 8

Figure 5   Air Flow Path

9

The nozzle spans may be varied by adjusting the internal flow passages to control the distribution and by closing the nozzle plate tightly to the flap upper surface to obtain the desired contour. Figure 6 shows the half-span wing nozzle with the nozzle calibration probes installed. These probes are removed after calibration and prior to data gathering runs. The total blowing air quantity is measured prior to entering the model. The individual blowing on each surface is then computed by the pressure ratio and nozzle exit area. High pressure air introduced to the model in this manner may result in a force on the balance. The balance, therefore, is calibrated with the air sting in place and a pressure tare is used to account for the loads. The pressure tare is obtained by closing the model flow exits and pressurizing the model and sting.

During test the wing and canard placement on the fuselage was changed to reduce the balance nose-down pitching moment with the canard-off tests. This was done in order to increase the test speed envelope. The wing was moved from plug 6 to plug 8 and the canard from plug 1 to plug 9 which maintained the original relative spacing of the wing and canard. The moments were transferred to the leading edge of the wing mean aerodynamic chord (MAC) for all data reduction. The model designations referenced in this report identify the model configuration; i.e., B2C9W8V means body number 2 (the shaped body), canard located at plug 9, wing located at plug 8, and vertical tail included.

2.2   Model Installation

The model was installed in the NASA 4 x 7 meter wind tunnel on air sting #1. The installation of the model is seen in Figures 7 and 8. The model was sting-mounted with the high pressure blowing air supplied through the air sting. The tares due to the air flow were minimized by a pipe/coil arrangement within the sting. Model height in the tunnel and the model angle of attack were controlled through vertical and tilt motion of the aft strut. Air was supplied to the model through two flexible hoses which enter the test section through the vertical strut, exit the strut above the floor and are ducted externally to the air sting. One of the external hoses can be seen in Figure 8. The second hose is on the opposite side of the sting. Air from both hoses enter the sting through the "T" fitting visible on top of the sting.

Weight tares and hose tares were required for each model installation and major configuration change. Instrumentation wiring was attached to the sting and exited the test section through the strut.

2.3   Model Instrumentation

The model installation incorporated the NASA air sting #1 and air station #3. These provided the model with a dry air supply heated slightly to prevent icing, and the associated air flow measuring instrumentation. Additional model and tunnel instrumentation included a six-component force balance, wing surface static pressure instrumentation, internal pressure measuring instrumentation, and a flow-field survey rake.
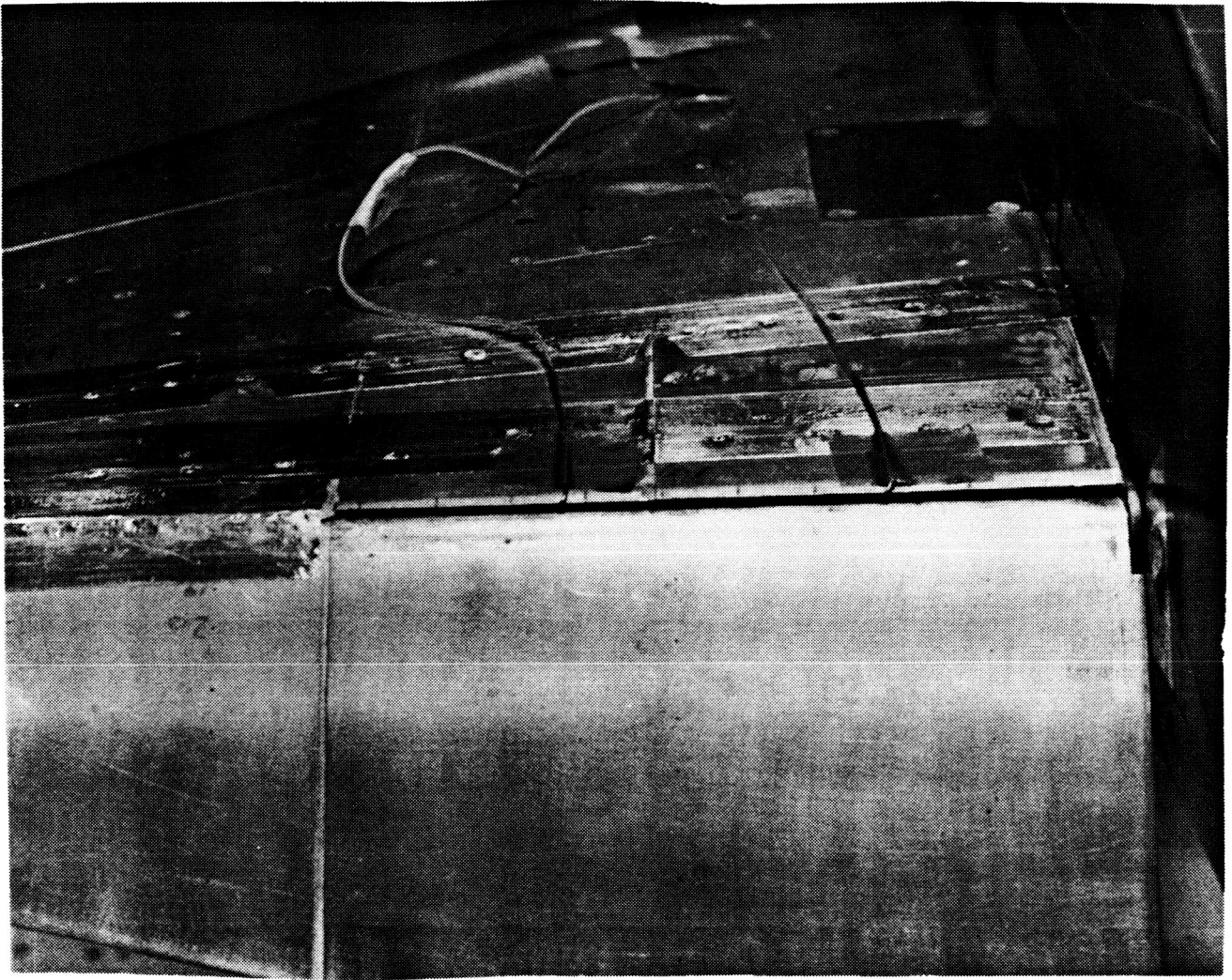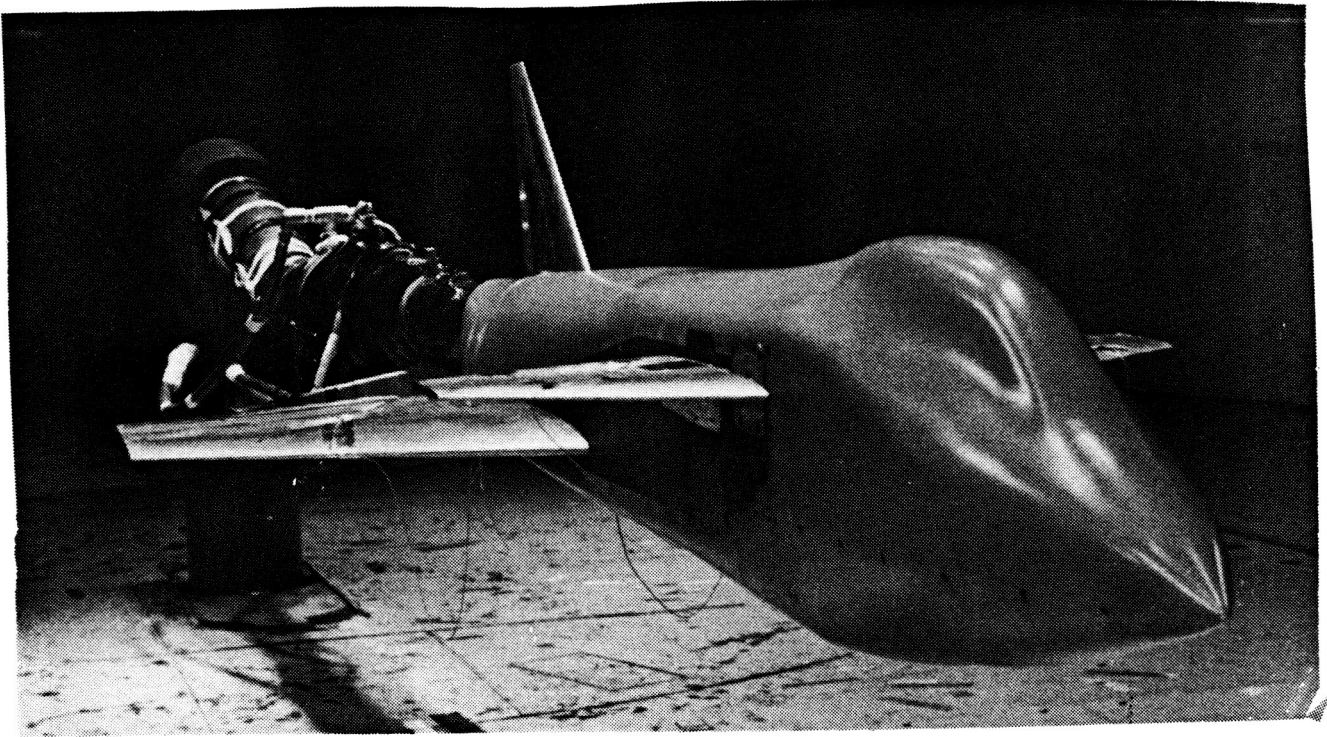
10

Figure 6   Wing Half-Span Nozzle

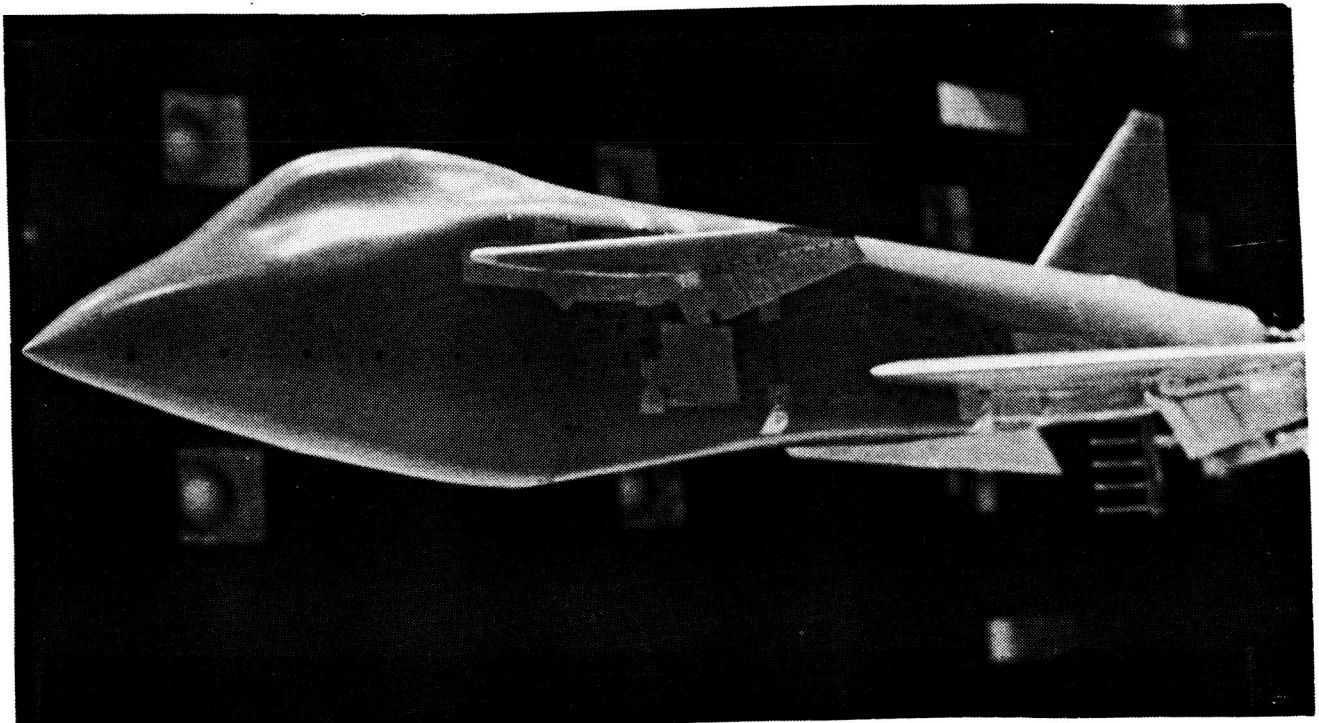Figure 7   Model Installed in NASA LaRC Tunnel-Flap Deflection of Zero Degrees

Figure 8   Model Installed in NASA LaRC Tunnel-Flap Deflection of Forty Degrees

2.3.1 Internal Force Balance

The NASA six-component internal balance 1621B was selected for this test based upon the balance allowable forces. Balance 1621B is limited to a pitching moment component of 10,000 inch-pounds, which was adequate for most desired testing. The pitching moment could have been exceeded at one test condition (C_μ = 0.5) so the tunnel dynamic pressure and nozzle total pressure were reduced slightly for that condition. This did not result in any data limitations. The balance calibrations utilized standard NASA procedures.

2.3.2 Wing Surface Pressures

The model wing was instrumented with five chordwise rows of pressure ports. The locations of the pressure ports are shown in Figure 9. The pressure ports are connected through standard 0.06 inch quick disconnects to ESP pressure recorders. The ESP recorders were connected to the data system through a decision switch which permitted real time selection of pressure measurements during the test.

2.3.3 Internal Pressure Instrumentation

Various pressure instrumentation was available within the model. The balance cavity pressure and the model base pressure were measured and applied to the balance reading as corrections. The air flow pressures were measured at several internal locations. Each plenum had a total pressure gage which was used for nozzle calibration. The main plenum also had a total pressure pickup which was used to interconnect with the NASA air safety system to assure that the model would not be overpressurized.

2.3.4 External Flow Field Measuring Rake

A NASA rake was used for flow field measurement. The NASA survey rake consists of seven five-hole, directionally sensitive probes. The probes are located in a row and spaced two inches apart. The rake was sting mounted behind the wing, as shown in Figure 10, for most of the testing. The rake provides a vertical slice through the downwash at a position 15 inches behind the wing MAC, with the top probe located 4 inches above the wing chord plane.

Figure 11 shows the rake installation for the flow field survey in the canard wake. The measurements were made at three longitudinal locations aft of the canard in a flow field area extending 30 inches vertically (6 inches above to 24 inches below the canard) and 26 inches laterally (just outboard of the fuselage to well outboard of the canard tip). The rake was mounted 66 inches above the floor and the lateral excursion was made by moving the rake in an inboard-outboard direction on its mount. The NASA pitch sting apparatus was used to vary the model height through the vertical range of

13

B.P. = 2 IN.
6
12
16
22
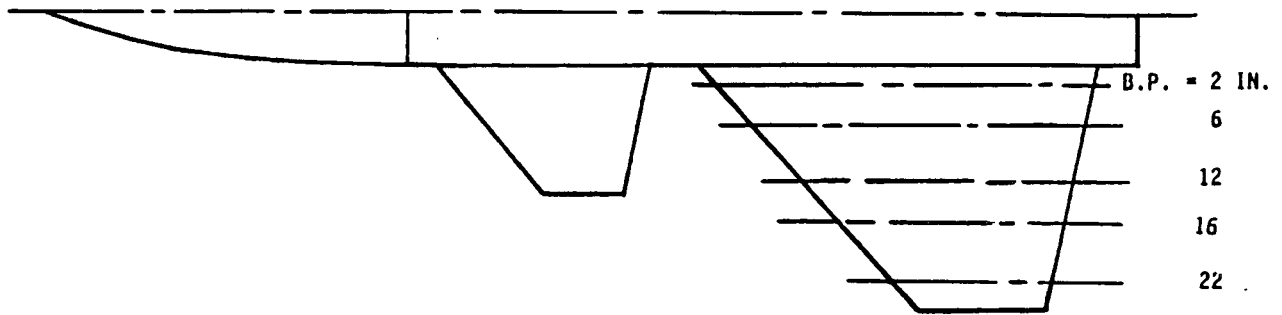
WING STATIC PRESSURE TAP LOCATIONS										
	Y_w (Distance to Root Chord)									
%	2		6		12		16		22	
Chord	Up	Lwr	Up	Lwr	Up	Lwr	Up	Lwr	Up	Lwr
0	L.E.		L.E.		L.E.		L.E.		L.E.	
2.5	X	X	X	X	X	X	X	X	X	X
5	X	X	X	X	X	X	X	X	X	X
10	X	X	X	X	X	X	X	X	X	X
15	X		X		X		X		X	
24	X	X	X	X	X	X	X	X	X	X
33	X	X	X	X	X	X	X	X	X	X
54	X	X	X	X	X	X	X	X	X	X
65	X		X		X		X		X	
73.5		X		X		X		X		X
78.5	X		X		X		X		X	
79.5	X		X		X		X		X	
80.5	X		X		X		X		X	
81.25	X		X		X		X		X	
82	X		X		X		X		X	
84	X	X	X	X	X	X	X	X	X	X
87	X		X		X		X		X	
89	X		X		X		X		X	
93	X				X		X		X	
96	X	X		X	X	X	X	X	X	X
100	T.E.		T.E.		T.E		T.E		T.E	

Figure 9   Wing Surface Pressure Tap Locations

14
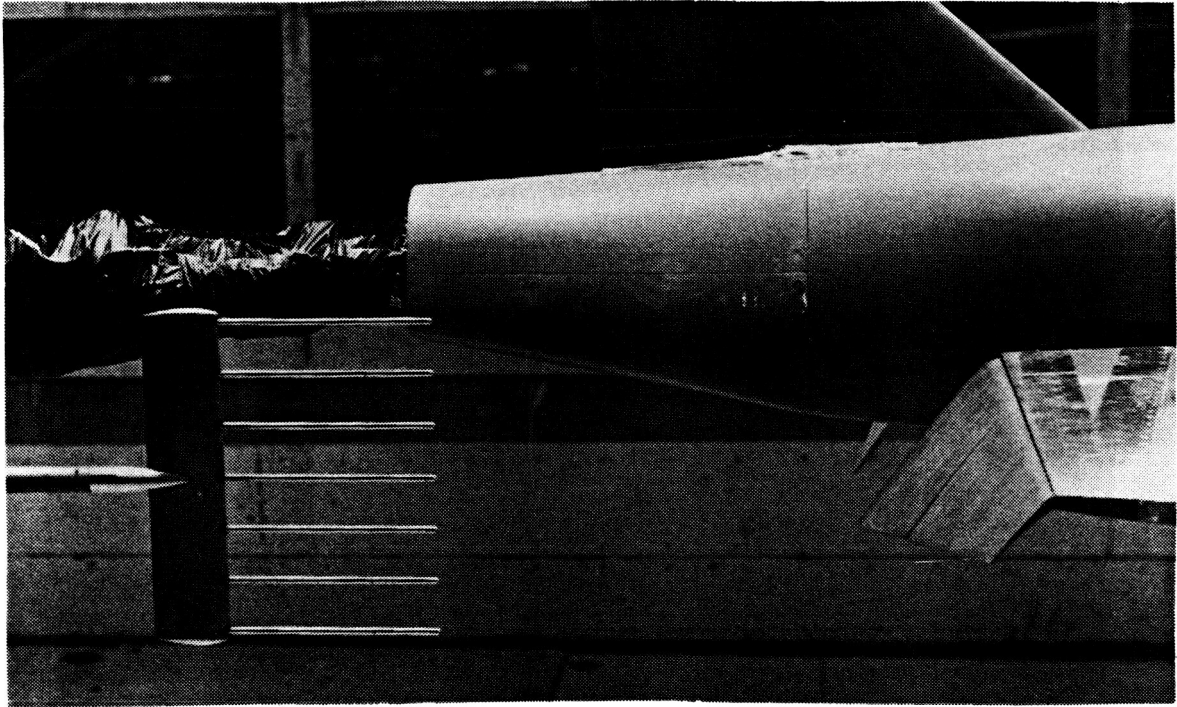
Figure 10   Downwash Probe Installation
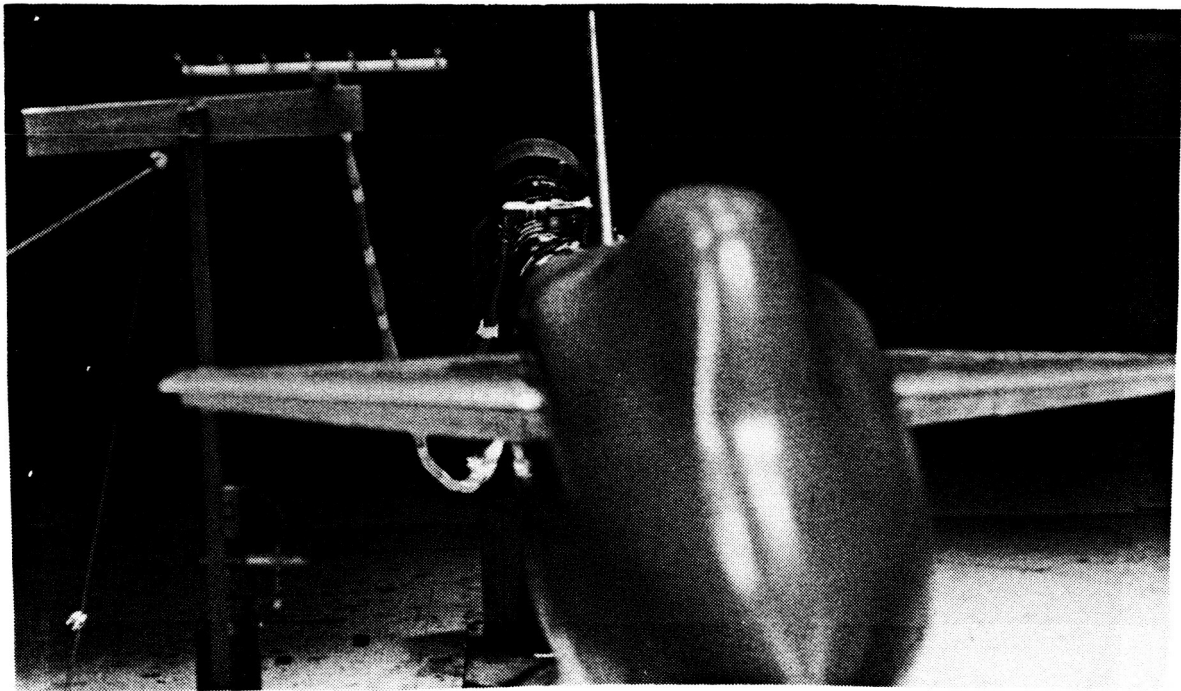
Figure 11   Survey Rake Installation

the survey area. In order to maintain zero angle of attack with vertical movement of the model the sting apparatus moves the model along a line inclined 7.25° to the vertical. This resulted in a 7.25° inclination of the survey area plane. Detailed probe locations are identified in Volume II.

2.4 Test Description

This test continued an earlier investigation of the same wing and canard which had been mounted on a rectangular fuselage (Reference 1). The rectangular fuselage was designed such that the wing and canard relative placement could be varied to investigate canard interference effects on the wing. Several objectives of that study were not completed due to time limitations and the unknown effects of the rectangular fuselage. A relative canard/wing placement was selected based on the original testing and a revised fuselage simulating a low aspect ratio, high power installation fighter was fabricated. The purpose of this test was, therefore, to complete the objectives of the Reference 1 investigation and to test those configurations and concepts which may have been affected by the rectangular fuselage shape.

The major areas of investigation in this test program were:

Longitudinal Characteristics: The pitch characteristics of the propulsive wing/canard were investigated to determine the effects of the shaped body. Configurations from the previous test which were repeated included the partial span nozzles on the wing. An intermediate flap deflection of 30 degrees was tested for the first time.

Lateral/Directional Characteristics: This data was measured to provide information on low aspect ratio fighter configurations with powered lift. The small amount of data available pertains to high aspect ratio transport configurations.

Ground Effects: Ground effects data for STOL vehicles is also currently limited to high aspect ratio configurations.

Wing/Canard Flow Field: This data was not taken during the first test series because of test time limitations.

16

2.4.1   Force and Moment Tests

The model was tested for the range of variables shown in Table 3:

TABLE 3   TEST VARIABLES

C_{μ_W}	0, 0.5, 1.0, 2.0, 4.0, 8.0
C_{μ_C}	0, 0.25, 0.5, 1.0, 2.0, 4.0
C_{μ_T}	0, 0.75, 1.5, 3.0, 6.0, 12.0
h/c	0.5, 1.0, 2.0, free air
δ_F	0, 15, 30, 45 degrees
α	-2 to 22 degrees
β	-15 to 15 degrees

Force and moment data were recorded for the full range of variables shown in Table 3. The tests were made with the model located as near to the center of the test section as possible for all tests except the ground effects tests. As the model is yawed the tunnel sting moves the whole assembly and at pitch angles above approximately 18 degrees the model pitch system can no longer maintain the model in the tunnel center. The excursions from the tunnel center are not large, however, and do not influence the test results. Wing static pressures were also recorded during the force tests for appropriate pitch runs. The pressure data were recorded by ESP pressure sensors.

2.4.2   Ground Proximity Tests

Ground proximity effects were measured for several conditions. Most measurements were taken with the ground belt stationary due to a belt drive failure. The model forces and pressures were recorded at various heights above the floor for several fixed conditions. The test procedure was to set the desired condition; i.e., configuration, angle of attack, blowing coefficient, and flap deflection, and to record data for several model heights above the tunnel floor. Tunnel floor boundary removal bleed was on for these tests except for an investigation of boundary layer effects.

17

2.4.3　Flow Field Surveys

The flow field was surveyed behind the wing and behind the canard. The flow field measurements behind the wing consisted of measurement of a vertical slice one-half chord length behind the wing trailing edge. The seven probe rake used provided a vertical flow measurement from 4 inches above the wing to eight inches below the wing plane. These data are available for all pressure recorded data points. The flow field behind the canard was measured at three locations aft of the canard trailing edge. At each longitudinal station a flow area of approximately 30 inches high by 24 inches wide was measured.

2.5　Data Reduction

The data reduction procedures used in the propulsive wing/canard test were standard tunnel procedures except for special cases pertaining to nozzle blowing. Special treatment was required for calculating the blowing coefficient (C_μ) and for removing the blowing thrust effect in determining circulation lift and other aerodynamic coefficients.

2.5.1　General Discussion

The overall force data were recorded by a six component internal balance. The data have been reduced in the standard manner to both body and stability axis coefficients with total wing geometry utilized for reference dimensions. Wing surface pressures are converted to pressure coefficients utilizing free stream dynamic pressure as the reference. The flow field survey and the downwash probe data are reduced to local velocity and flow angles (alpha and beta) by the NASA probe calibration program.

2.5.2　Blowing Coefficient

The propulsive wing/canard model used in this test had four separate nozzles; i.e., right and left canard nozzles and right and left wing nozzles. The air was supplied to the model through a common, high pressure pipe and distributed to each nozzle as described in Section 2.1. The nozzle areas were preset to provide a balanced flow at a balanced pressure ratio. The actual individual nozzle blowing coefficient was computed based on the preset nozzle area and the average nozzle total pressure. The nozzle spanwise flow distribution was critical for the data reduction methods used. The flow distribution was controlled as discussed in Section 2.1 by valves, flow passages and screens. The nozzle pressure ratio balance between the four nozzles was attained by use of the calibration probes shown in Figure 6. The calibration probes were used to determine the nozzle average pressure referenced to an upstream pressure source. The probes were removed during testing.

The model blowing coefficient is computed, as described in Reference 6, by:

$$C_\mu = \dot{m}\, V_j / qS$$

18

2.5.3   Thrust Removed Aerodynamic Coefficients

Blowing on the lifting surfaces produces two force changes, one of which is the direct thrust vector of the nozzle. The thrust produces a lift force and a drag force equal to the appropriate component of the thrust vector. The thrust also produces a moment which is equal to the product of the thrust and the moment arm of the jet. The second force change produced by blowing is an effect on the aerodynamic forces of the configuration. Blowing effects the lift coefficient by altering the circulation of the flow field. This also changes the pitching moment and induced drag coefficients. The analysis of the propulsive wing and propulsive wing/canard configurations requires that the overall forces be converted into direct thrust coefficients and induced, or purely aerodynamic, forces. For this investigation the aerodynamic data were calculated by removing the thrust vector from the balance recorded data and computing the aerodynamic (thrust removed) data in the same way that the total coefficients are normally computed. This method accounts for the nozzle efficiency and scrubbing drag of the jet and only assumes that the jet attachment is unaffected by the external airstream.

(THIS PAGE INTENTIONALLY LEFT BLANK)

3.0 SUMMARY OF TEST RESULTS

The data presented and discussed here provides an extension of the data base for powered-wing fighter aircraft. The previous data base on powered configurations was generally limited to higher aspect ratios and to specific configurations and specific test objectives. This test and that of Reference 1 represent a generic approach to the subject of powered-wing fighter configurations. Reference 1 investigated the effects of relative wing/canard placement and flap nozzle span on longitudinal effects of the propulsive wing/canard. Longitudinal data is also presented here, and lateral/directional and flow field characteristics are included. The influence of ground proximity on longitudinal characteristics is discussed. The moving ground board was not available for most of the testing of the propulsive wing/canard model.

3.1 Longitudinal Characteristics

The propulsive wing/canard concept evolved in an effort to provide a powered wing configuration which could be trimmed without the lift loss associated with conventional tail trim. The loss in trimmed lift is particularly great with a powered wing which produces large nose down moments because of the aft location of the flap. A canard configuration contributes forward lift which provides nose up trim with a positive lift. The canard also produces large downwash angles ahead of the wing, however, which reduce the wing lift and increase drag by tilting the wing normal force vector aft.

3.1.1 Wing-Body

The aerodynamic characteristics of the propulsive wing are dominated by large lift coefficients and large nose down pitching moment coefficients. The lift, drag, and pitching moment coefficients of the wing-body combination at flap deflections of 0, 15, 30, and 45 degrees are presented in Figures 12 through 15, respectively. Blowing at the flap knee increases the lift coefficient at all conditions and angles tested. At zero flap deflection there is an increase in lift at zero angle of attack as well as at positive angles of attack. The lift increase due to blowing at zero angle of attack and zero flap deflection is the result of surface camber and an upper surface angle of approximately 10 degrees on the trailing edge flap. The total, or thrust included, aerodynamic coefficients are presented in Figures 12a, 13a, 14a, and 15a for each flap deflection while the thrust removed coefficients are presented in the accompanying Figures 12b, 13b, 14b, and 15b. A significant circulation can be seen on the airplane.

The effect of the blowing coefficient on the lift coefficient can be seen in Figures 16 and 17. Figure 16 compares the total wing-body lift curve slope to the thrust removed lift curve slope. The thrust removed (aerodynamic or circulation) lift curve slope is increased by 50% due to the
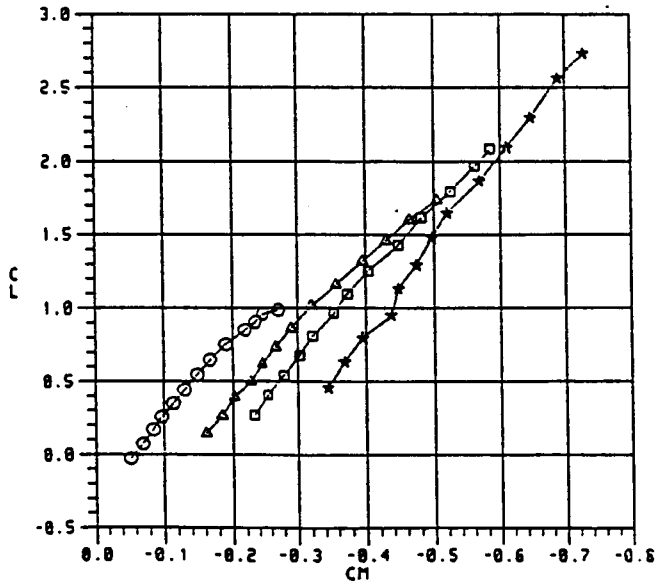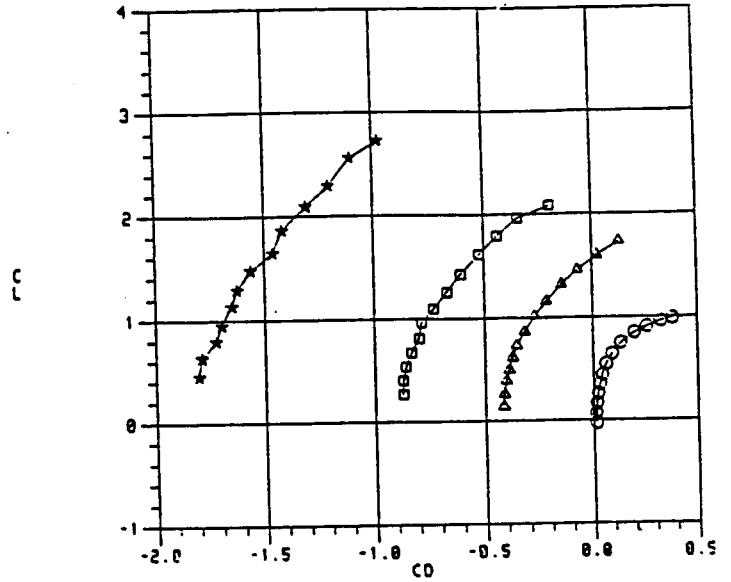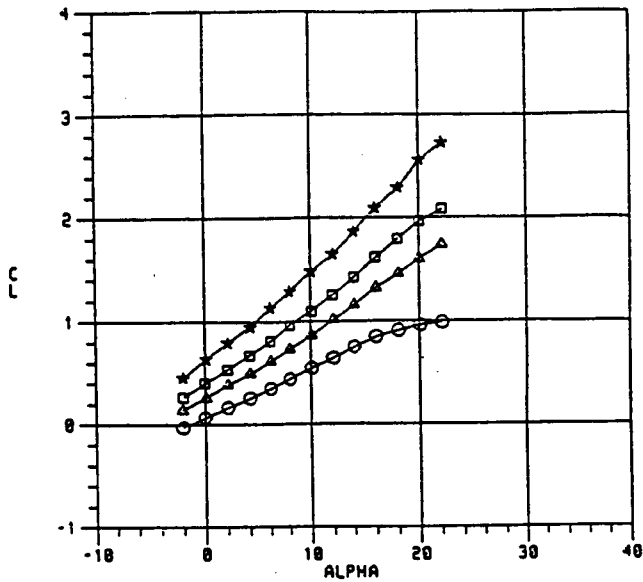
SYM	RUN	CMUT
O	110	0.00
△	111	0.51
□	112	1.03
★	113	2.10

a. Total Aerodynamic Characteristics

Figure 12. Variation of Longitudinal Aerodynamic Characteristics, B2W6V, $\delta_F = 0°$
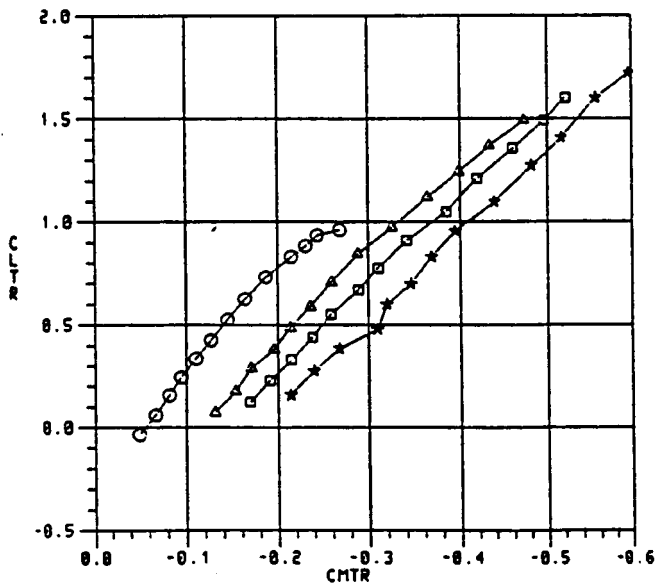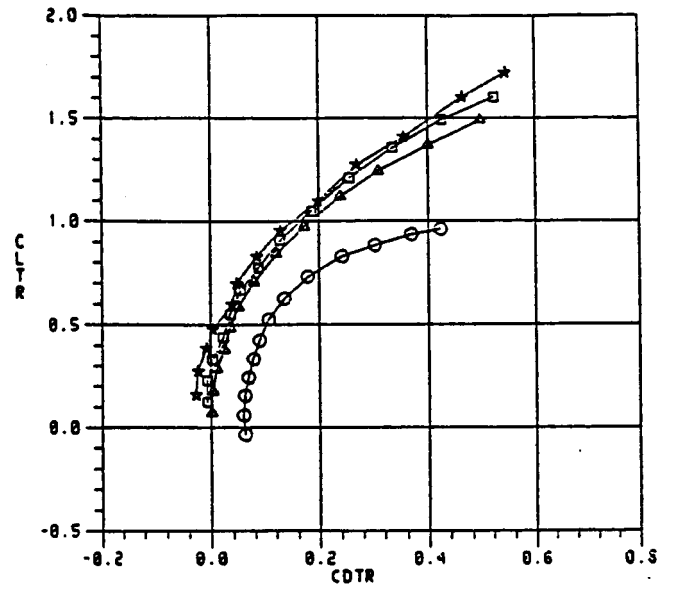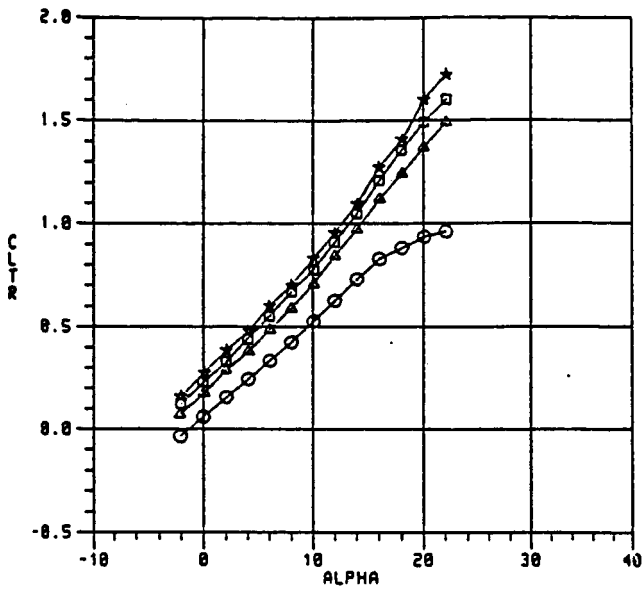
SYM	RUN	CMUT
O	110	0.00
△	111	0.51
□	112	1.03
★	113	2.10

b. Thrust Removed Aerodynamic Characteristics

Figure 12   Variation of Longitudinal Aerodynamic Characteristics, B2W6V, $\delta_F = 0°$

SYM | RUN | CMUT
O | 256 | 0.00
△ | 257 | 0.53
□ | 258 | 1.07
★ | 259 | 2.23

a. Total Aerodynamic Characteristics

Figure 13   Variation of Longitudinal Aerodynamic Characteristics, B2W8V, δ_F = 15°
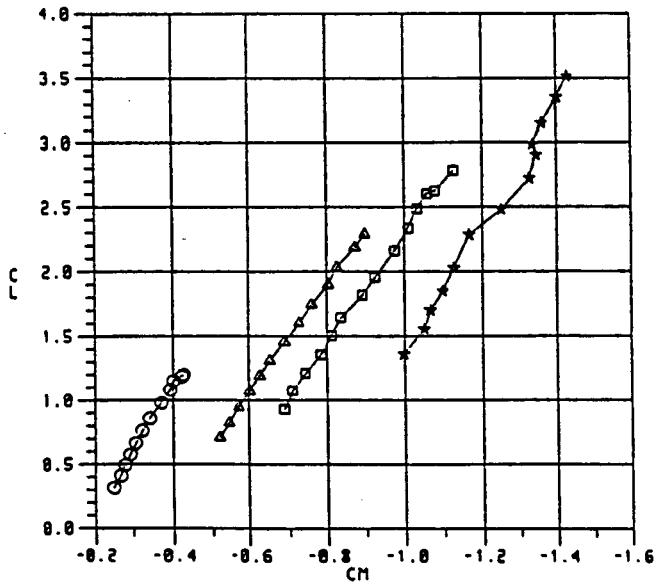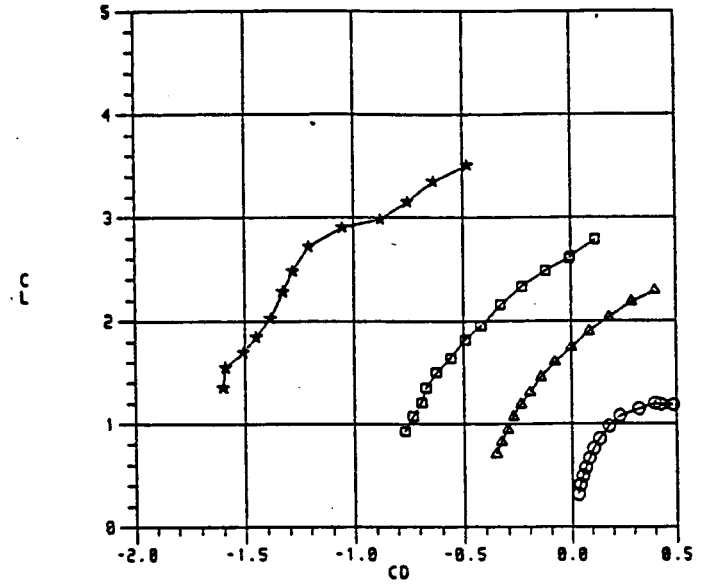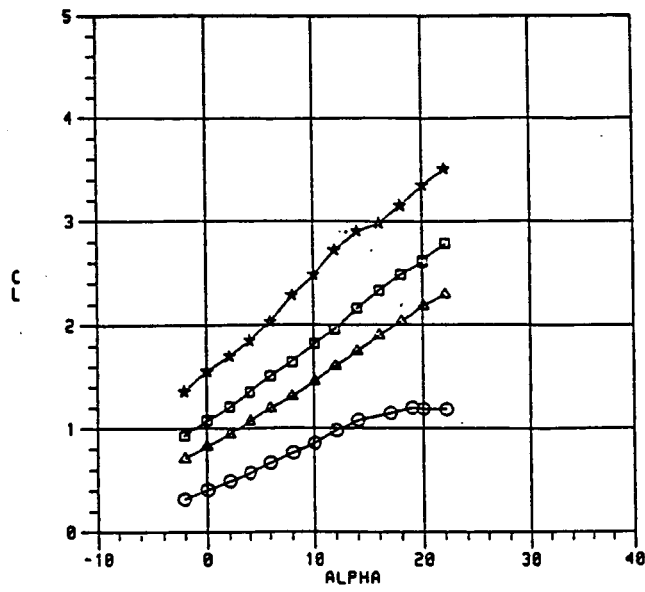
SYM	RUN	CMUT
○	256	0.00
△	257	0.53
□	258	1.07
★	259	2.23

b. Thrust Removed Aerodynamic Characteristics

Figure 13   Variation of Longitudinal Aerodynamic Characteristics, B2W8V, $\delta_F = 15°$
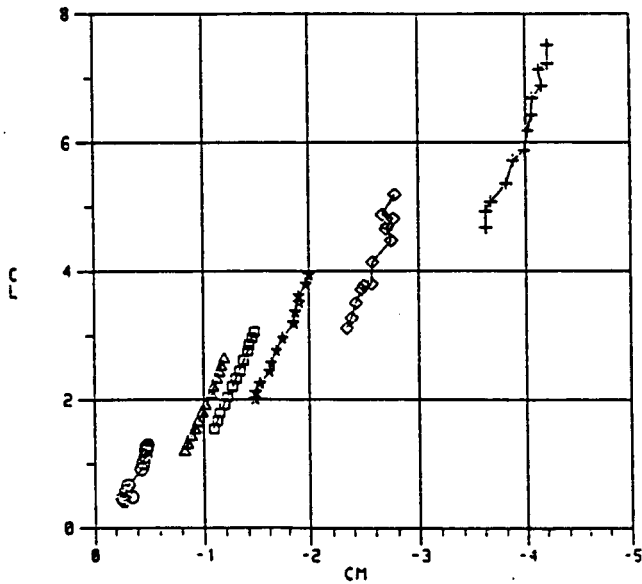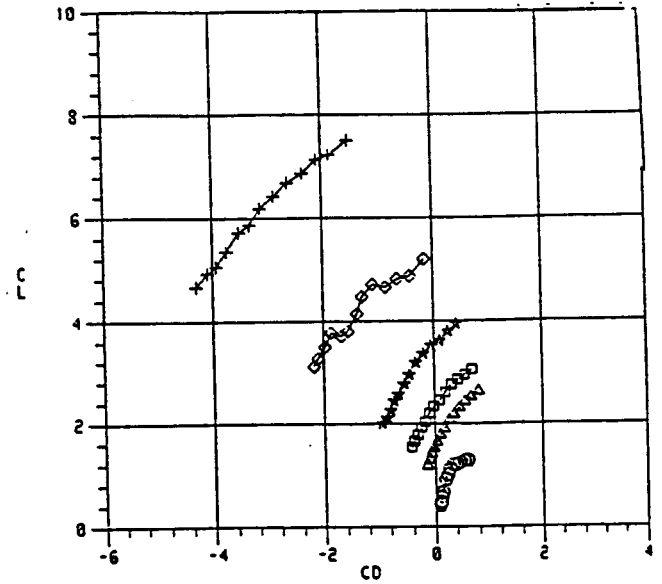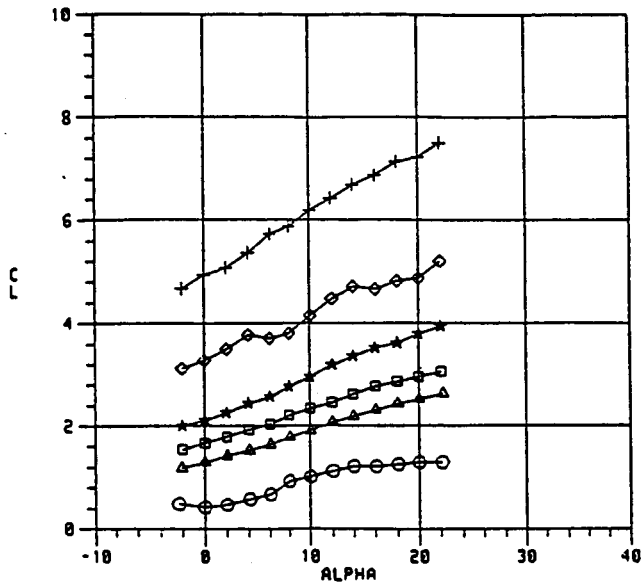
SYM   RUN   CMUT
O   235   0.00
△   236   0.48
□   237   0.95
★   238   1.71
◇   239   3.71
+   240   6.86

a. Total Aerodynamic Characteristics

Figure 14   Variation of Longitudinal Aerodynamic Characteristics,
B2W8V, $\delta_F = 30°$

26
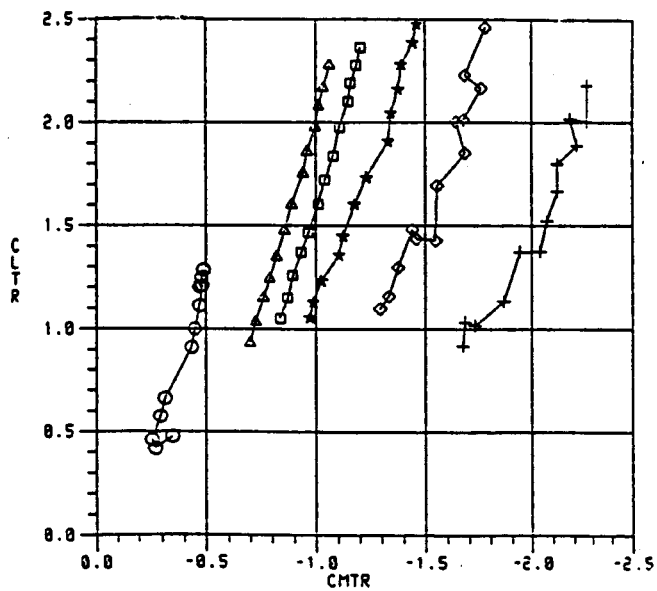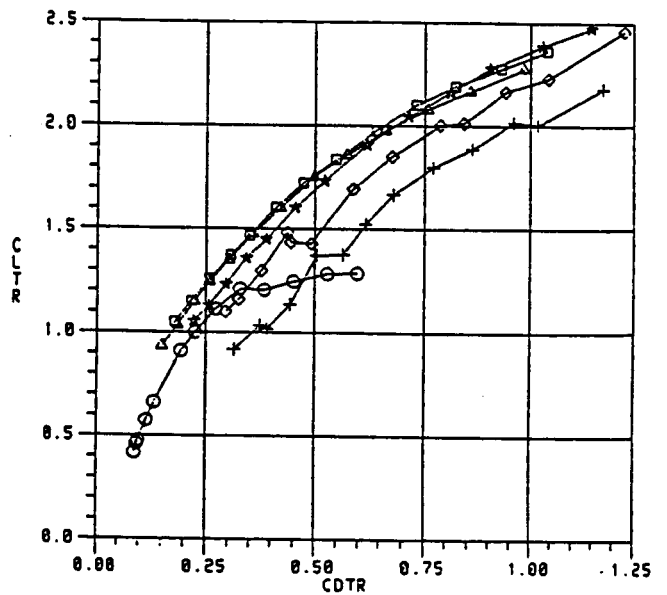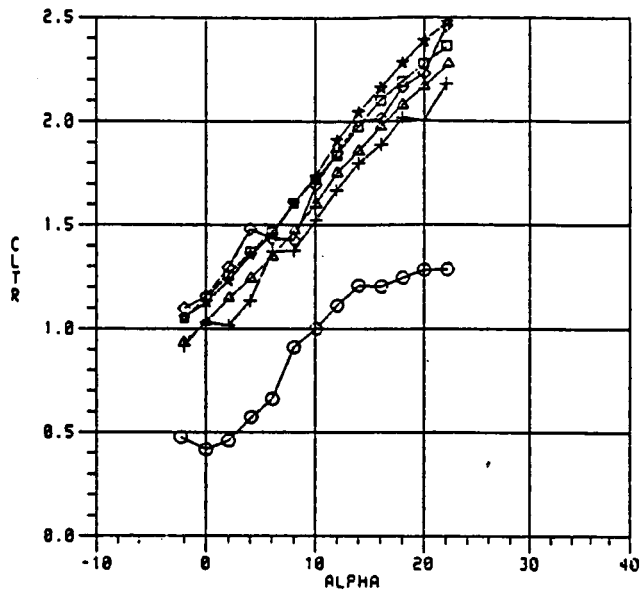
SYM	RUN	CMUT
O	235	0.00
△	236	0.48
□	237	0.95
★	238	1.71
◇	239	3.71
+	240	6.86

b. Thrust Removed Aerodynamic Characteristics

Figure 14   Variation of Longitudinal Aerodynamic Characteristics,
B2W8V, δ_F = 30°

27
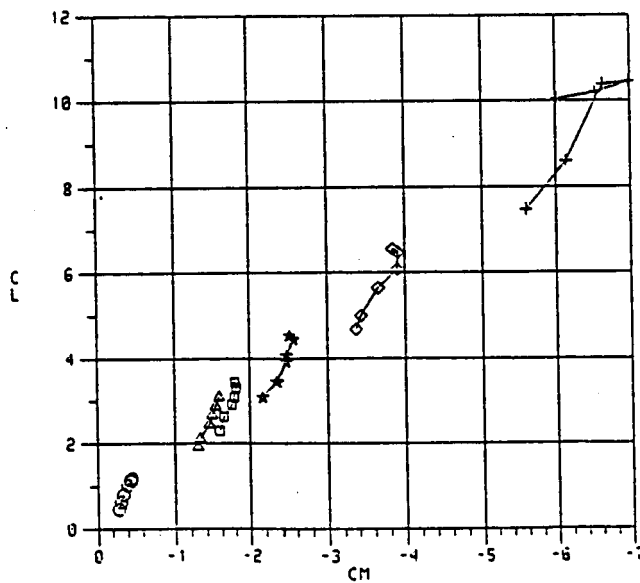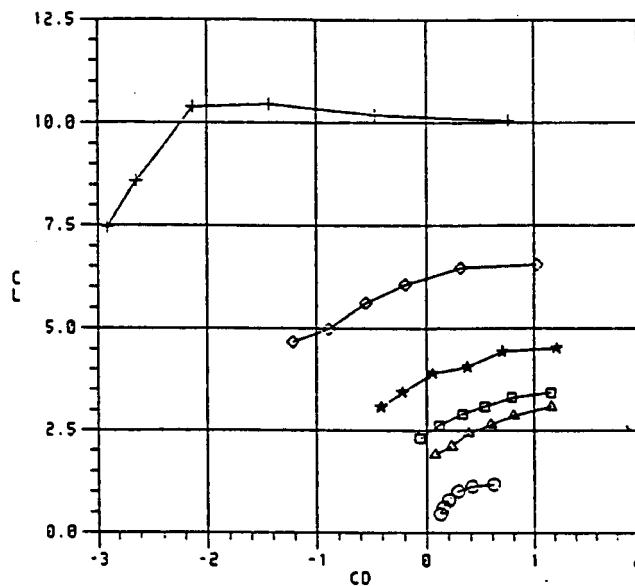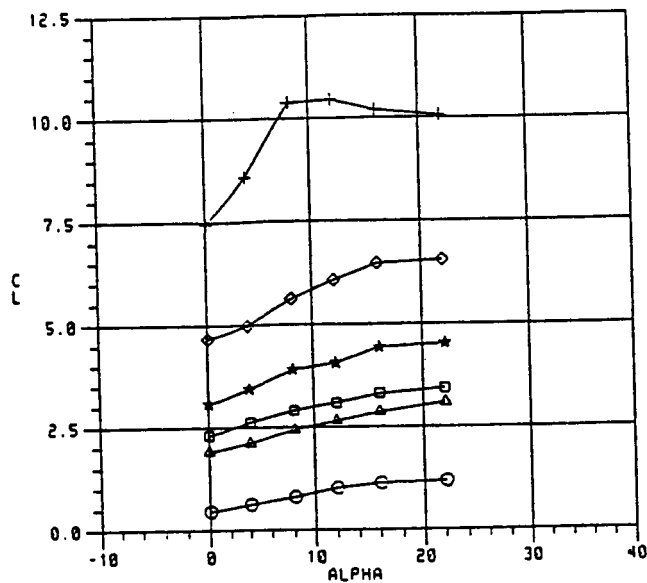
SYM	RUN	CMUT
O	362	0.00
△	363	0.63
□	364	1.07
★	365	2.04
◇	367	3.95
+	366	8.44

a. Total Aerodynamic Characteristics

Figure 15   Variation of Longitudinal Aerodynamic Characteristics,
B2W8V, δ_F = 45°

28
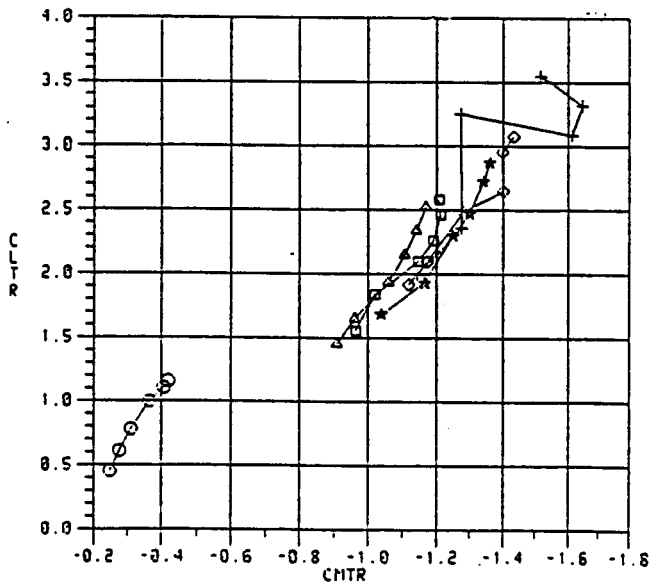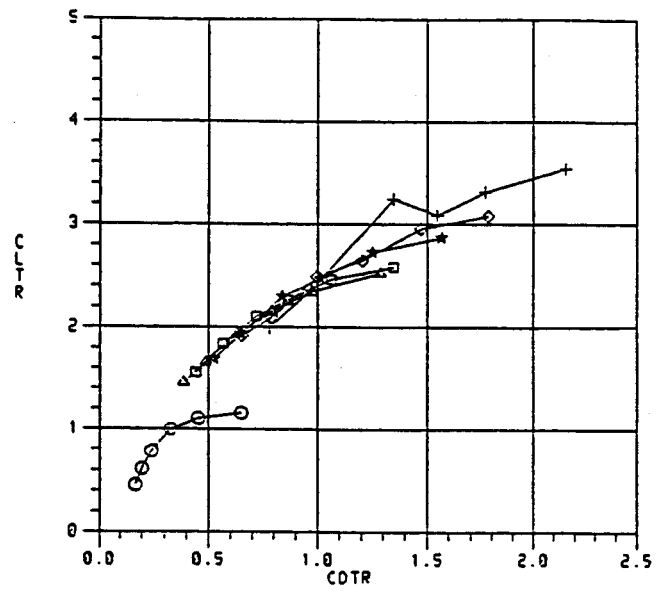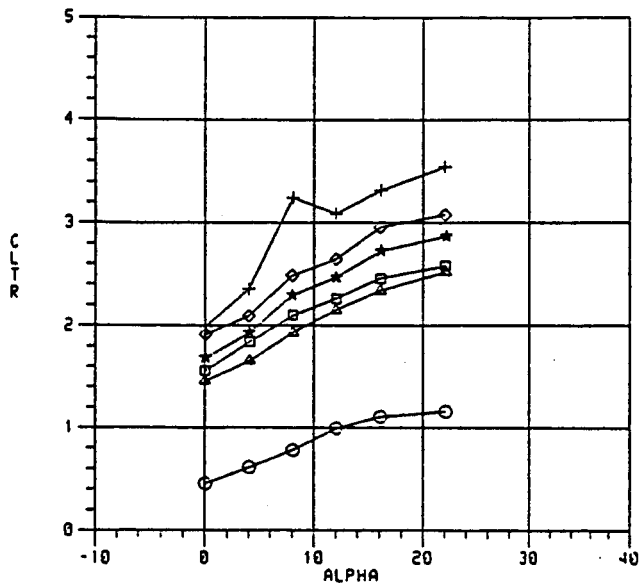
SYM	RUN	CMUT
O	362	0.00
△	363	0.63
□	364	1.07
★	365	2.04
◇	367	3.95
+	366	8.44

b. Thrust Removed Aerodynamic Characteristics

Figure 15   Variation of Longitudinal Aerodynamic Characteristics, B2W8V, $\delta_F = 45°$
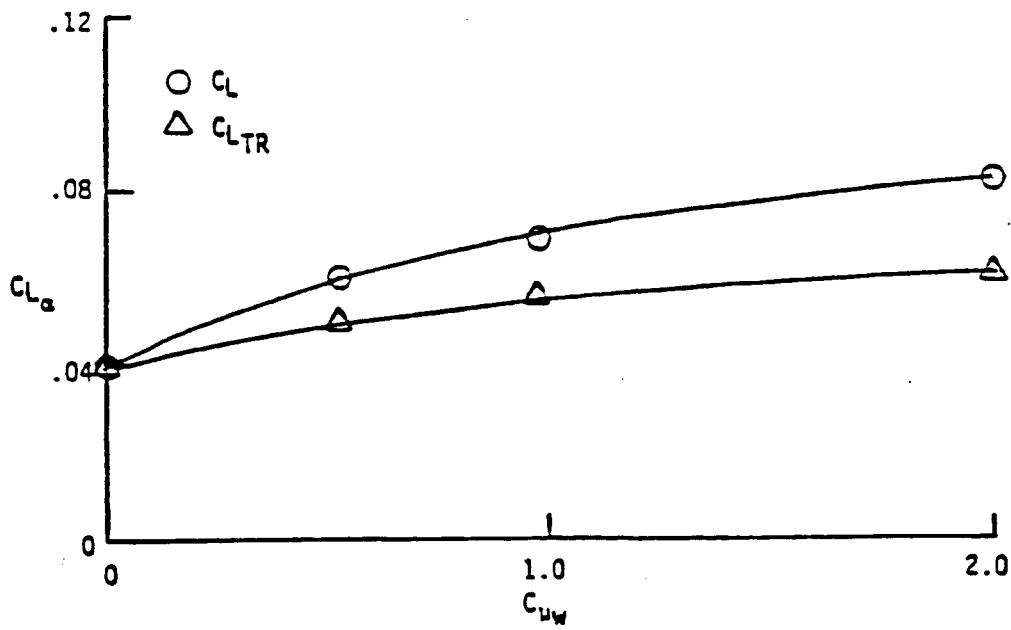
Figure 16   Effect of Blowing on C_{L_α}, $\delta_F = 0°$, $\alpha = 0°$, B2W8V
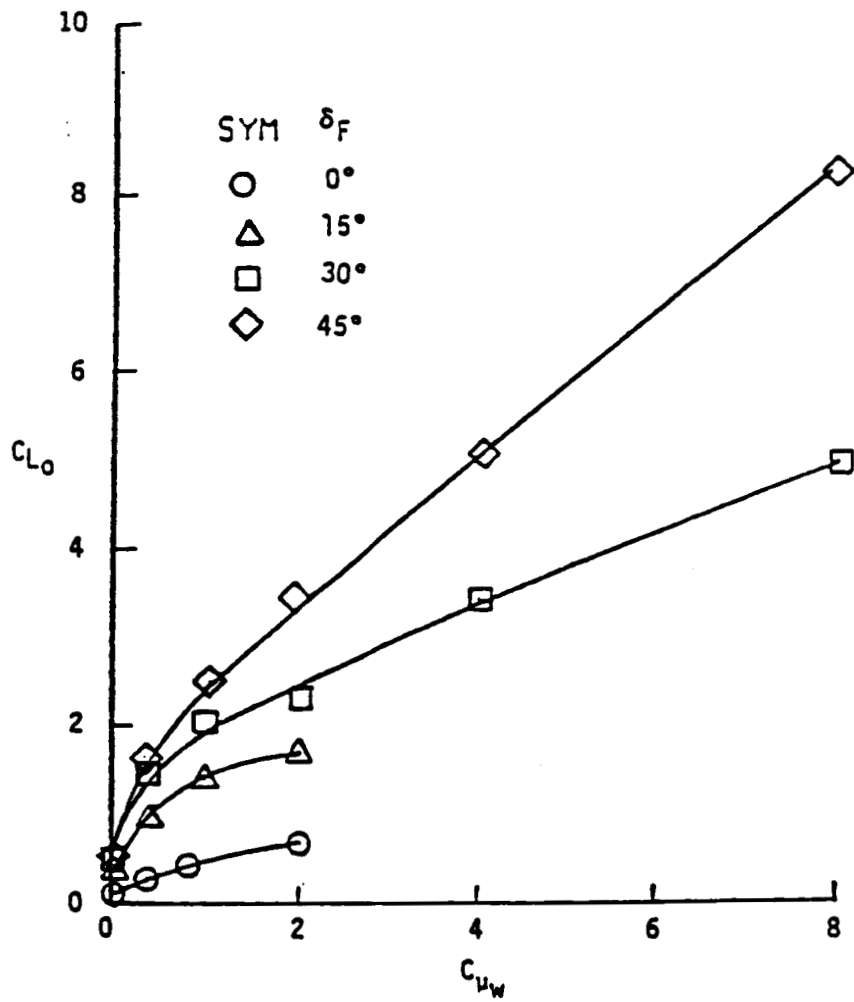
Figure 17 Effect of Flap Deflection on Lift Coefficient, $\alpha = 0°$, B2W8V

blowing. The data show that the lift curve slope is doubled at blowing
coefficients of 2.0 for the undeflected flap configuration. Figure 17
presents the variation of lift coefficient with blowing coefficient for
several flap deflections. The results indicate large increases in the lift
coefficient as the blowing is increased. Figure 18 presents a comparison
of lift coefficient due to flap deflection with that due to angle of attack
for a constant blowing coefficient. These data show that the lift variation
with flap deflection is nearly the same as with angle of attack except at a
flap deflection of 45 degrees where the angle of attack variation appears to
be higher. The condition of

$$C_{L_{\delta_F}}/C_{L_\alpha} = 1.0$$

was not expected because of the relatively short chord flap on the
propulsive wing model. The lift characteristics are apparently dominated by
the thrust vector addition to the lift coefficient and the effect of blowing
on the circulation lift.

The effect of the span of the blowing portion of the flap was also
investigated. Figure 19 presents the longitudinal axis data for the
quarter-span nozzle and Figure 20 presents the same data for the half-span
nozzle tests. The data indicate that the lift coefficient decreases as the
span of the blown section is reduced. Figure 21 presents the variation of
the thrust removed lift coefficient for the quarter, half, and full-span
nozzles with the coefficients based on the blown wing area. The results
show that at zero angle of attack, at least, the data correlate when based
on the blown wing area and referenced to a blowing coefficient based on the
same area. The data previously obtained on this propulsive wing with a
rectangular fuselage and with a root chord incidence of four degrees showed
a similar correlation when the wing incidence was properly considered.
Since the flap deflection lift for each of the two models is approximately
the same at the same wing angle of attack the fuselage shape change does not
appear to have affected the flap characteristics.

The previous tests of this propulsive wing configuration in February 1985
demonstrated maximum lift coefficients which approached 1.9 times the wing
aspect ratio. It has been suggested that the square fuselage tested at that
time may have contributed to the high maximum circulation lift coefficients
attained. The results of the latest test with the shaped fuselage is
compared to previous results in Figure 22. As seen, the maximum lift
coefficient with the shaped fuselage is at least as high as that of the
previous tests. This test data appears to confirm that the maximum
attainable circulation lift coefficient can approach 1.9 times the wing
aspect ratio. The maximum circulation lift coefficient from the shaped
fuselage test was reached at a higher blowing coefficient than that required
for the rectangular fuselage tests. The maximum lift coefficient was
attained at the most extreme conditions tested, see Figure 15. A positive
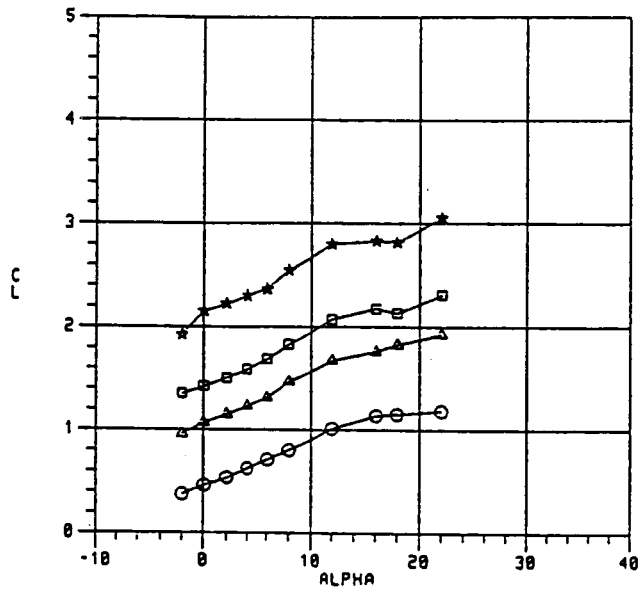
32
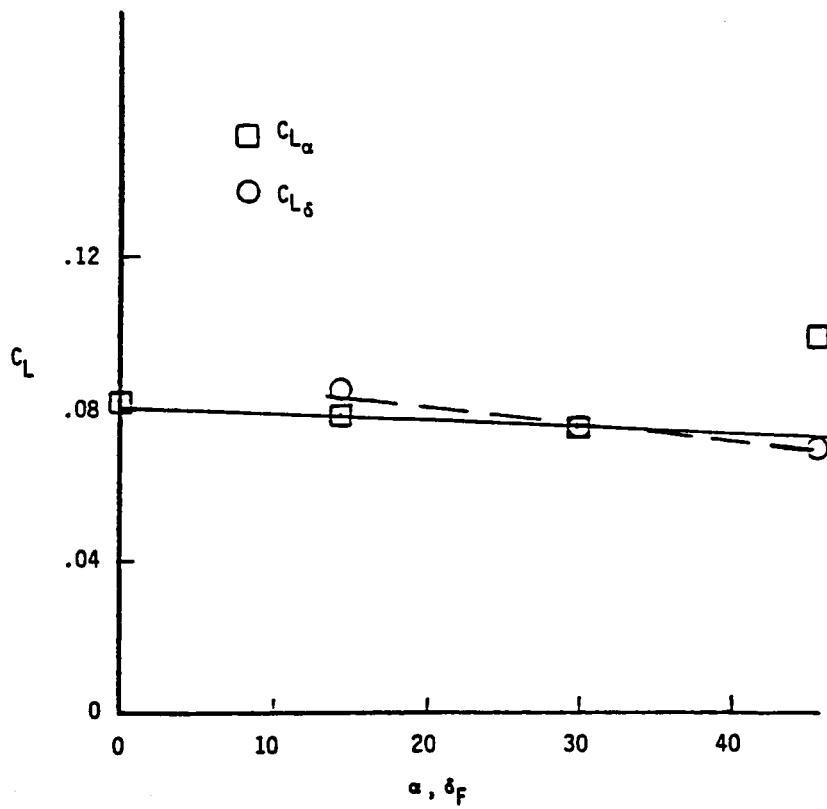
Figure 18   Comparison of Lift Due to Angle of Attack and Flap
Deflection, C_μ = 2.0, B2W8V
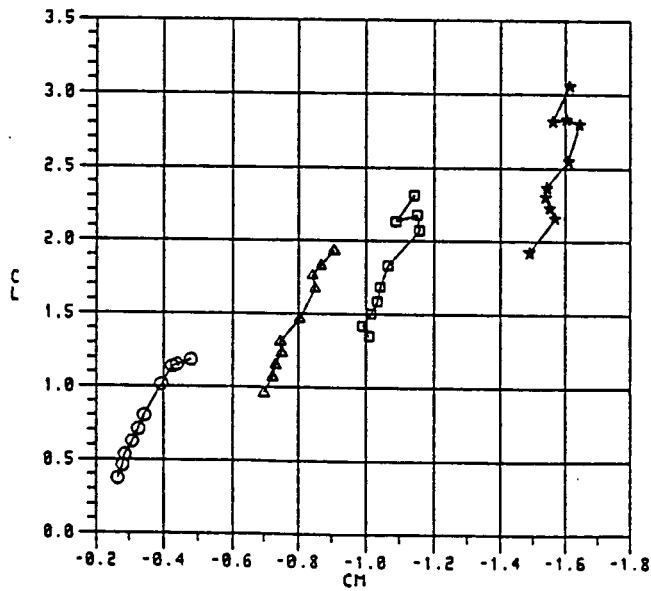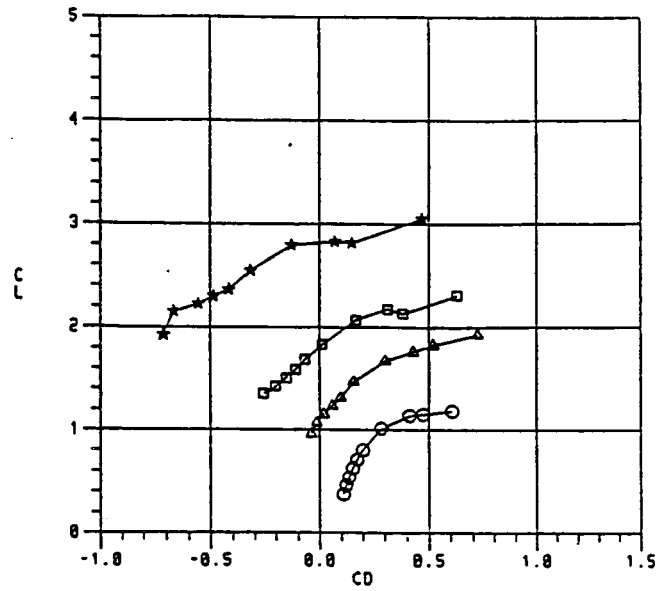
SYM	RUN	CMUT
○	273	0.00
△	274	0.50
□	275	0.98
★	276	2.07

a. Total Aerodynamic Characteristics

Figure 19   Variation of Longitudinal Aerodynamic Characteristics,
B2W8V, δ_F = 45°, Bn/N = .25

34

b. Thrust Removed Aerodynamic Characteristics

Figure 19   Variation of Longitudinal Aerodynamic Characteristics,
B2W8V, δ_F = 45°, Bn/B = .25
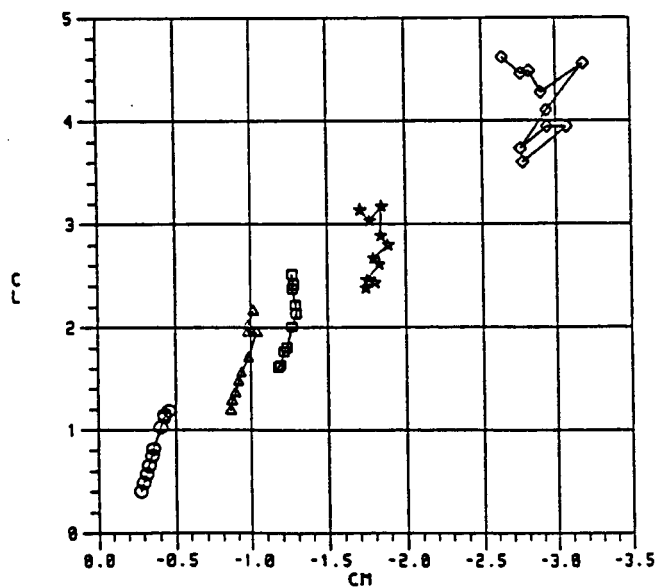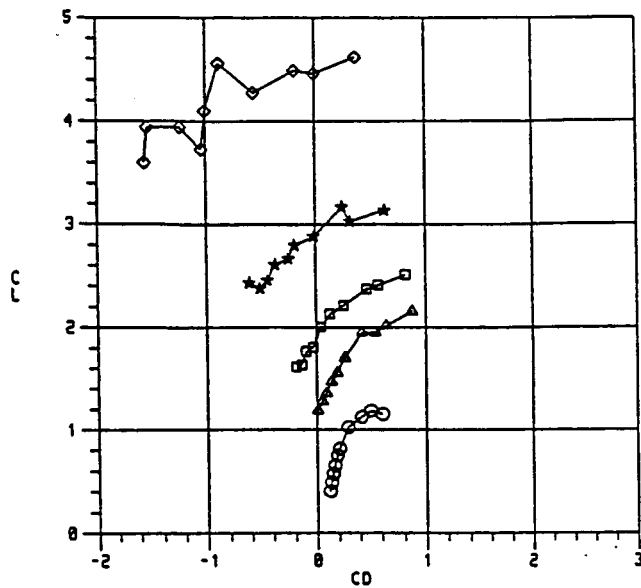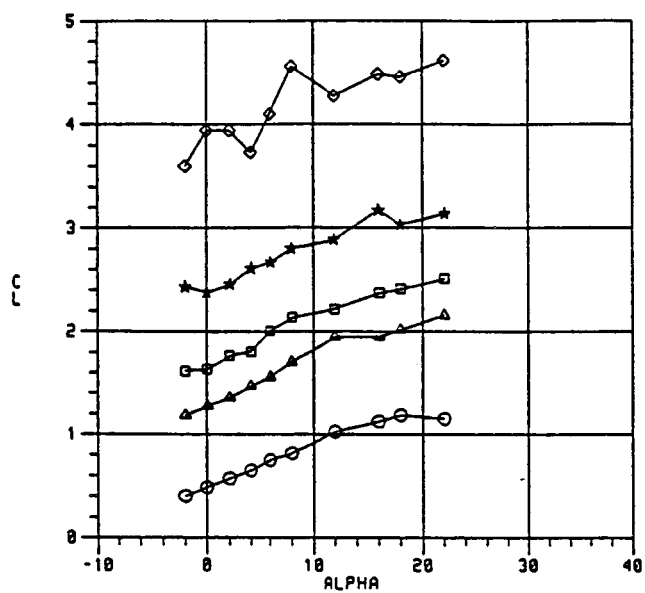
SYM	RUN	CMUT
○	299	0.00
△	307	0.50
□	306	0.99
★	305	1.95
◇	304	4.36

a. Total Aerodynamic Characteristics

Figure 20   Variation of Longitudinal Aerodynamic Characteristics,
B2W8V, δ_F = 45°, Bn/B = .5

36
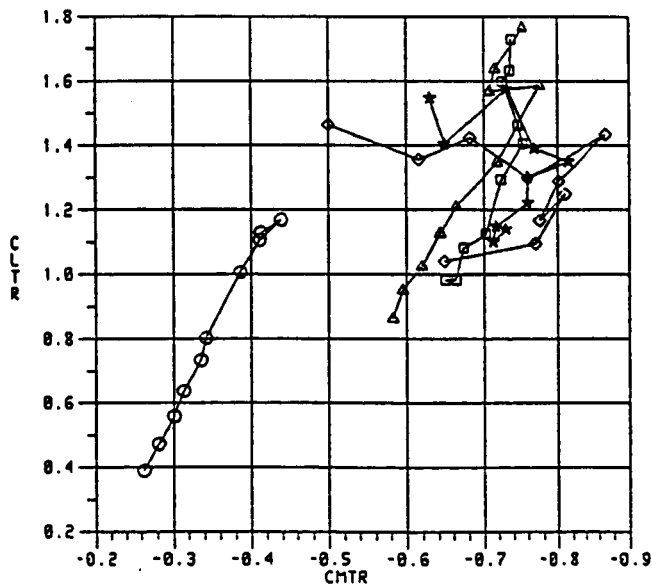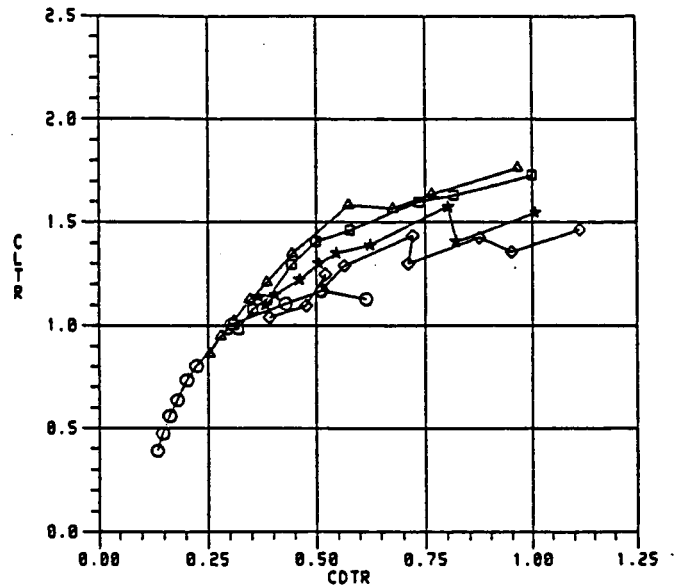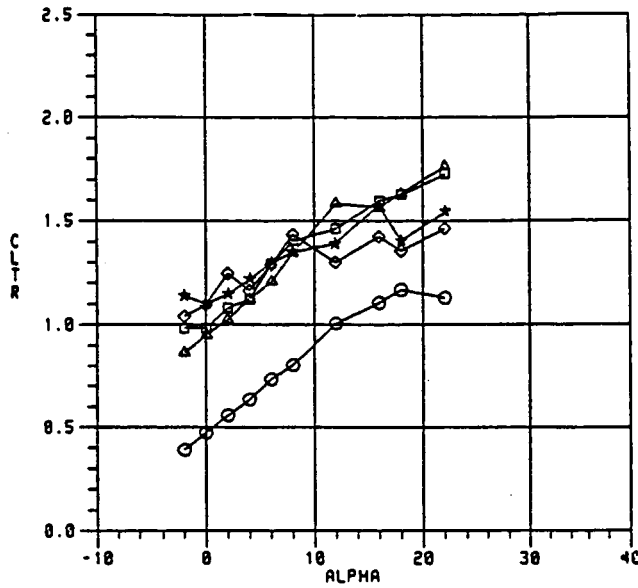
SYM   RUN   CMUT
○   299   0.00
△   307   0.50
□   306   0.99
★   305   1.95
◇   304   4.36

b. Thrust Removed Aerodynamic Characteristics

Figure 20   Variation of Longitudinal Aerodynamic Characteristics,
B2W8V, δ_F = 45°, Bn/B = .5

37
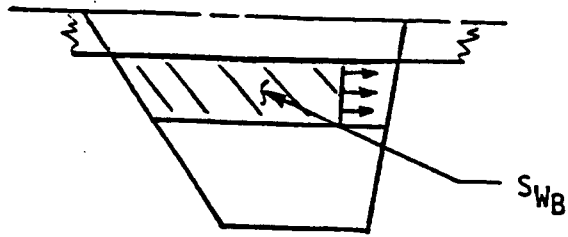
$$C_{L_{\Gamma_f}} = C_{L_{TR}} \left(\frac{S}{S_{W_B}} \right)$$

$$C_{\mu_f} = C_\mu \left(\frac{S}{S_{W_B}} \right)$$
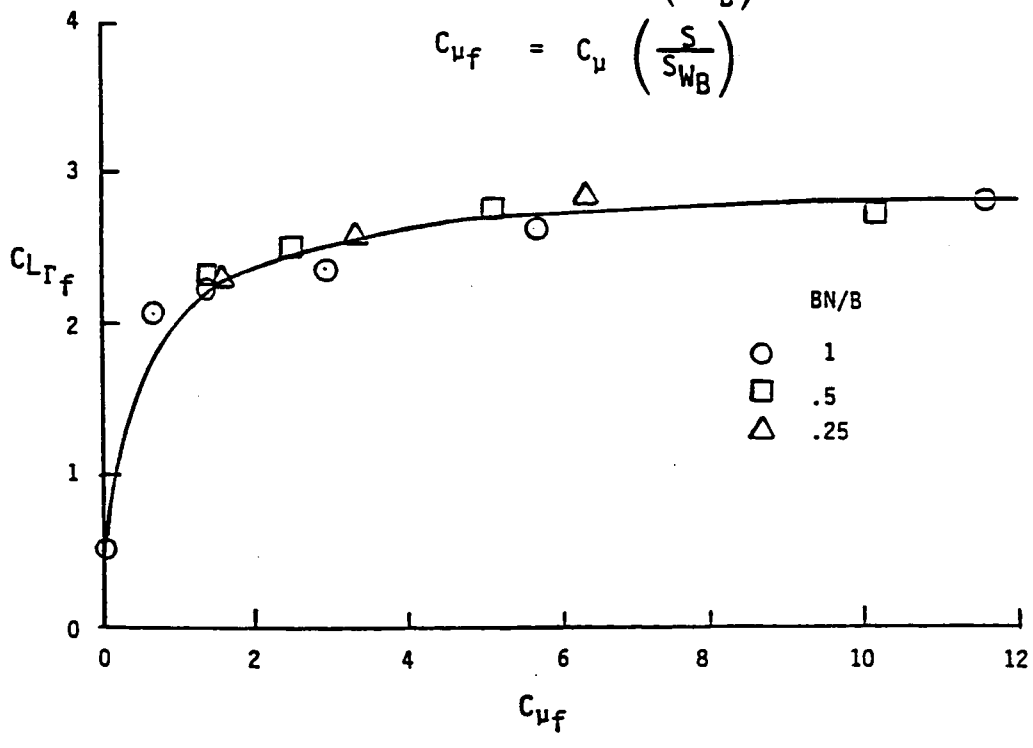
Figure 21   Effect of C_μ on Lift Coefficient, $\alpha = 0°$, $\delta_F = 45°$
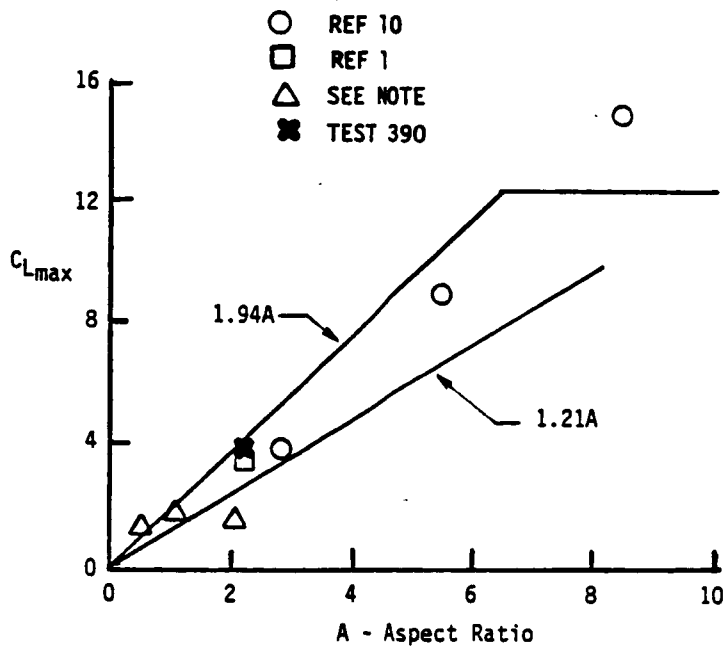
NOTE: Zimmerman, C. H., "Characteristics of Clark Y Airfoils of Small Aspect Ratio," NACA Unpublished Data, May 1932.

Figure 22 Comparison of Predicted and Test Maximum Lift Coefficient

lift curve slope is indicated at that condition confirming that the wing incidence reduction did affect the maximum attained lift condition. The effect of fuselage endplating on the flap cannot be determined from the available data.

3.1.2 Wing-Body-Canard

The large pitching moment coefficient developed by blowing on the flap of the propulsive wing requires a nose up pitching moment to balance the airplane. An aft tail will provide pitch trim by imposing a down load at the tail surface thus resulting in an overall lift loss. An alternative to the aft tail is the use of a blown canard which provides a control surface located forward of the center of gravity. The positive pitching moment required for trim is then provided with a positive lift. The canard, however, produces a large downwash angle on the inboard wing sections thereby detracting from the positive benefits of the forward control surface.

Most canard development studies have concluded that a canard located high and close-coupled relative to the wing is preferred. A program devoted to development of a V/STOL augmenter wing and canard ("XFV-12A V/STOL Fighter Attack Technology Prototype Program", Contract N00019-73-C-0053, Rockwell Unpublished Data) concluded, however, that the canard should be located below the wing plane. This investigation and two previous studies, References 1 and 4, have provided information which aids in understanding the canard interaction with the wing. Reference 1 provided an initial insight into canard/wing relative positions for STOL flap deflections. Reference 4 primarily investigated the high speed characteristics of the jet flap, but also provided some information on relative canard/wing placement for low flap deflections.

The downwash and jet sheet deflected from the trailing edge of a propulsive canard combine to produce an effect on the wing which is condition dependent. The studies mentioned above indicate that a high canard is preferred at cruise and takeoff flap deflections of less than 15 to 20 degrees. At the larger flap deflections required for STOL landing (greater than 30 degrees) a low canard is more advantageous. Figure 23 presents the calculated jet path for several canard flap deflections. The wing position for the model used in this investigation is shown in the figure for discussion purposes. For jet deflection angles of greater than 15 degrees the jet is shown to pass below the wing creating a large downwash angle on the wing. In addition, the jet passing in front of and below the wing acts as a blockage to the airflow at the wing leading edge. Figure 24 presents the measured local flow angles of the canard with the canard flap deflected 45 degrees. The inboard station shows relatively large downwash angles and relatively constant jet velocities outside the jet. The outboard station, BP12, in addition, shows the tip vortex effects carried inboard of the canard tip. These data indicate the jet sheet to be deflected slightly more than calculated. The calculated jet sheet path shown in Figure 23 indicates that at canard flap deflections of less than 15 degrees the jet passes over the wing leading edge and in fact may impinge on the aft wing chord to produce a beneficial upper surface blowing effect.
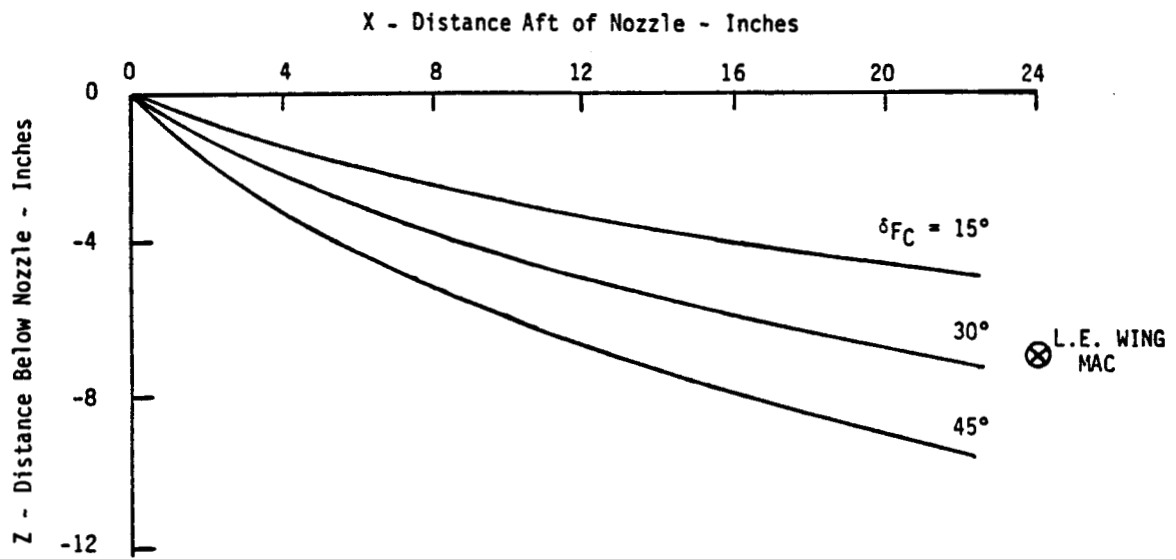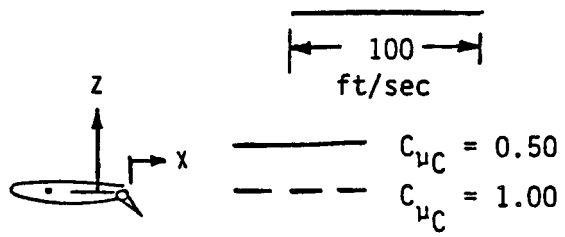
X - Distance Aft of Nozzle - Inches
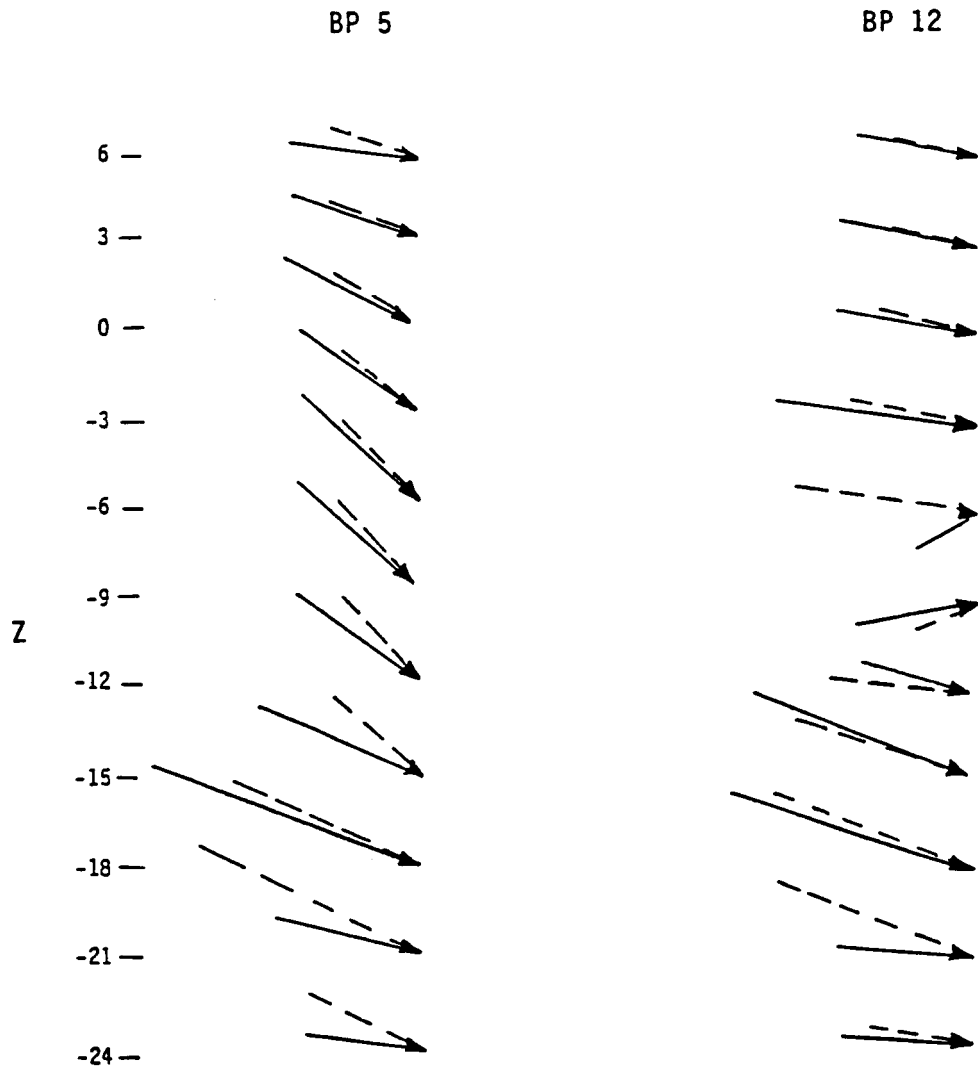
Figure 23   Canard Jet Sheet Paths

Figure 24   Canard Flow Field

42

The previous studies conducted on the propulsive wing/canard have suggested that the high canard may be the best compromise for the overall missions of a STOL fighter wing/canard configuration. The canard was located in the high position for all data presented in this report.

The longitudinal characteristics of the propulsive wing/canard model are presented in Figures 25 through 28 for flap deflections of 0, 15, 30, and 45 degrees, respectively. The characteristics are well behaved for most levels of blowing coefficient except for the very high blowing rates and large deflections. The data show considerable scatter at very high blowing coefficients, greater than 10.0. It appears that this data scatter is the result of variations in the thrust coefficient magnified by the low dynamic pressure. These variations can mostly be eliminated by utilization of the thrust removed coefficients. The thrust removed lift and drag coefficients also show the interference effects which are apparent with the canard configuration.

At blowing coefficients of three or less the characteristics exhibit the expected variations with attitude. However, at the higher blowing coefficients the longitudinal characteristics exhibit separation tendencies which are reflected in nonlinear lift, drag, and pitching moment. These high blowing coefficients occur at only very slow speeds when the use of power controls may be required and such characteristics may be acceptable.

Figure 29 presents the lift characteristics of the canard and wing at a blowing coefficient of 2.0 and a flap deflection of 45 degrees. The canard-on lift coefficient is approximately the same as the wing-alone lift coefficient while the thrust removed lift coefficient is actually reduced.

Figure 30 presents the lift coefficient required and blowing coefficient available for a weight and thrust typical for the landing configuration of a wing/canard fighter. The lift coefficients available from the wing/canard configuration at wing and canard flap deflections of 30 and 45 degrees are also presented on Figure 30. These untrimmed data show that if trim can be provided without losing lift, the lift coefficient for the configuration is sufficient to fly at 40 knots and 57 knots with 45 and 30 degrees flap deflection, respectively.
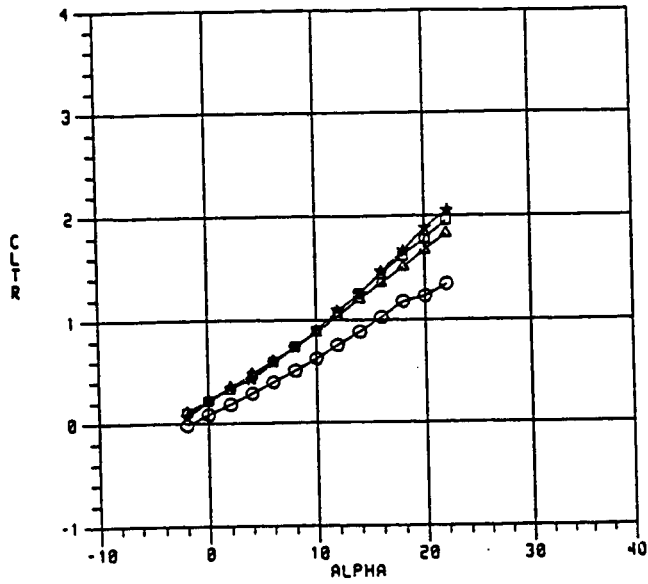
Providing sufficient trim for the propulsive wing canard is somewhat alleviated by the forward location of the canard. However, if the thrust split of 33% for the canard and 67% for the wing is maintained the canard will not provide sufficient nose-up pitch to trim with the center of gravity at the leading edge of the mean aerodynamic chord, as required for a wing/canard configuration. Trimming is additionally complicated by canard interference effects on the wing, as discussed above. Figures 31 to 34 show the effect of canard interference as the deflection is increased. These figures present the lift, drag, and pitching moment coefficients for the wing flap deflection at 30 degrees and the canard flap at 45, 30, and canard-off conditions and several blowing coefficients. The data show an increase in nose up moment as the canard flap deflection is changed from 30 to 45 degrees. The additional lift and thrust forward of the center of
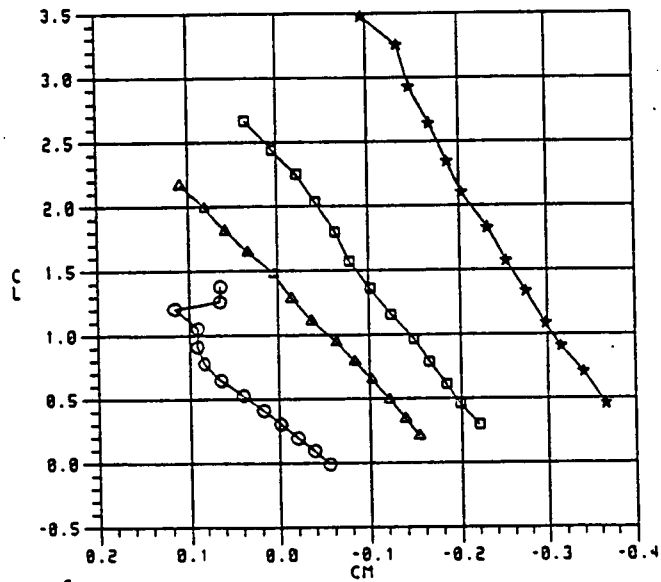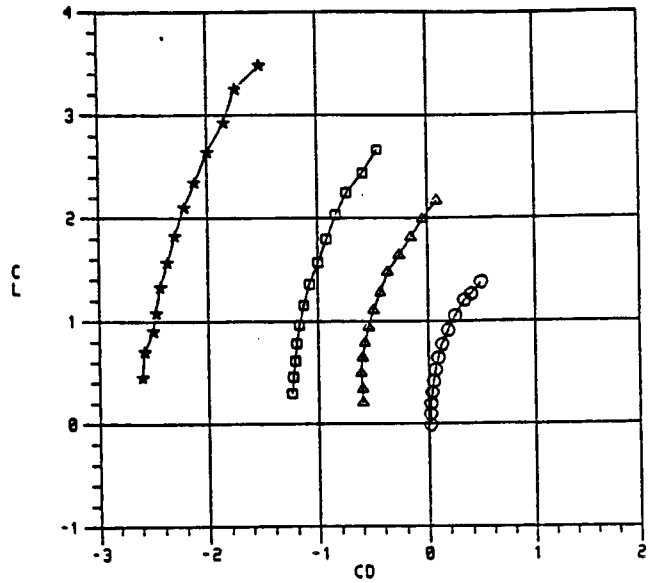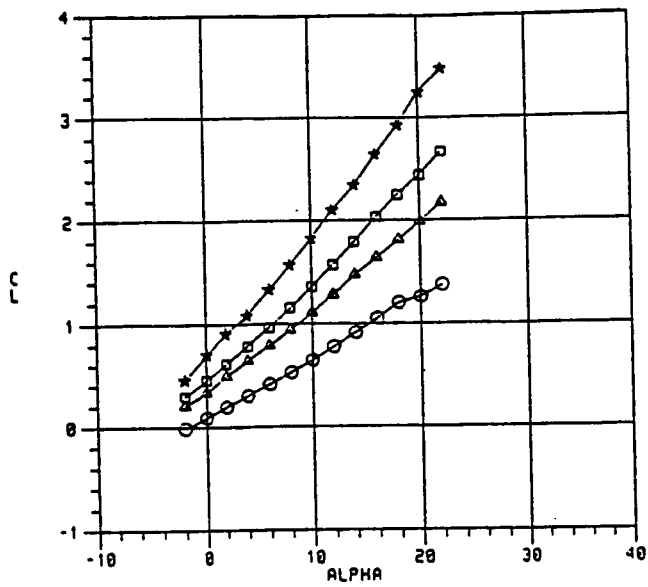
SYM RUN CMUT
○   105 0.00
△   106 0.74
□   107 1.43
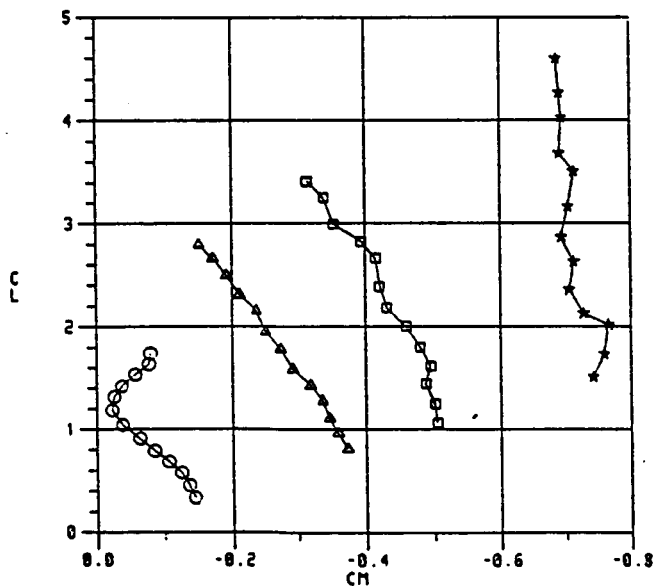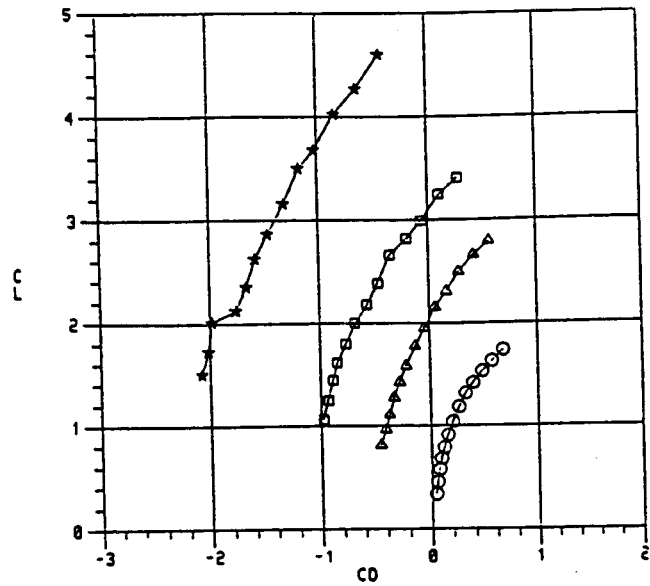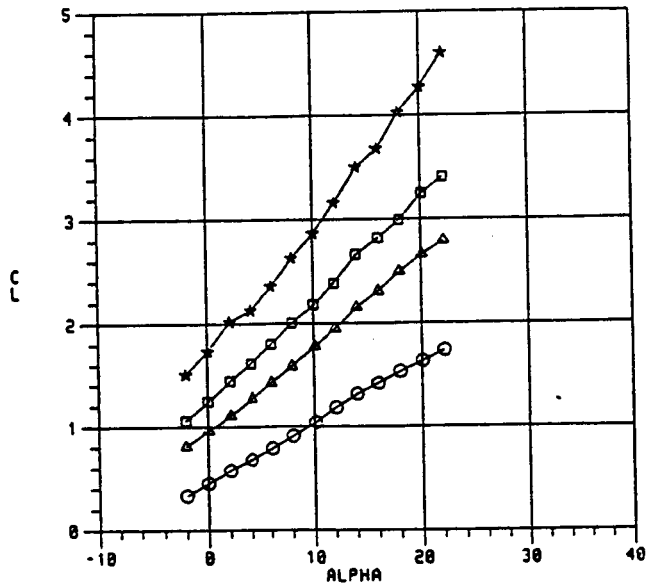★   108 2.98

a. Total Aerodynamic Characteristics

Figure 25. Variation of Longitudinal Aerodynamic Characteristics,
B2C1W6V, $\delta_F = 0°$

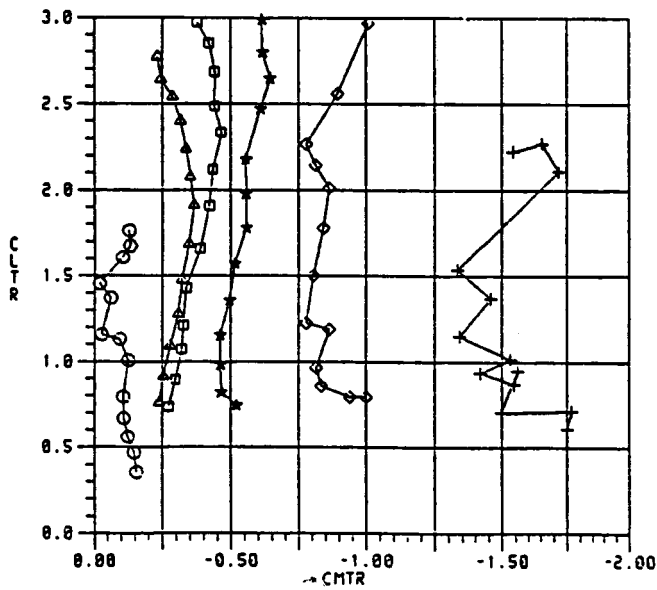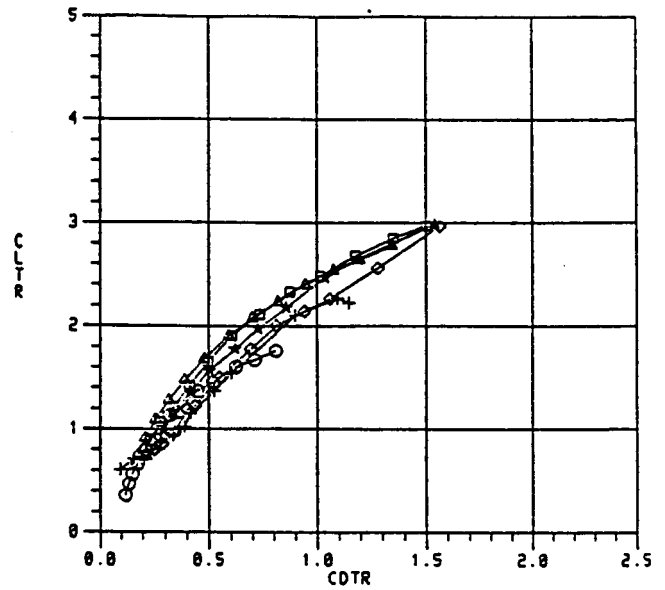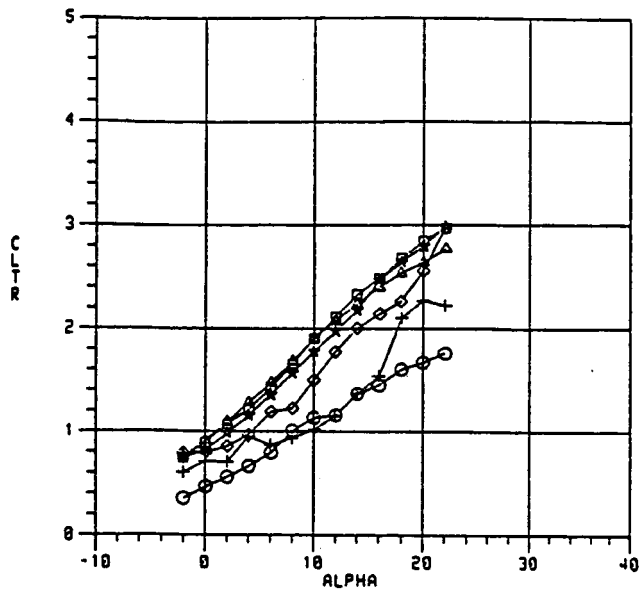| SYM	RUN	CMUT
O	105	0.00
△	106	0.74
□	107	1.43
★	108	2.98

b. Thrust Removed Aerodynamic Characteristics

Figure 25   Variation of Longitudinal Aerodynamic Characteristics,
B2C1W6V, $\delta_F = 0°$

45

SYM	RUN	CMUT
O	262	0.00
△	263	0.69
□	264	1.39
★	265	2.89

a. Total Aerodynamic Characteristics

Figure 26   Variation of Longitudinal Aerodynamic Characteristics,
B2C9W8V, δ_F = 15°

46
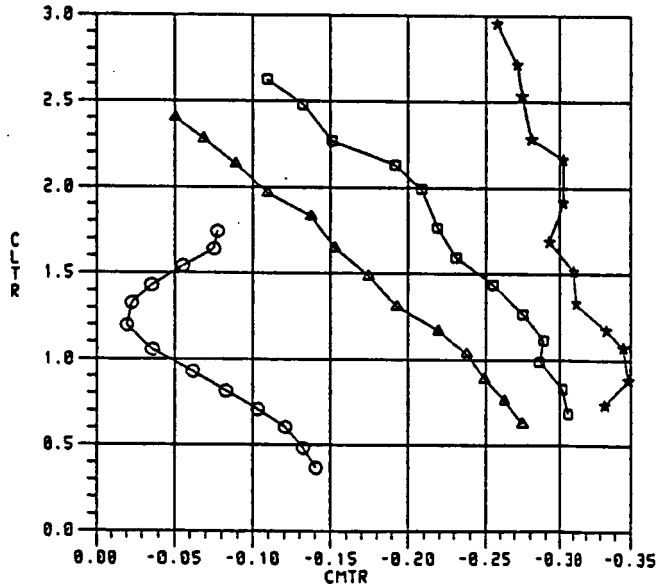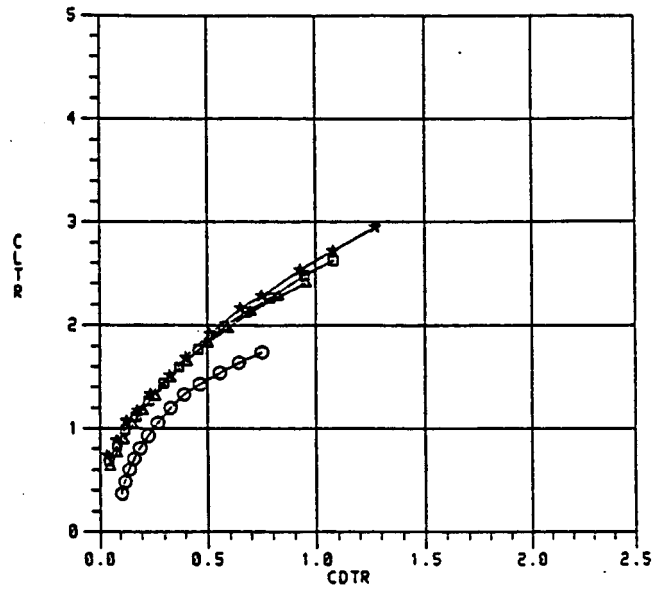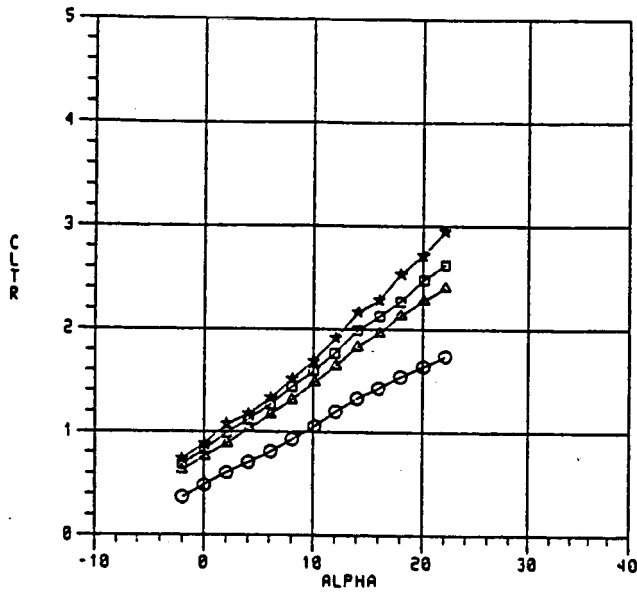
SYM	RUN	CMUT
O	262	0.00
△	263	0.69
□	264	1.39
★	265	2.89

b. Thrust Removed Aerodynamic Characteristics

Figure 26   Variation of Longitudinal Aerodynamic Characteristics,
             B2C9W8V, δ_F = 15°
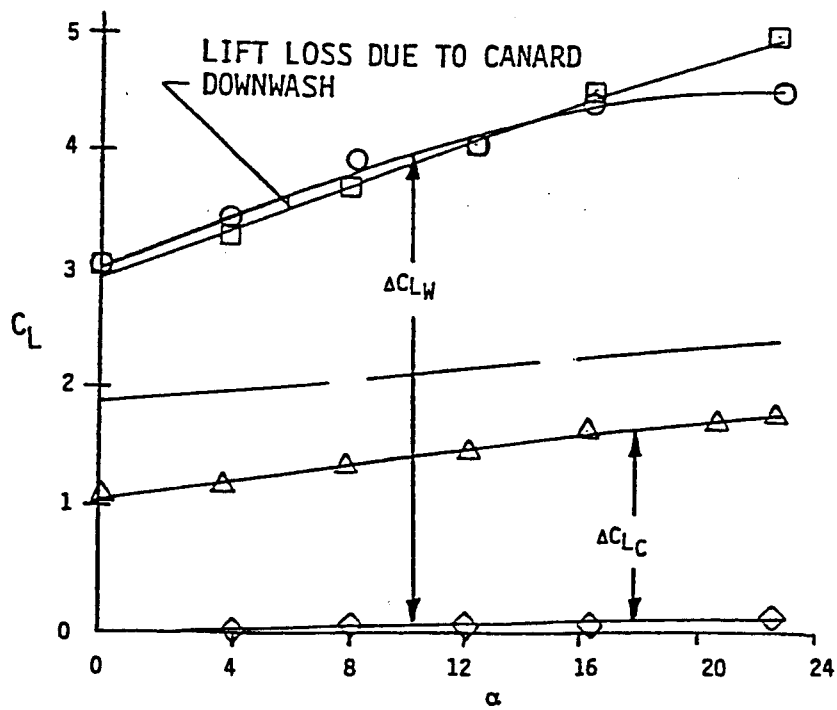
47

a. Total Aerodynamic Characteristics

Figure 27   Variation of Longitudinal Aerodynamic Characteristics,
B2C9W8V, δ_F = 30°

48
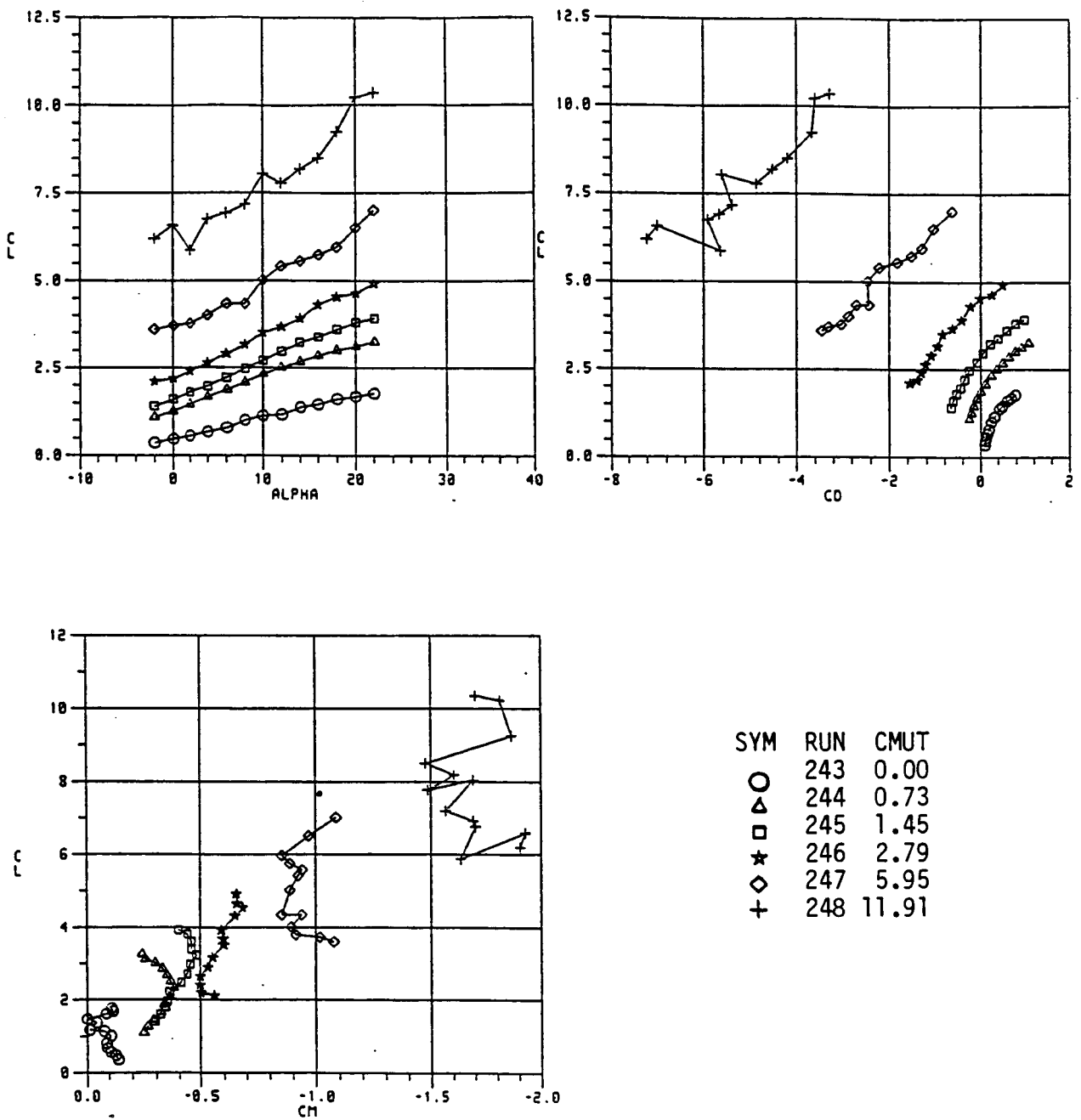
SYM RUN CMUT
○   243 0.00
△   244 0.73
□   245 1.45
★   246 2.79
◇   247 5.95
+   248 11.91

b. Thrust Removed Aerodynamic Characteristics

Figure 27. Variation of Longitudinal Aerodynamic Characteristics,
B2C9W8V, δ_F = 30°

49

SYM	RUN	CMUT
O	369	0.00
△	370	0.64
□	371	1.38
★	372	2.74
◇	373	5.48
+	374	10.58

a. Total Aerodynamic Characteristics

Figure 28   Variation of Longitudinal Aerodynamic Characteristics, B2C9W8V; $\delta_F = 45°$
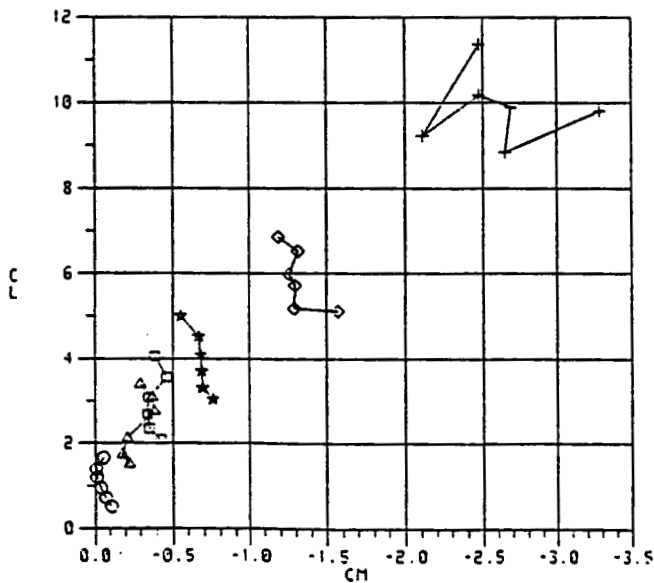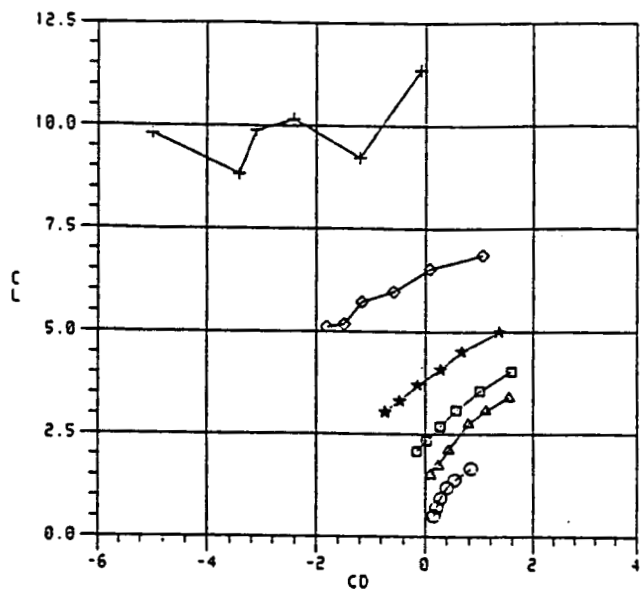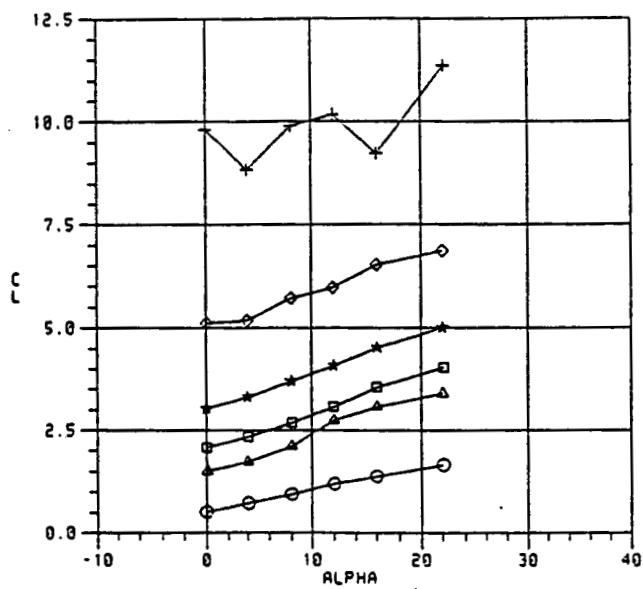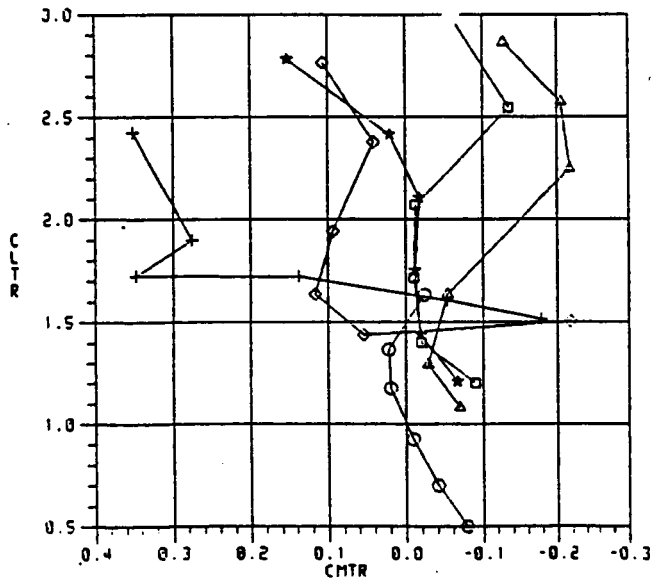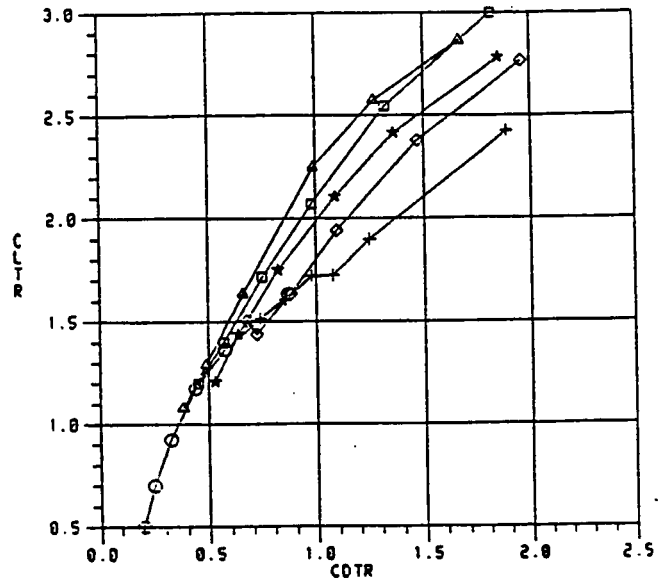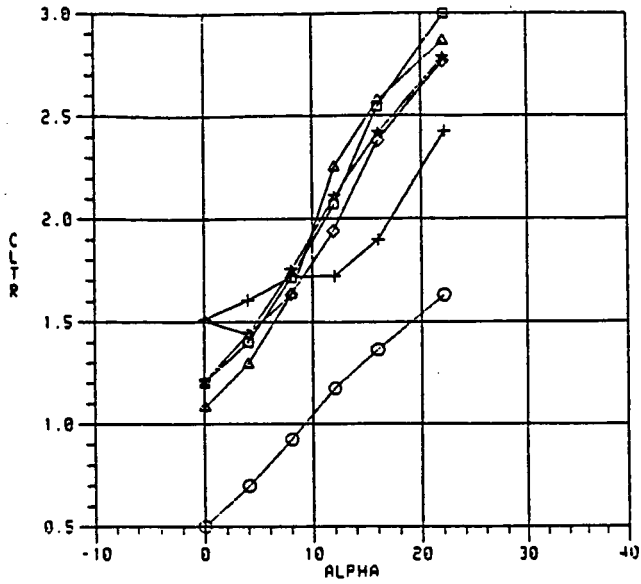
SYM RUN CMUT
○ 369 0.00
△ 370 0.64
□ 371 1.38
★ 372 2.74
◇ 373 5.48
+ 374 10.58

b. Thrust Removed Aerodynamic Characteristics

Figure 28   Variation of Longitudinal Aerodynamic Characteristics,
B2C9W8V, δ_F = 45°

51
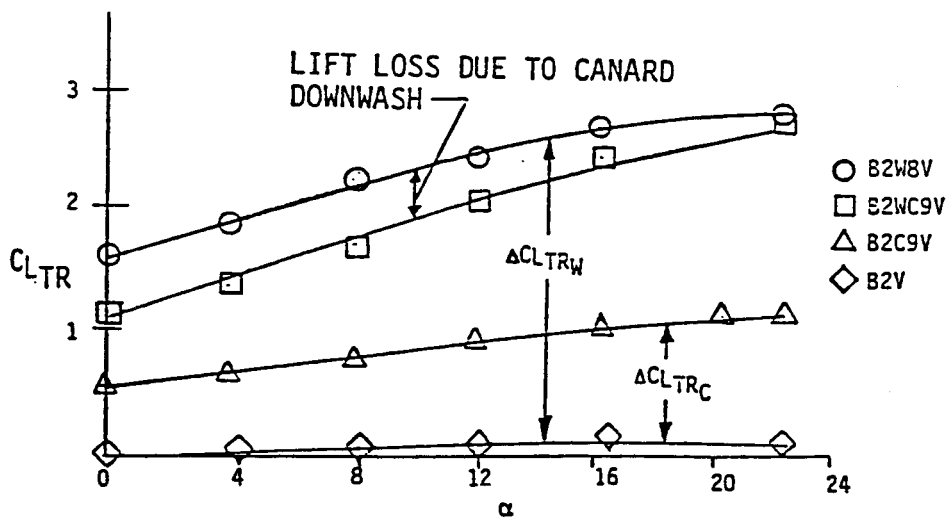
a. Thrust Removed Lift

Figure 29   Lift Coefficient Buildup, $C_\mu = 2.0$, $\delta_F = 45°$

52

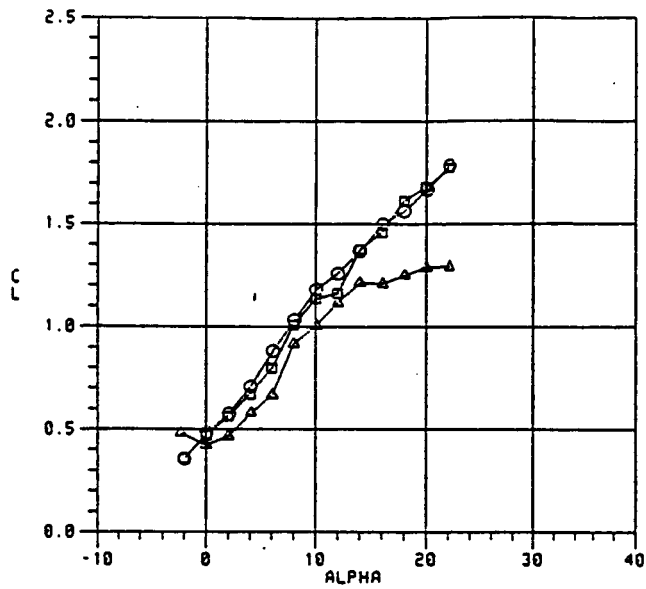LIFT LOSS DUE TO CANARD DOWNWASH

ΔC_{L_W}

ΔC_{L_C}

b. Total Lift

Figure 29   Lift Coefficient Buildup, $C_\mu = 2.0$, $\delta_F = 45°$
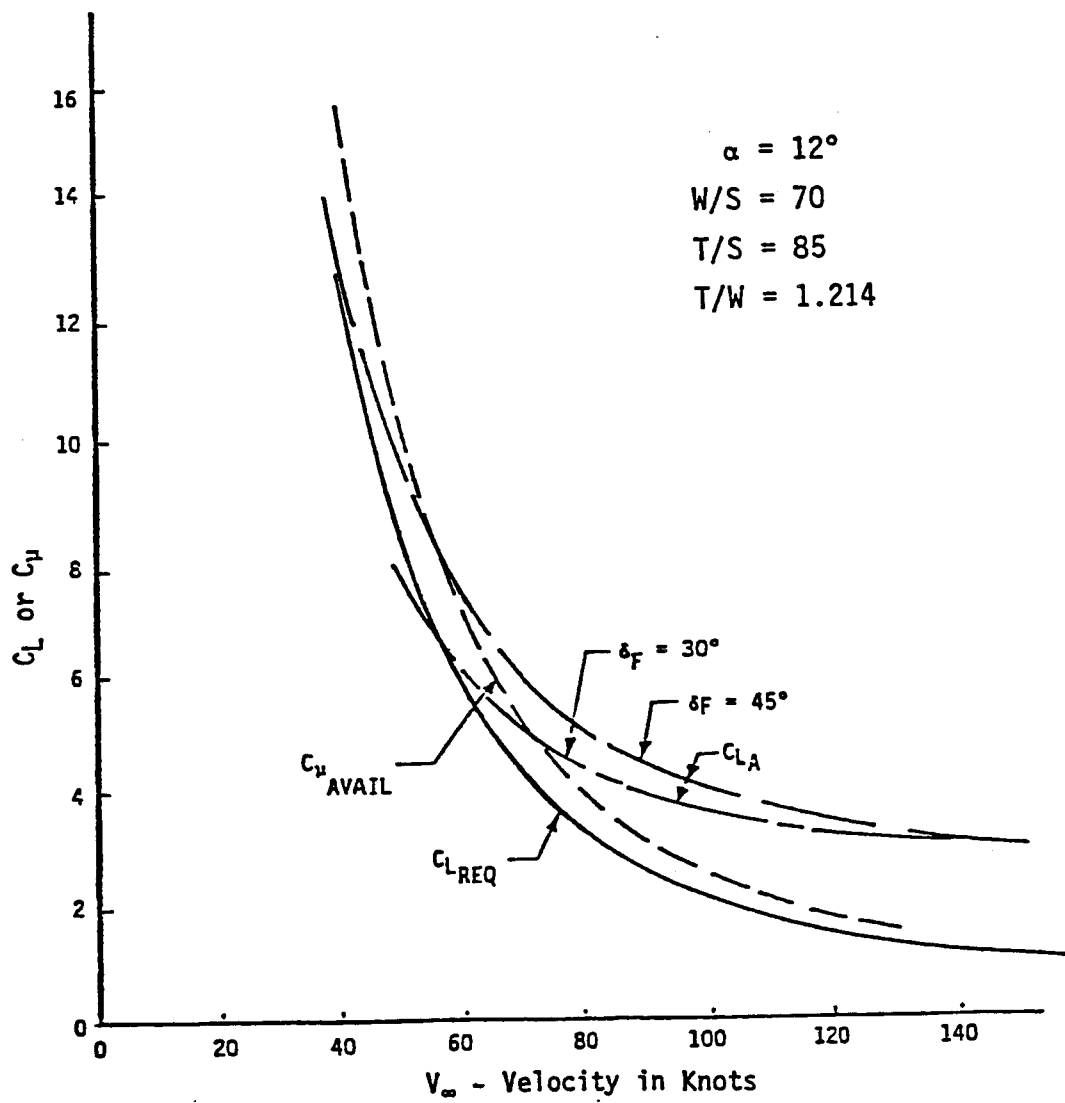
Figure 30   Lift and Blowing Coefficient Required and Available

54
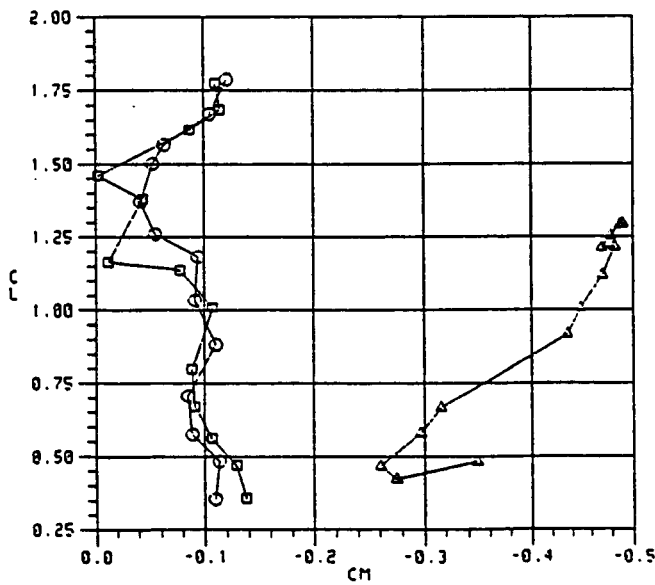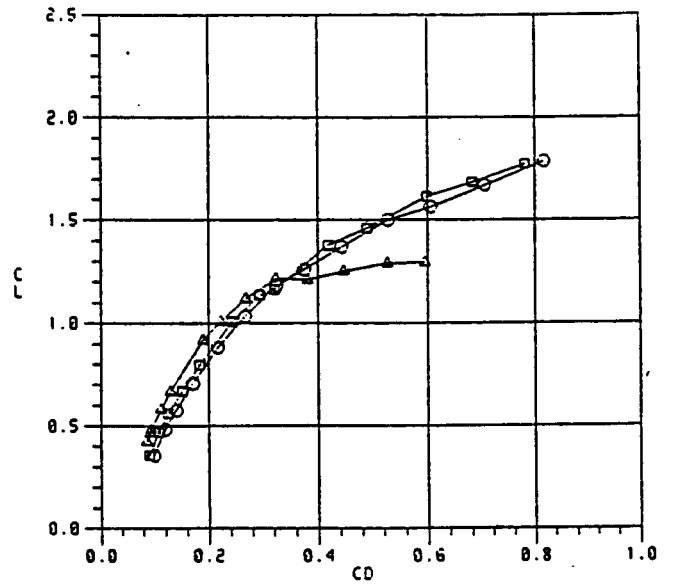
Figure 31   Variation of Longitudinal Aerodynamic Characteristics
             For Trim, $C_\mu = 0$
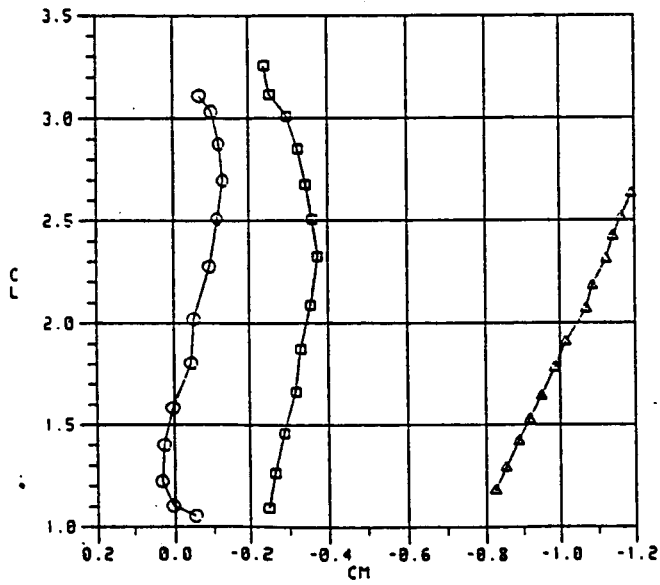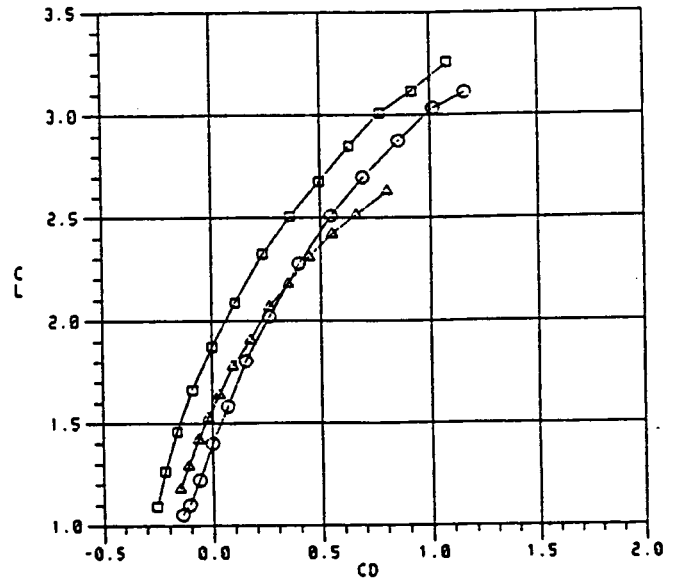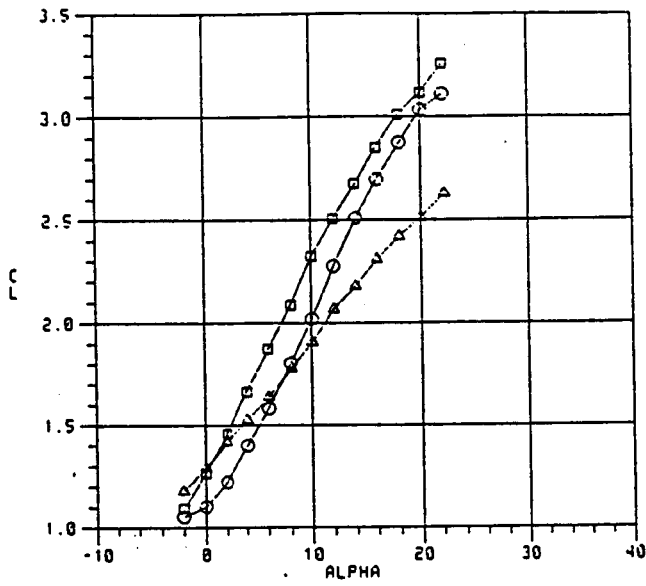
SYM	RUN	CMUT
○	231	0.67
△	236	0.48
▢	244	0.73

a. Total Aerodynamic Characteristics

Figure 32   Variation of Longitudinal Aerodynamic Characteristics
for Trim, C_{μ_W} = .5

56

SYM	RUN	CMUT
O	231	0.67
△	236	0.48
□	244	0.73

b. Thrust Removed Aerodynamic Characteristics
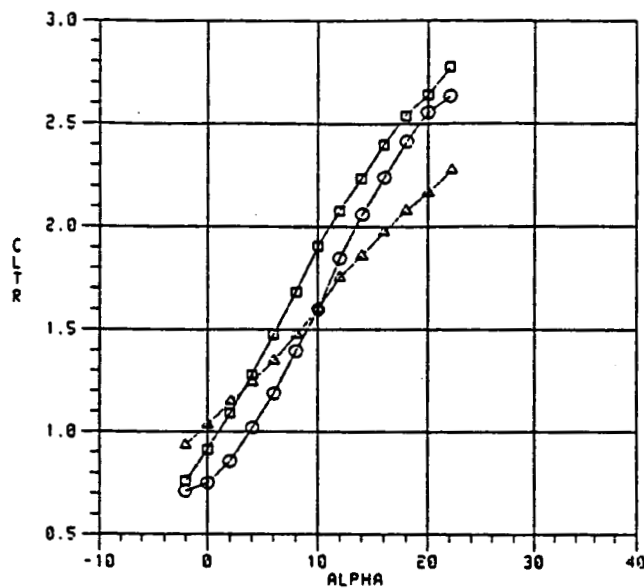
Figure 32   Variation of Longitudinal Aerodynamic Characteristics
             for Trim, C_{μ_W} = .5

57

SYM RUN CMUT
O   232 1.34
△   237 0.95
□   245 1.45
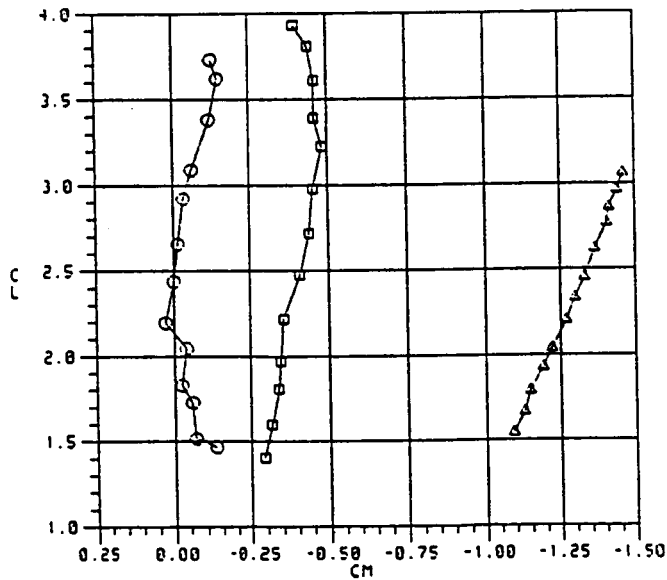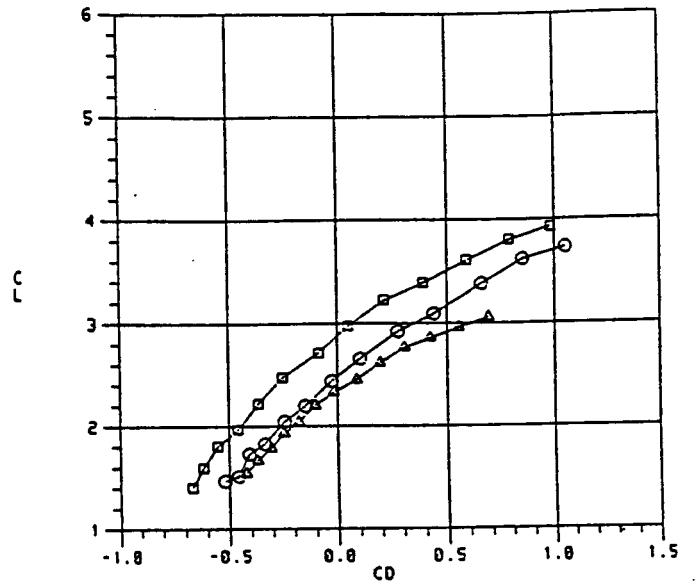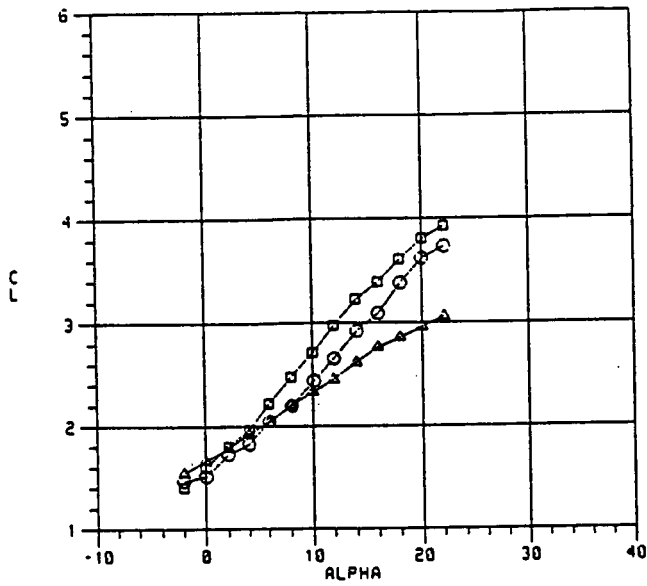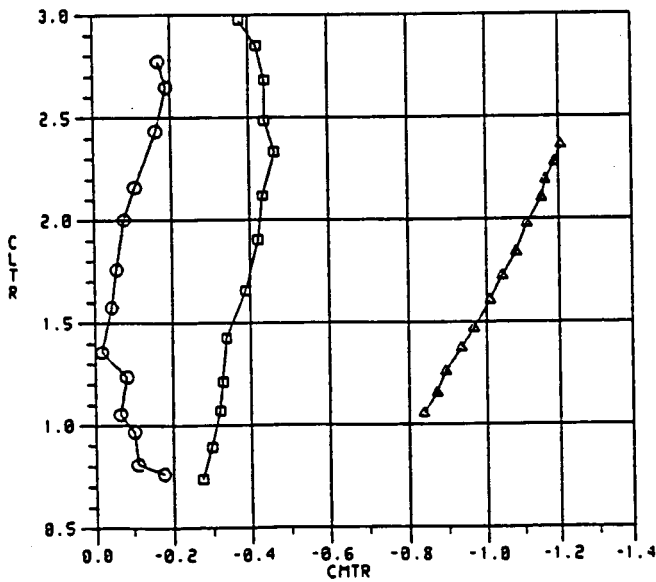
a. Total Aerodynamic Characteristics

Figure 33   Variation of Longitudinal Aerodynamic Characteristics
for Trim, C_{μ_w} = 1.0

58
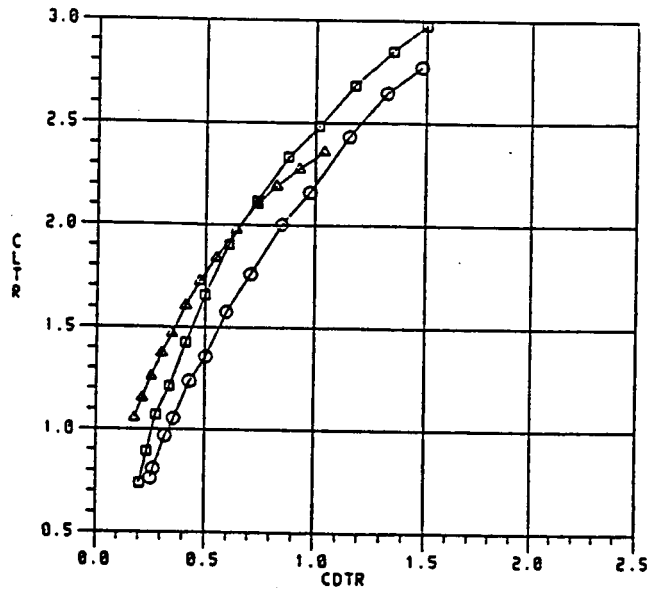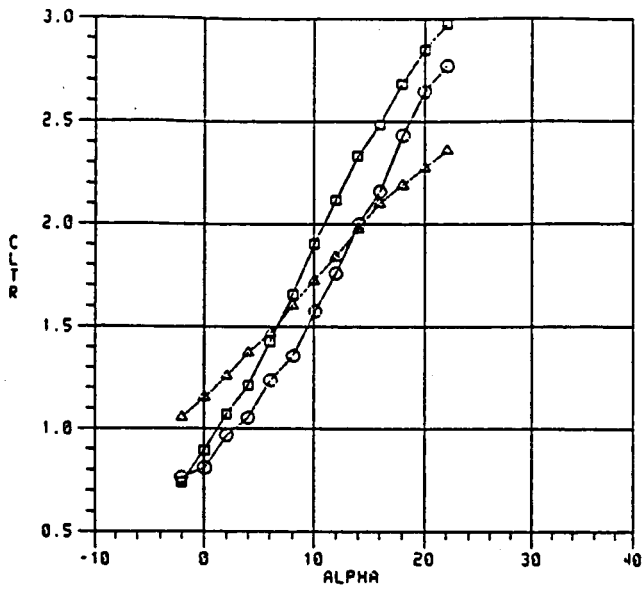
SYM	RUN	CMUT
○	232	1.34
△	237	0.95
□	245	1.45

b. Thrust Removed Aerodynamic Characteristics

Figure 33   Variation of Longitudinal Aerodynamic Characteristics for Trim, C_{μ_W} = 1.0

a. Total Aerodynamic Characteristics

Figure 34 Variation of Longitudinal Aerodynamic Characteristics
for Trim, C_{μ_W} = 2.0

60

b. Thrust Removed Aerodynamic Characteristics

Figure 34   Variation of Longitudinal Aerodynamic Characteristics
for Trim, C_{μ_W} = 2.0

61
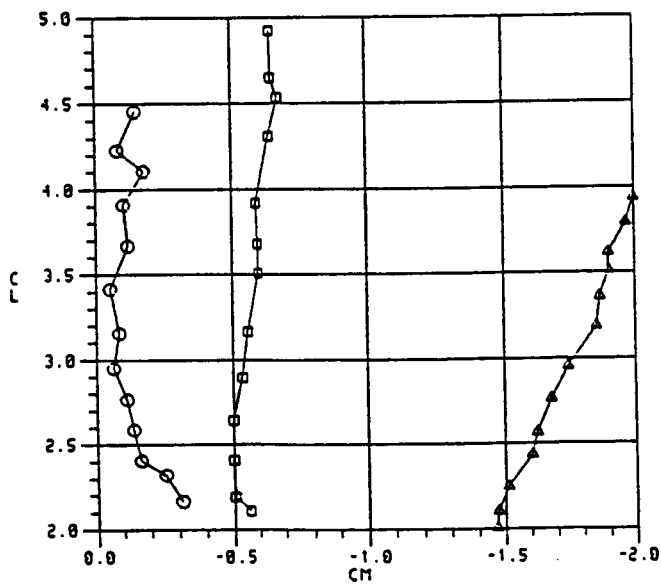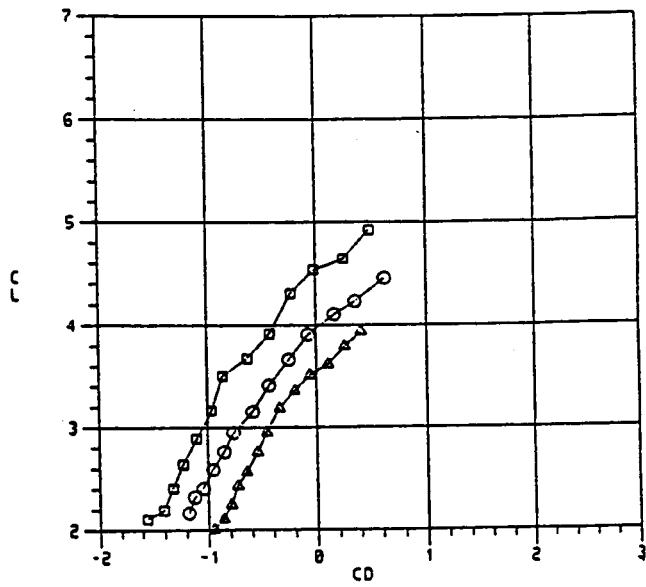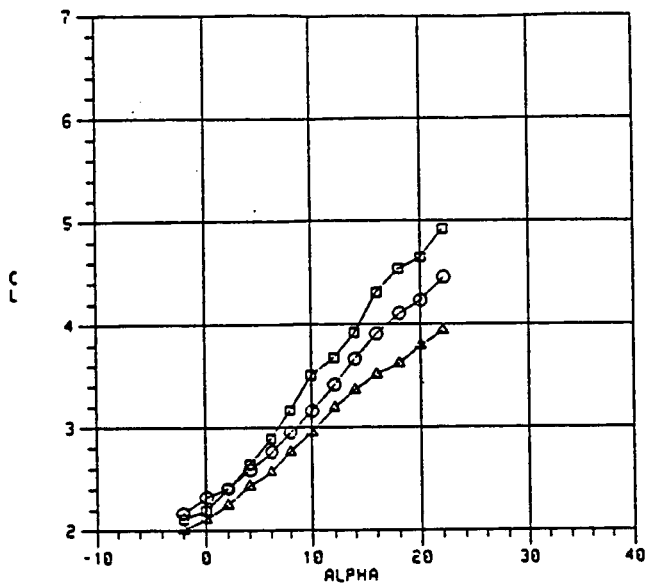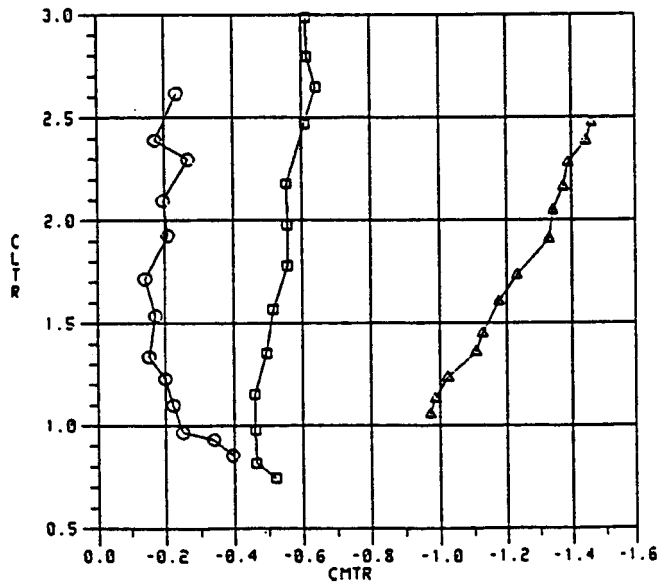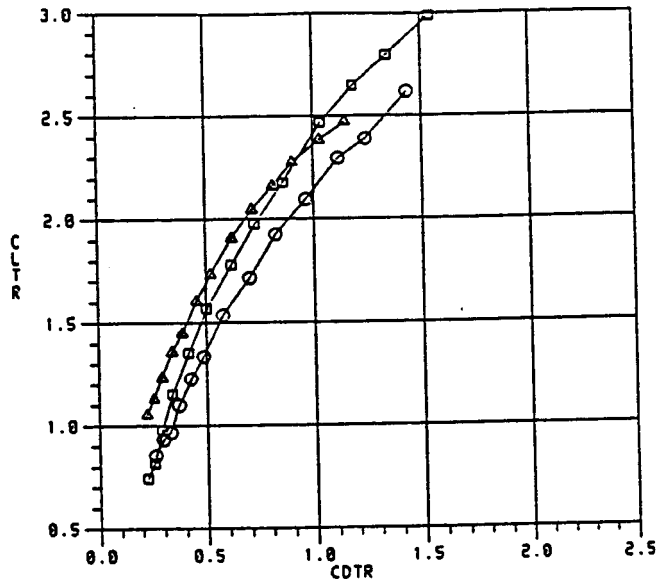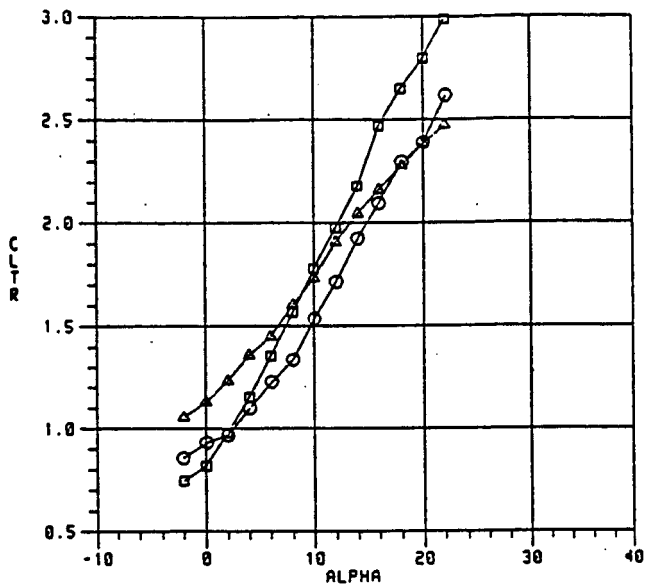
gravity produce this moment, however, the interference of the increased canard flap deflection on the wing produces a sizable loss in lift coefficient compared to the lower canard flap deflection. The data show a positive increment in lift for the 45 degree canard flap and 30 degree wing flap, as opposed to the essentially zero lift increment discussed for the 45 degree wing flap configuration. The different wing circulation accounts for the different induced effects.

3.1.3   Propulsive Configuration Concept

The longitudinal characteristics of the propulsive wing concept suggest that a three-surface airplane configuration with a blown wing, blown canard and horizontal tail may be the most appropriate concept for a STOL fighter. A three-surface concept allows the center of gravity to be moved aft and reduces the canard flap deflection required to trim the vehicle. In addition, the canard of the three-surface configuration will not require as much load input for high speed conditions and, therefore, may be positioned lower relative to the wing. Locating the canard lower will allow the canard jet sheet to pass further below the wing and decrease interference effects. Alternately, if the canard can be raised above its current water plane or can be moved nearer to the wing leading edge it may be possible to extend the flap deflection at which an upper surface blowing effect is realized.

3.2   Lateral/Directional Characteristics

The lateral/directional characteristics of the propulsive wing/canard model were investigated at flap deflections of zero and forty-five degrees. The shaped fuselage model utilized an existing vertical tail which was originally sized for a conventional wing-tail configuration. This resulted in an unstable total configuration because of the aft center of gravity location. While this condition is unsatisfactory for an airplane configuration the test results and conclusions regarding incremental effects resulting from the canard and blowing are valid.

3.2.1   Effect of Blowing

The effects of flap blowing on lateral/directional characteristics can be attributed to several aspects of blowing. A significant increase in lift coefficient is experienced with blowing at any selected angle of attack. While some effect on lateral/directional stability has normally been observed as lift coefficient has been increased through angle of attack increases, the increase of lift coefficient due to blowing tends to result in a translation of lateral/directional characteristics with lift coefficient rather than the expected continuation of the parameter slopes as lift increases. Figure 35 presents the lateral/directional stability parameters at several blowing coefficients and as a function of lift coefficient. These data at zero flap deflection show little effect of blowing on directional stability.

Vertical Tail On

$\delta_F = 0°$

C_μ

○ 0
◇ 1
△ 2

$C_{Y\beta}$

$C_{n\beta}$

$C_{\ell\beta}$

C_L

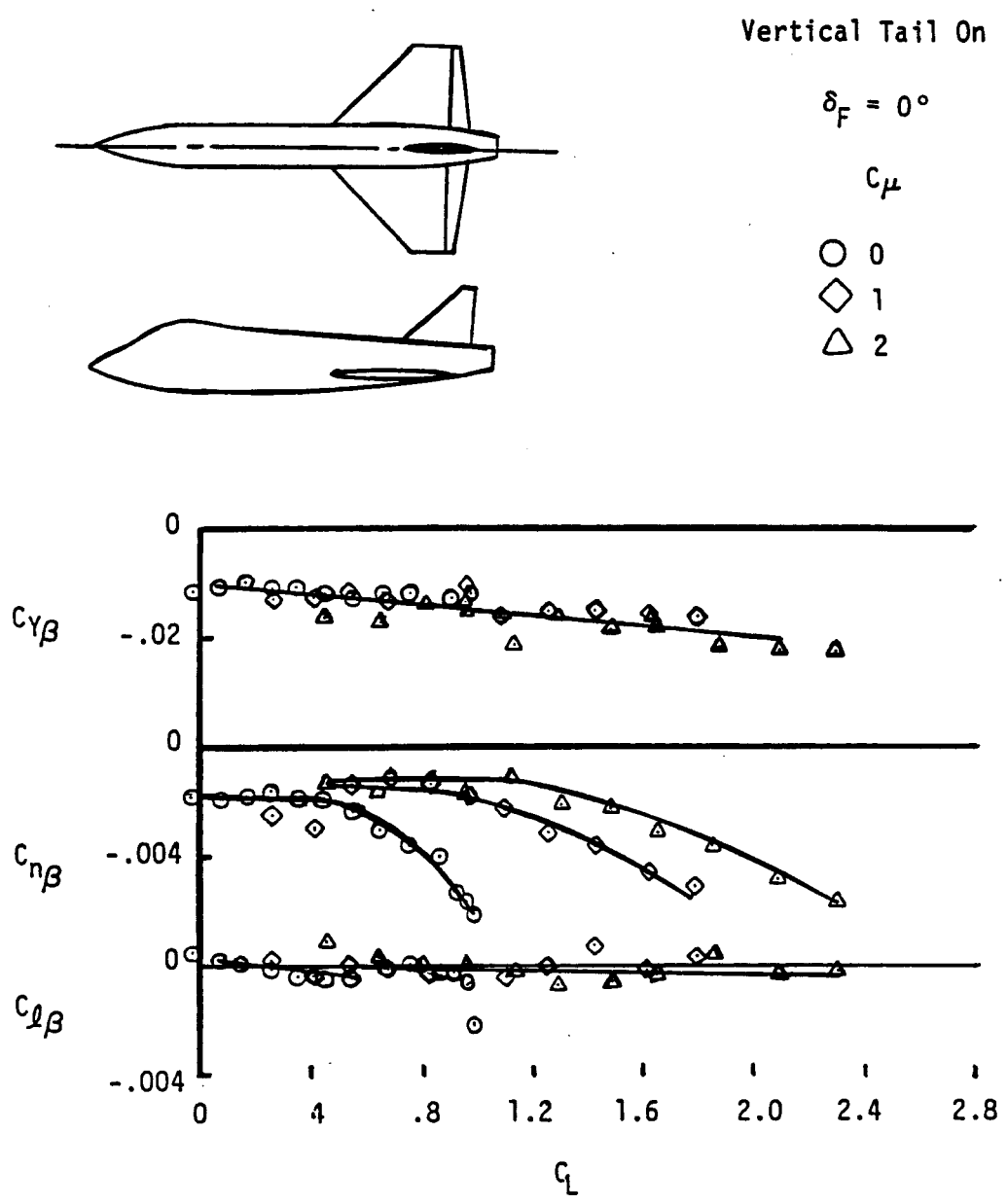Figure 35   Lateral/Directional Aerodynamic Characteristics, B2W6V

63
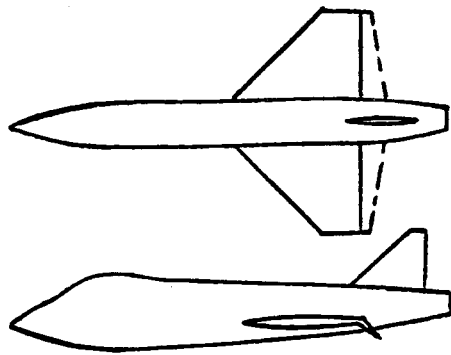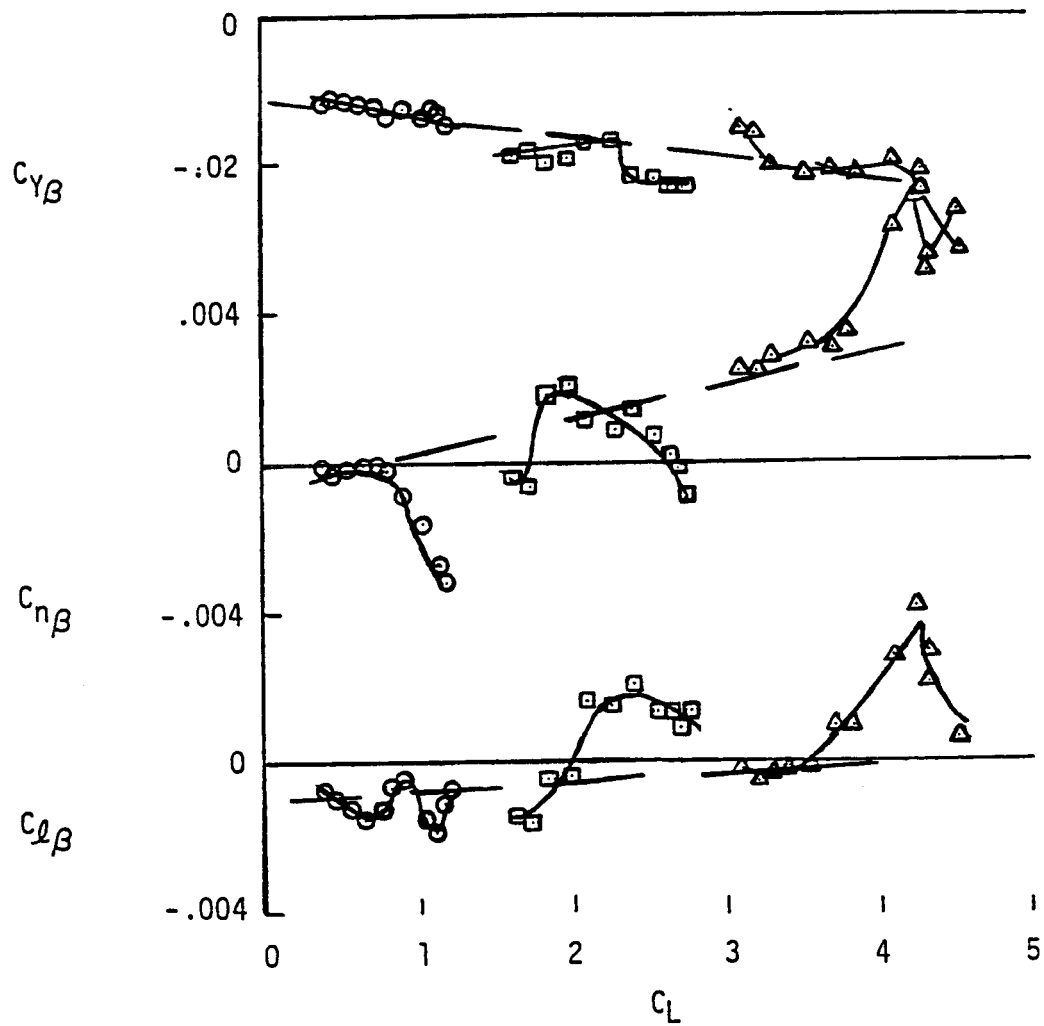
Figure 36. Lateral/Directional Aerodynamic Characteristics, B2W8V

64
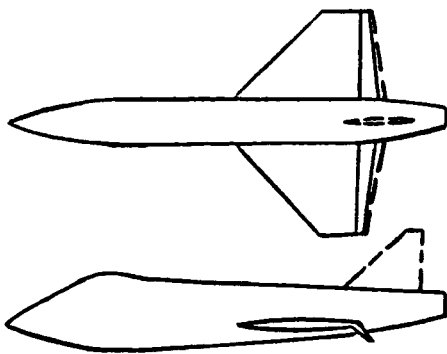
Vertical Tail Off

$\delta_F = 45°$

C_μ

○ 0
☐ .5
△ 2.0
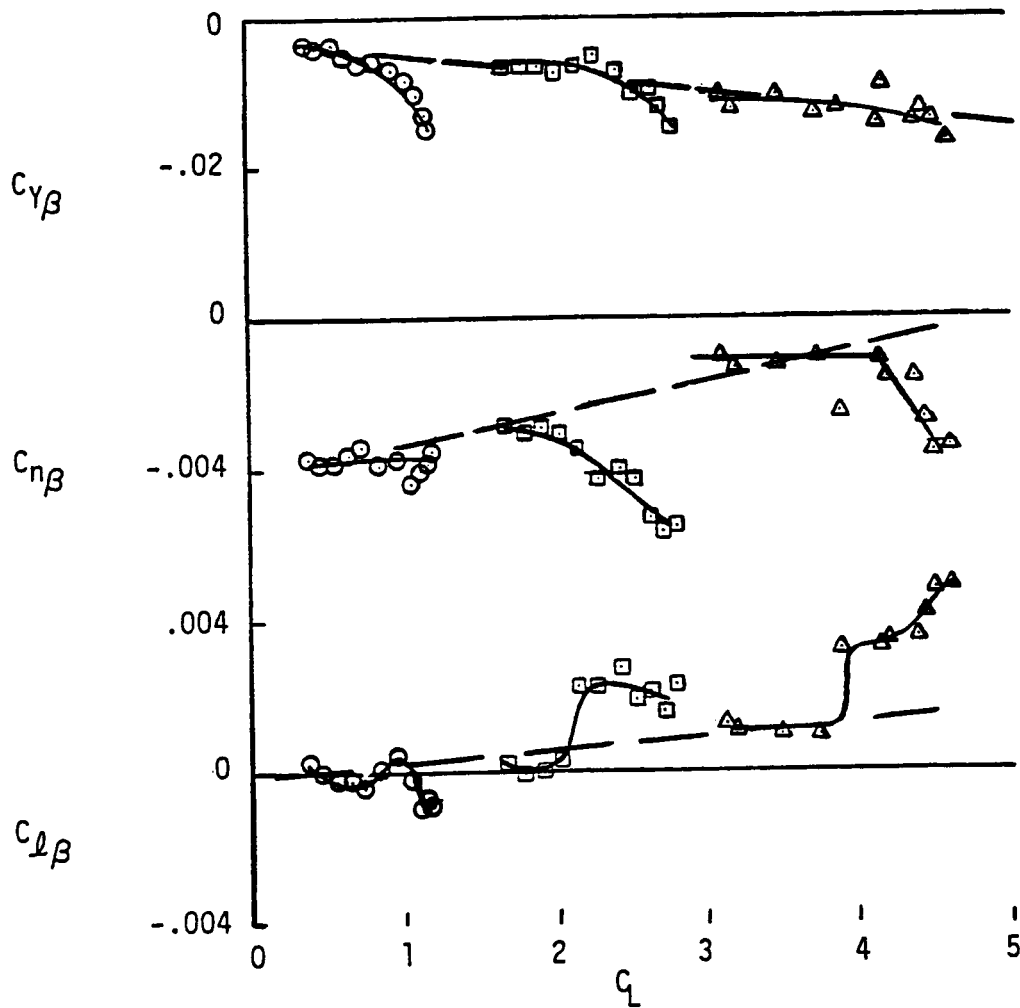
Figure 37. Lateral/Directional Aerodynamic Characteristics, B2W8
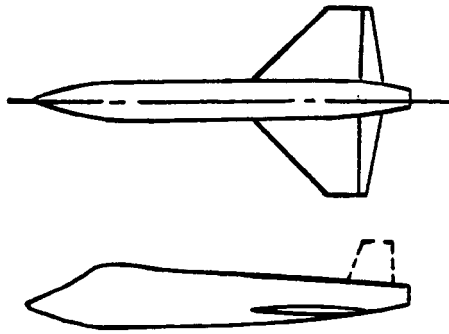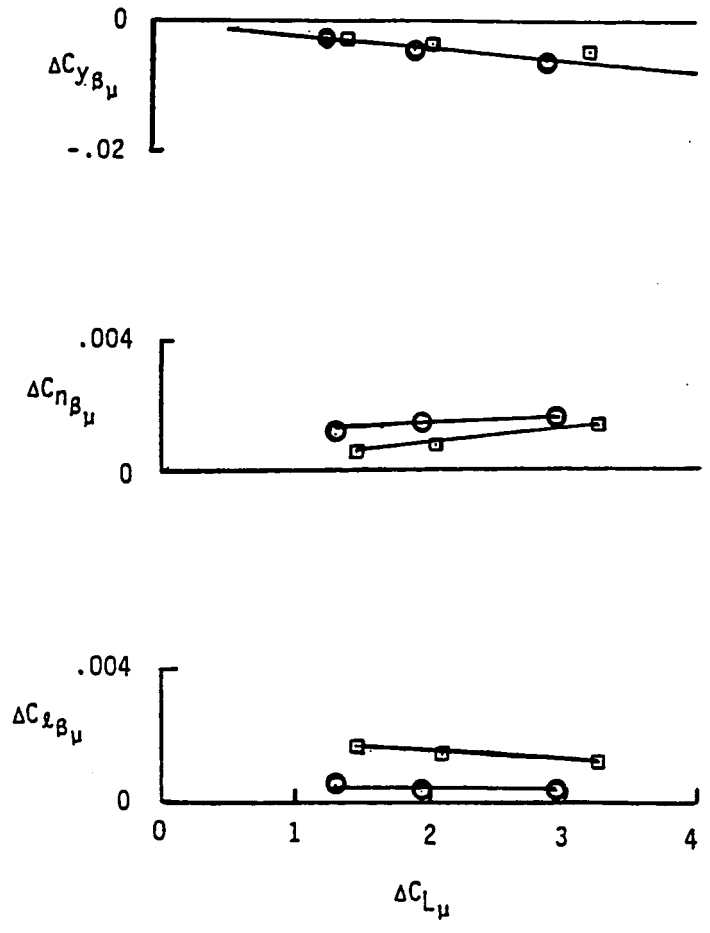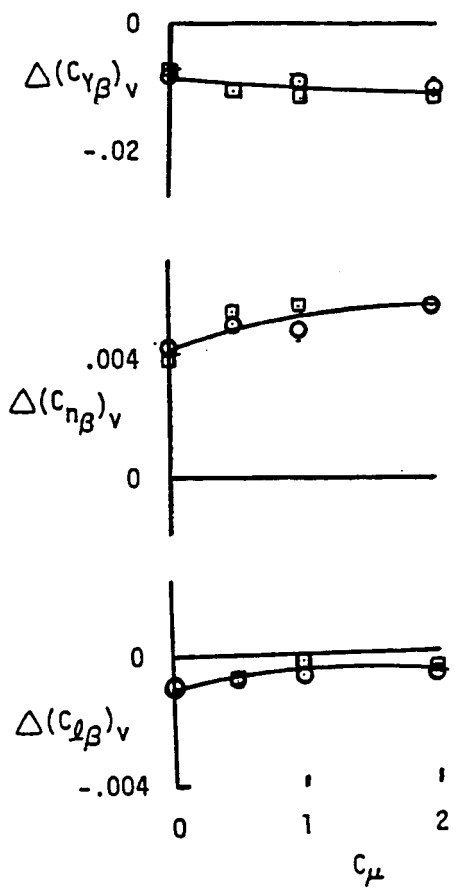
a. Vertical Tail Increments   b. Vertical Tail On and Off

Figure 38   Effect of Blowing on Vertical Tail Contribution

$$\Delta(C_{\ell_\beta})_C = \frac{\ell'_C/b}{57.3} \Delta(C_{L_W})_C$$
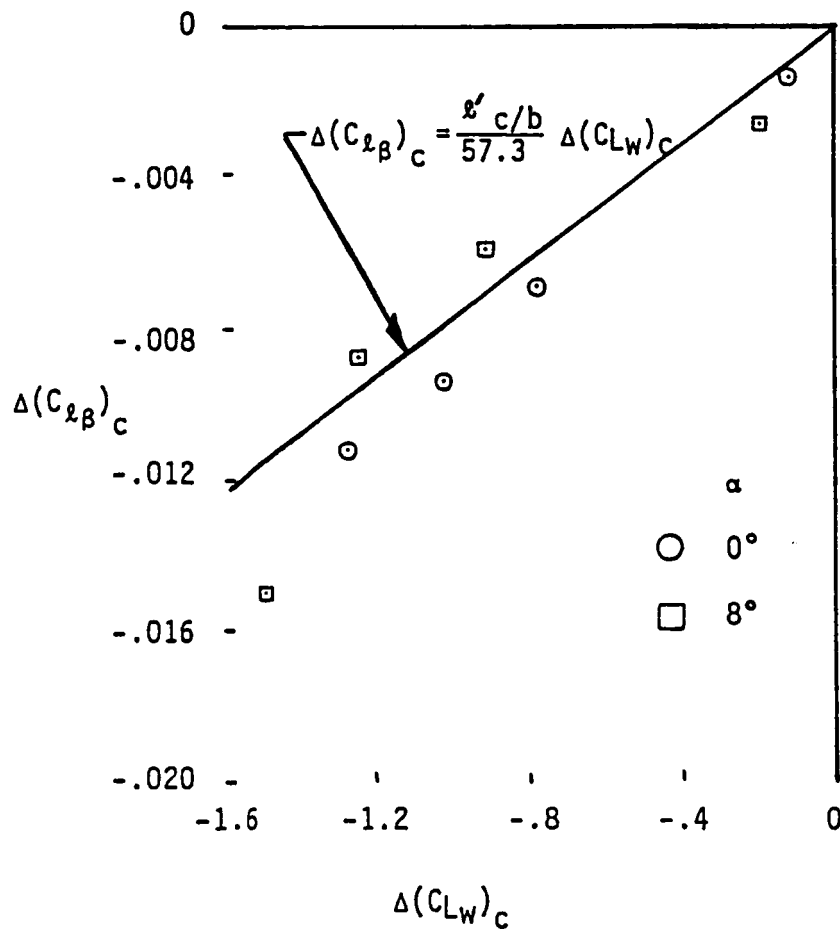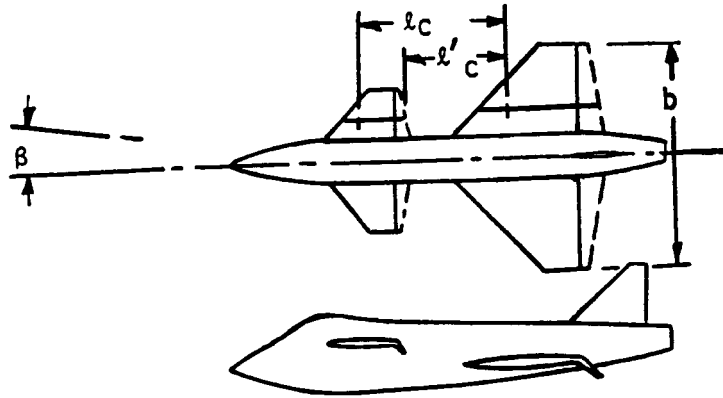
Figure 39   Effect of the Canard Downwash on the Effective
Dihedral Parameter

67
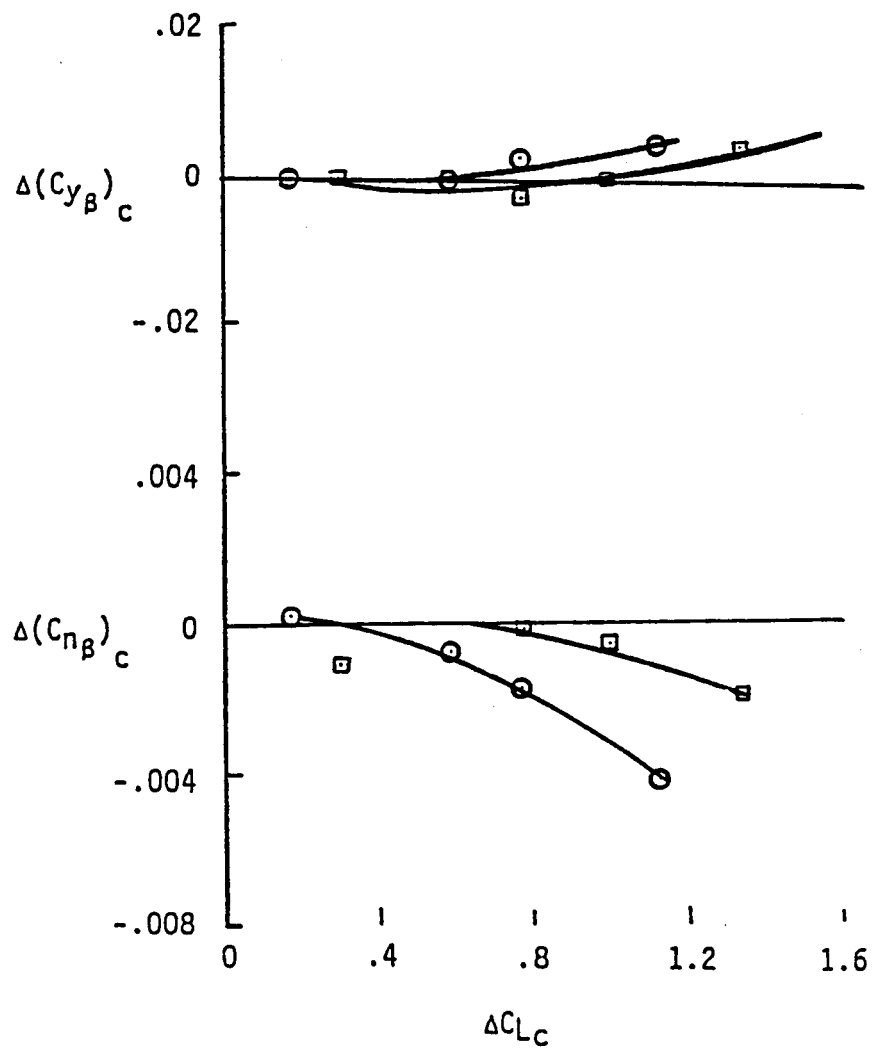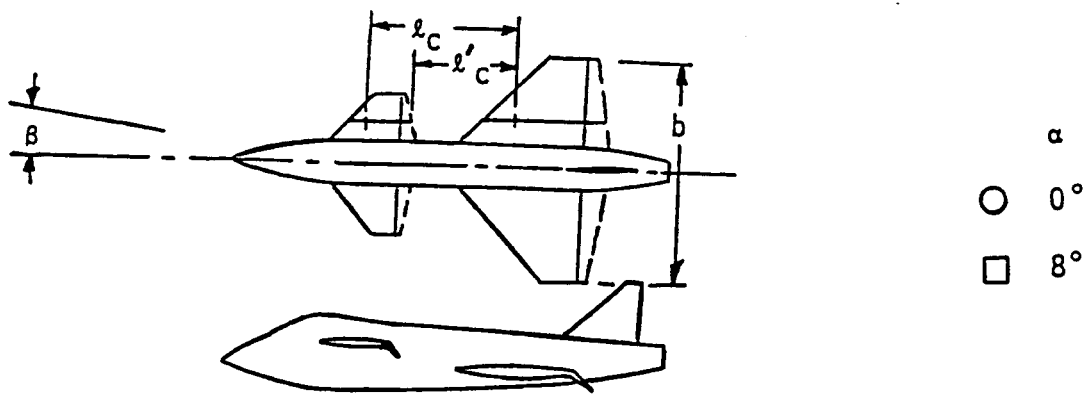
Figure 40   Effect of the Canard on Side Force and Yawing Moment Parameters

Figure 36 presents the same parameters for a flap deflection of 45 degrees. These data indicate an increase in directional stability with blowing. The same trend is seen with the vertical tail removed in Figure 37 indicating that blowing is not affecting the tail effectiveness appreciably. Figure 38 presents the lateral/directional increments of the vertical tail. A small increase in side force and yawing moment coefficients due to blowing is shown. This small increase most likely results from a velocity increase due to entrainment into the jets.

The addition of a canard to the wing-body does not materially change the side force or yawing moment coefficients, but does show a sizable increase in the dihedral parameter (C_{ℓ_β}). This increment can

be attributed to the downwash of the canard on the wing. As seen in Figure 39, the increment is related to the wing lift loss and the canard distance ahead of the center of wing lift. Figure 40 presents the effect of the canard on the side force and yawing moment parameters. As stated, these increments are insignificant.

3.3 Ground Effects

Ground effects on the longitudinal characteristics of the propulsive model were investigated with and without the canard. This data is the first set of low aspect ratio jet flap ground effect data generally available. Most available propulsive wing data was obtained for considerably higher wing aspect ratio configurations.

Previous analysis and testing of powered configurations was accomplished to establish a need for removal of the ground boundary layer by incorporating a moving belt. These data have generally shown that if the circulation lift coefficient is less than about two:

$$C_{L_\Gamma} = 2.0$$

a positive lift will be induced by the ground, see Stewart and Kuhn, Reference 7. In addition, Turner, Reference 8 has shown that if the lift coefficient is:

$$C_L = 20 \cdot h/b$$

a moving ground board is necessary. Stewart and Kuhn in Reference 7 also showed that a ground vortex may be encountered outside the boundaries established by Turner. The effect of this ground vortex on the lift coefficient was not adequately determined in Reference 7 because of model and test limitations. The ground vortex was established for jet flap testing at lift coefficients of:

$$C_L = 7 \cdot h/b$$

Tests of the propulsive wing-body at these lift coefficients and ground proximity have provided an additional insight into ground effects. The lift coefficient data presented in Figure 41 show that at the higher levels of blowing a large negative lift coefficient increment is realized as the ground is approached. The data shown in Figure 41 are with the ground fixed, but with the boundary layer removal operating. Figure 42 presents the thrust removed lift coefficient for the ground effect data. The thrust removed lift coefficient data show that the thrust removed, or circulation lift coefficient, never exceeds two. The previous studies would indicate that a small positive ground effects increment would be expected rather than the large negative lift increment shown in Figure 41. There are no data to indicate that the increment would be different if the boundary layer were removed by moving the ground belt. The lift loss experienced with this propulsive wing test appears to correlate well with the vortex occurrence lift coefficient discussed by Stewart and Kuhn in Reference 7. Figure 43 presents a comparison of the vortex formation lift coefficient from Reference 7 with the lift-loss lift coefficient of the propulsive wing and to the moving ground board requirement observed by Turner in the earlier tests. The vortex and lift loss occur at the same lift coefficients while the Turner data indicate a much higher lift coefficient prior to ground-induced lift loss. This is believed to be a result of aspect ratio differences of the two sets of data.

The effect of ground proximity on the pitching moment coefficient for the propulsive wing is presented in Figure 44. The data show a large reduction in the negative pitching moment coefficient at high blowing coefficients as the ground is approached. This characteristic indicates that the reduction of lift coefficient results from a lift loss on the wing or aft fuselage. The center of pressure of the lift loss is seen to be at approximately 65 percent of the mean aerodynamic chord (MAC).

The complete configuration, body-canard-wing-vertical tail, produced entirely different incremental ground effects. Figures 45 and 46 present the lift and pitching moment coefficients, respectively, of the body-canard-wing-vertical tail configuration. The complete configuration shows a lift increase and an incremental nose down pitching moment at the low ground heights and high blowing coefficients. This characteristic could result from a reduction in canard downwash and an associated increase in wing lift as the ground is approached.

The propulsive wing with half-span jet nozzles was tested with both moving and stationary ground boards. Figure 47 presents the lift coefficient for the half-span blowing jet with the moving and stationary belts. The data do not indicate an effect of the moving belt on the lift of the blown wing in proximity of the ground. The thrust removed lift coefficient for these half-span nozzle data points show very low levels of circulation lift coefficient, see Figure 48. The maximum circulation lift coefficient in free air was:

$$C_L = 1.1$$
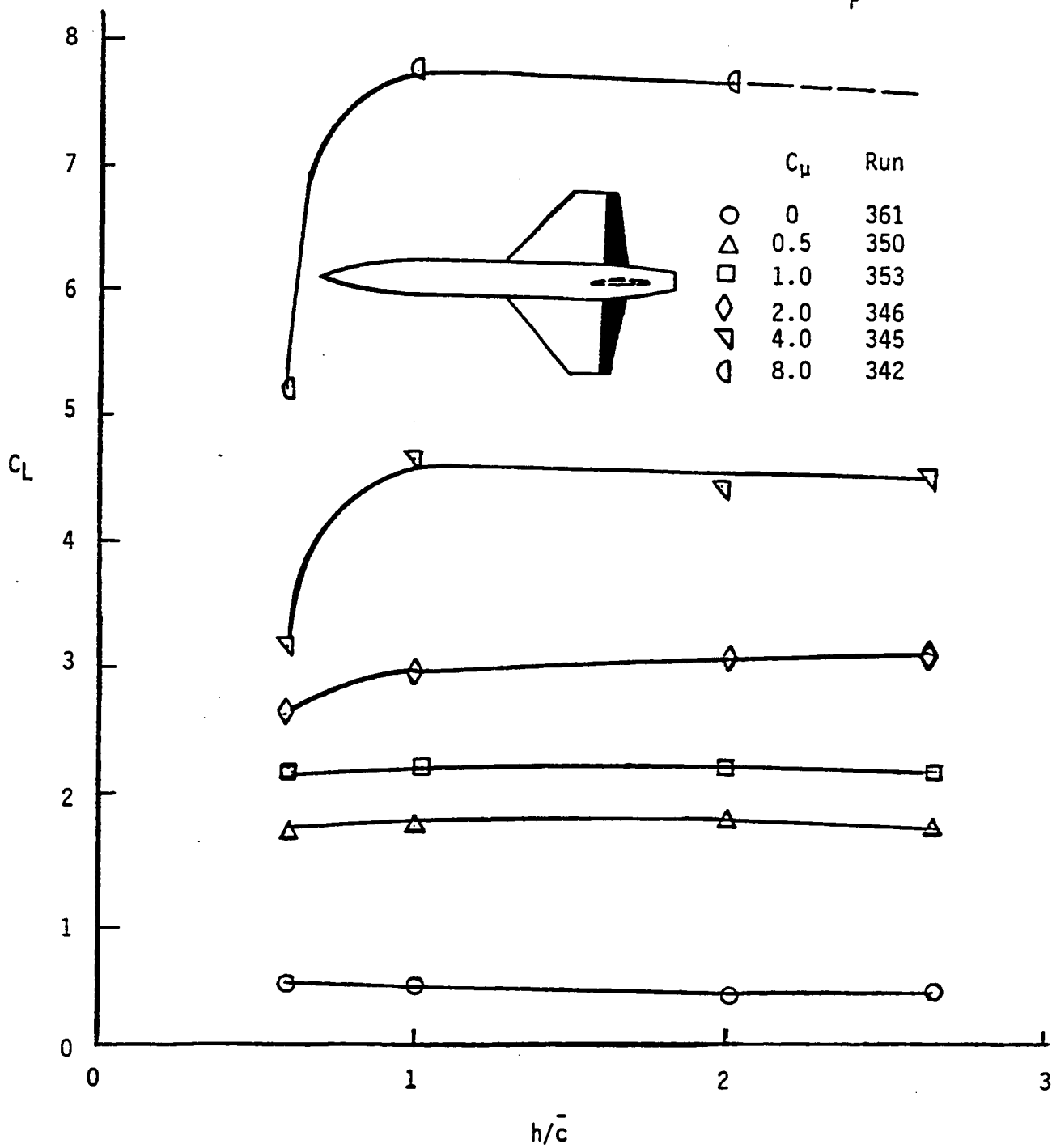
Figure 41   Effect of Ground Proximity on Lift Coefficient, B2W8V
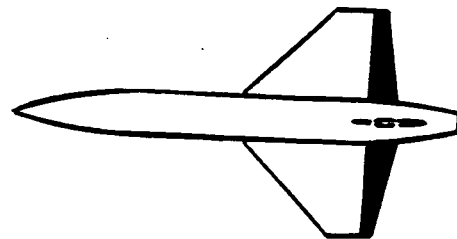
	C_μ	Run
○	0	361
△	0.5	354
□	1.0	353
◇	2.0	346
▽	4.0	345
◖	8.0	342

$\delta_F = 45°$
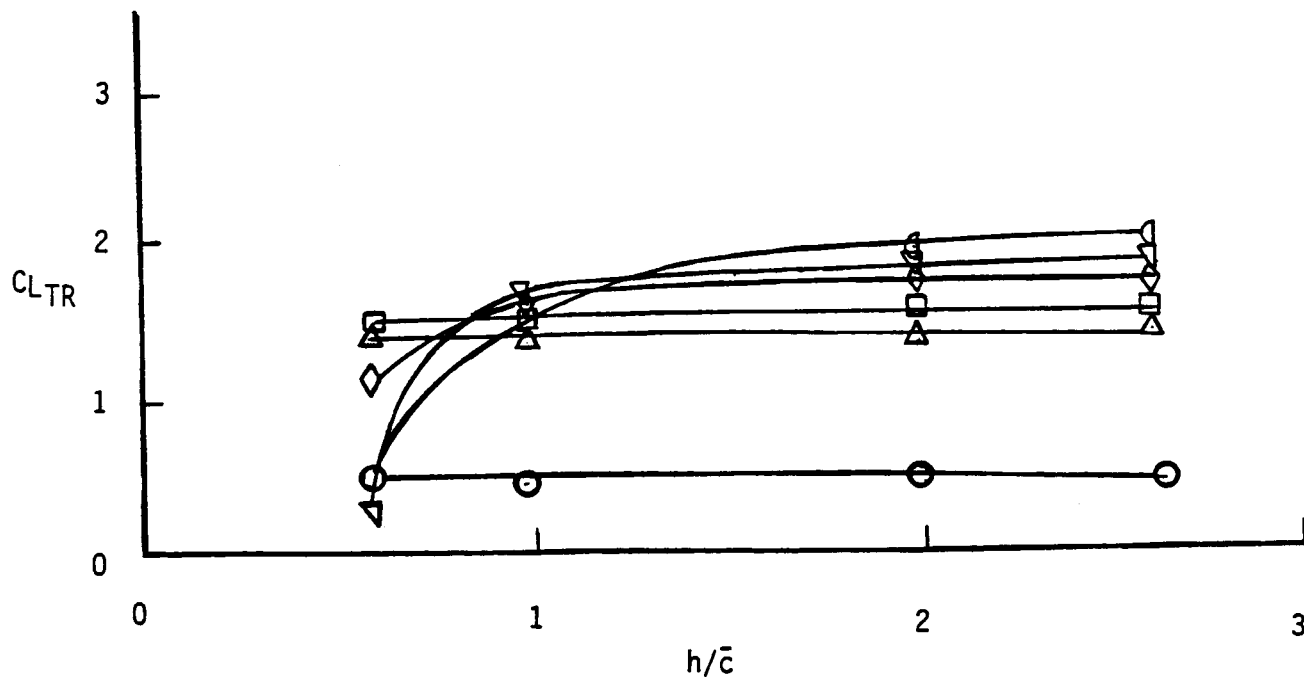
Figure 42   Effect of Ground Proximity on Thrust Removed Lift
Coefficient, B2W8V

● JET FLAP (VORTEX)

□ PROPULSIVE WING MODEL
(LIFT LOSS)

VORTEX FORMED
LOW ASPECT RATIO

MOVING BELT REQUIRED
(TURNER HIGH ASPECT RATIO)

h/b

$C_L = C_{L_\Gamma} + C_\mu \sin \theta$
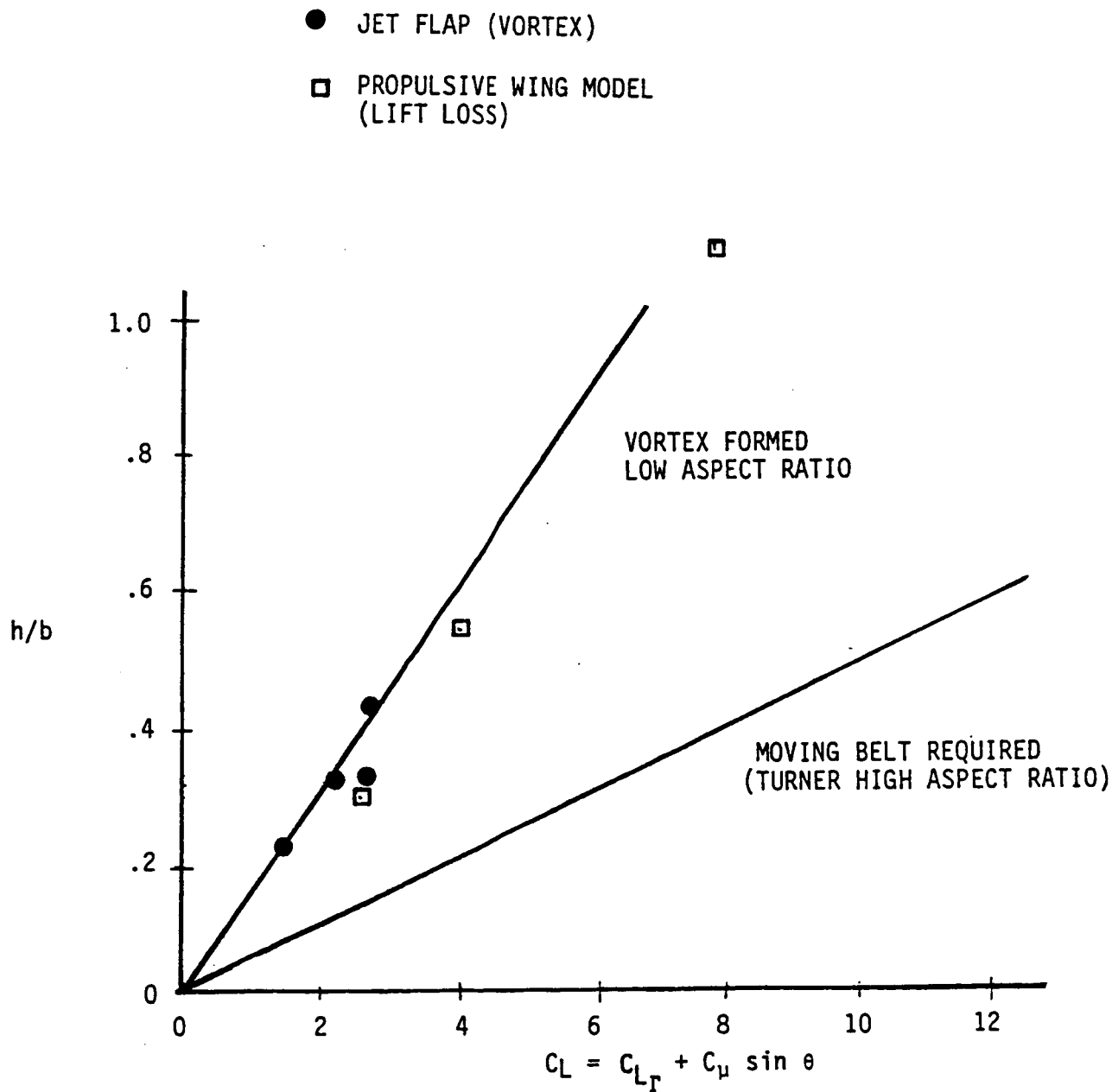
Figure 43   Requirement for Moving Ground Belt

	C_μ	Run
○	0	361
△	0.5	350
☐	1.0	353
◇	2.0	346
▽	4.0	345
◖	8.0	342
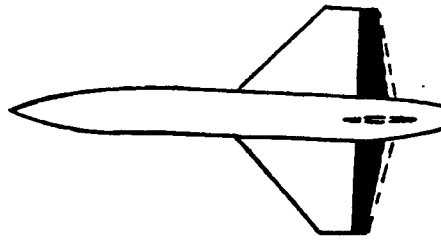
$\delta_F = 45°$

Figure 44   Effect of Ground Proximity on Pitching Moment Coefficient, B2W8V

74

Figure 45   Effect of Ground Proximity on Lift Coefficient, B2C9W8V

Figure 46   Effect of Ground Proximity on Pitching Moment Coefficient, B2C9W8V

Figure 47. Effect of Belt Velocity on Lift Coefficient
Half Span Nozzle, B2W8V

Figure 48. Circulation Lift Coefficient with Half-Span Nozzle,
Free Air
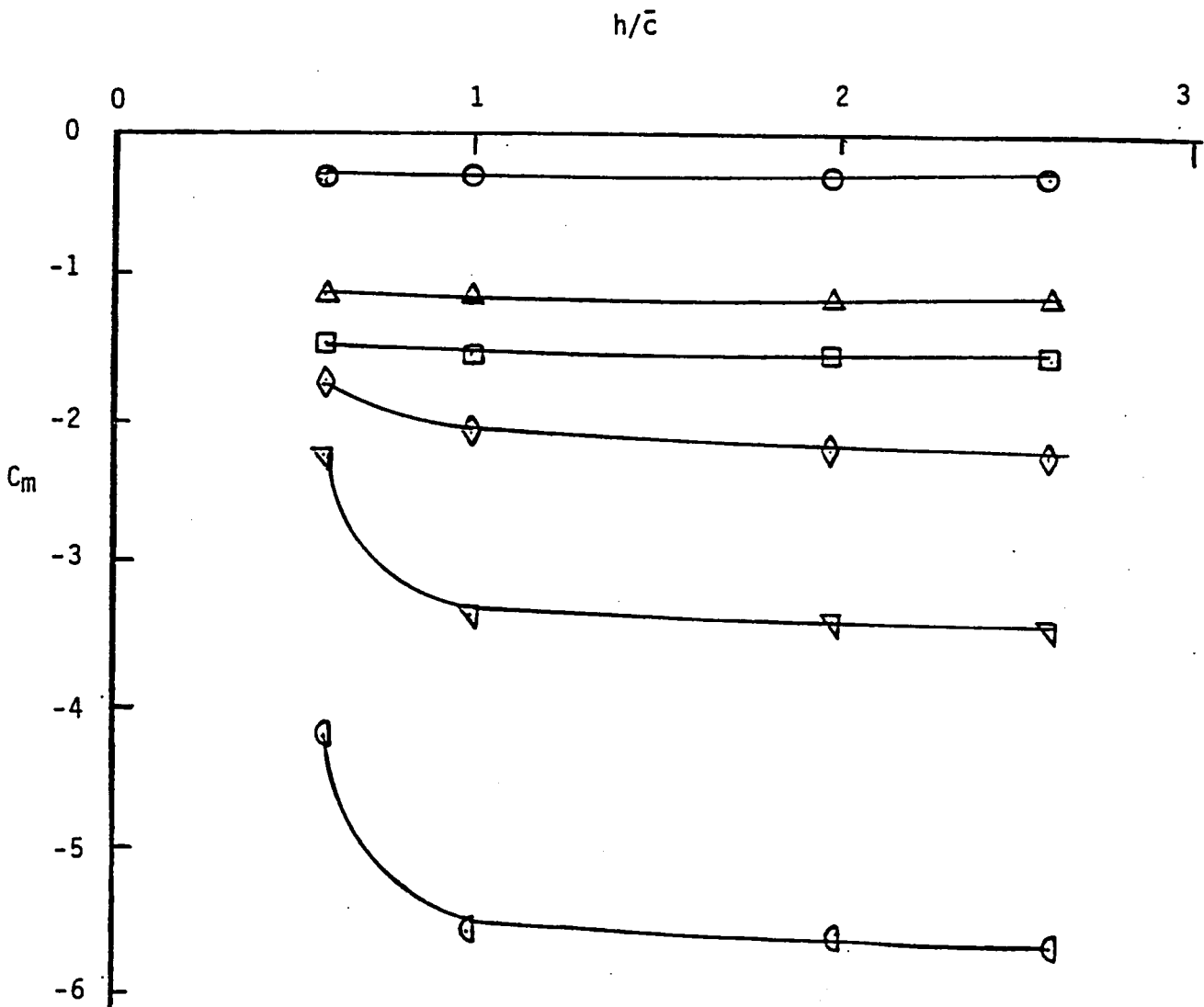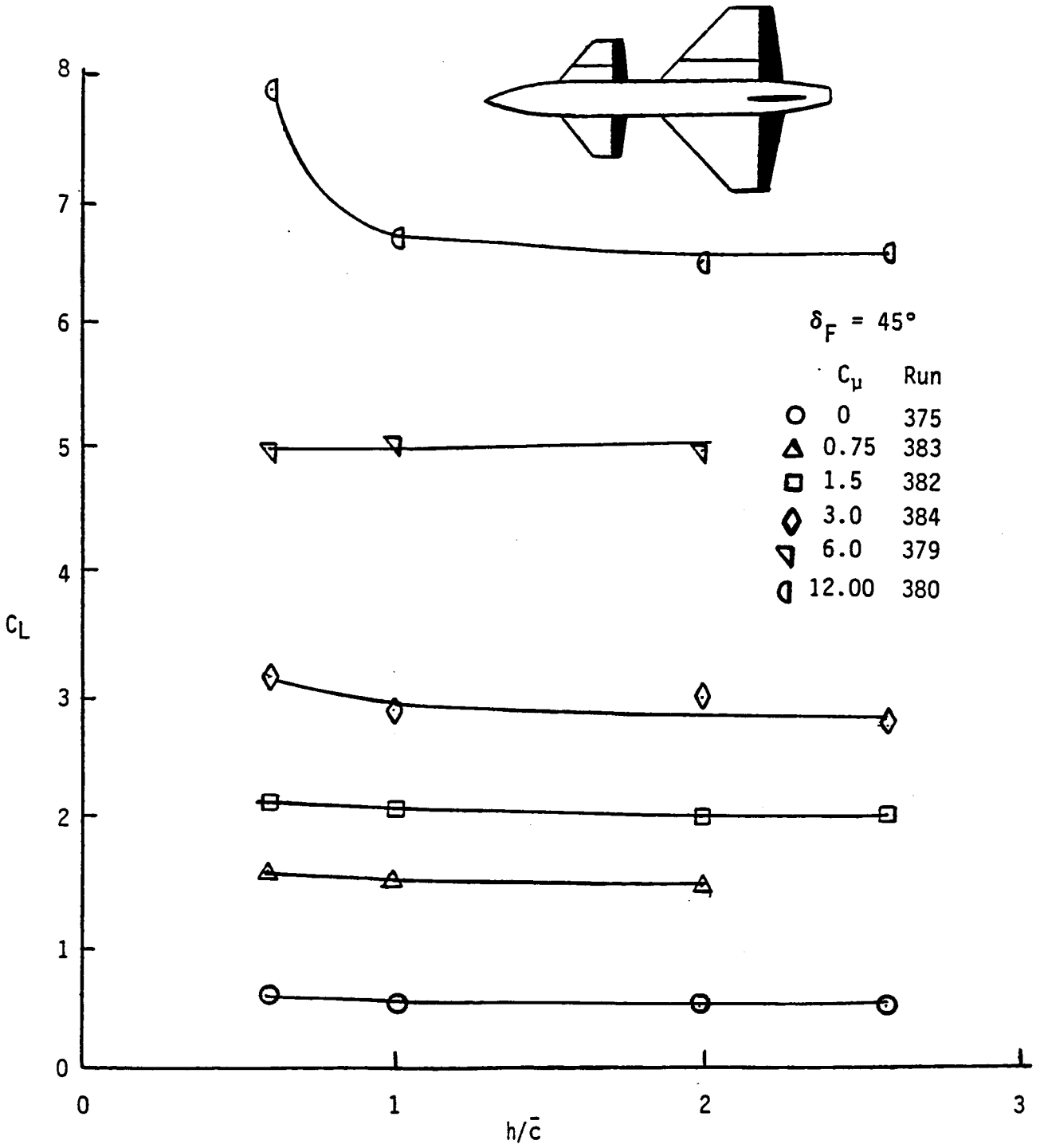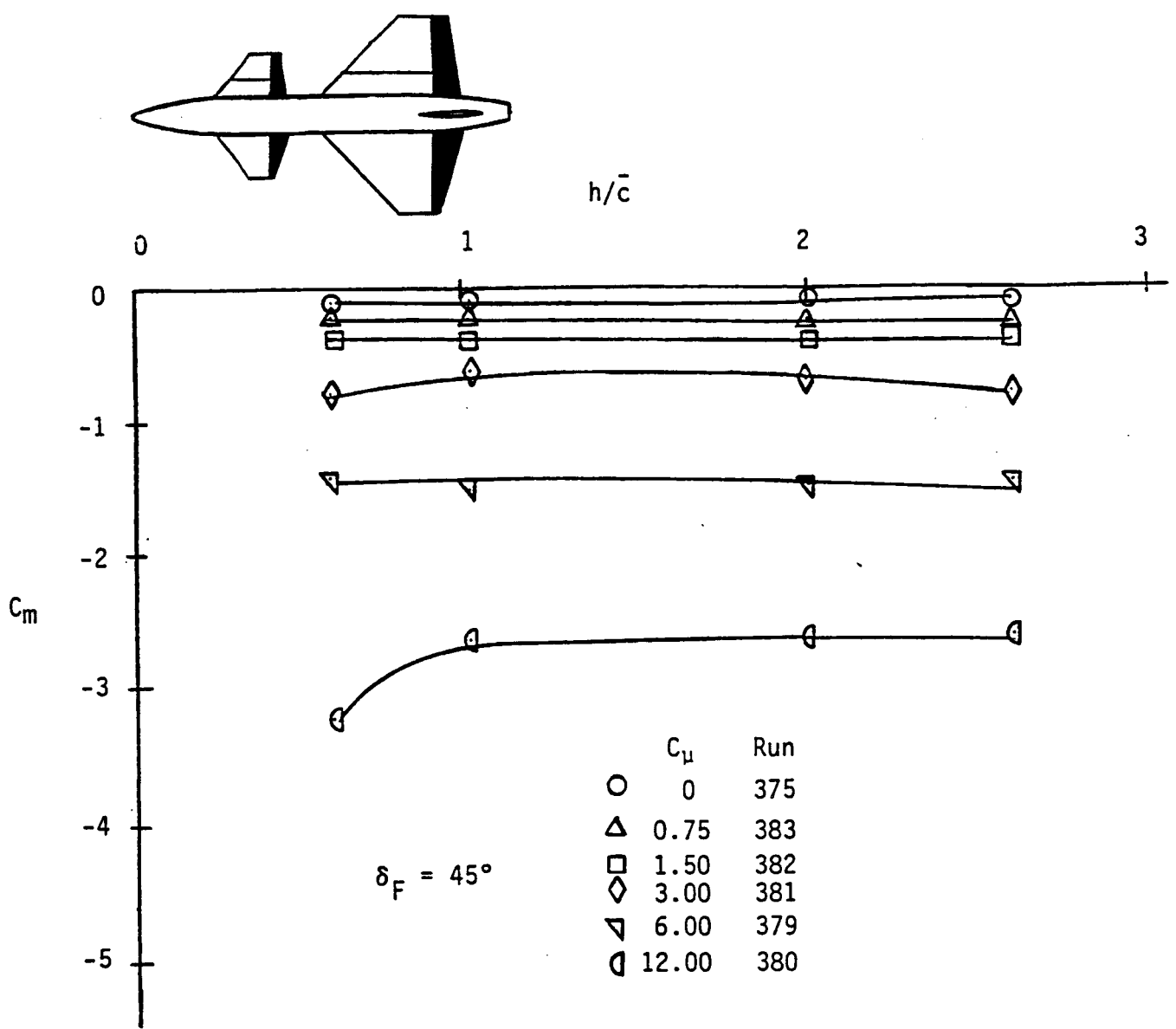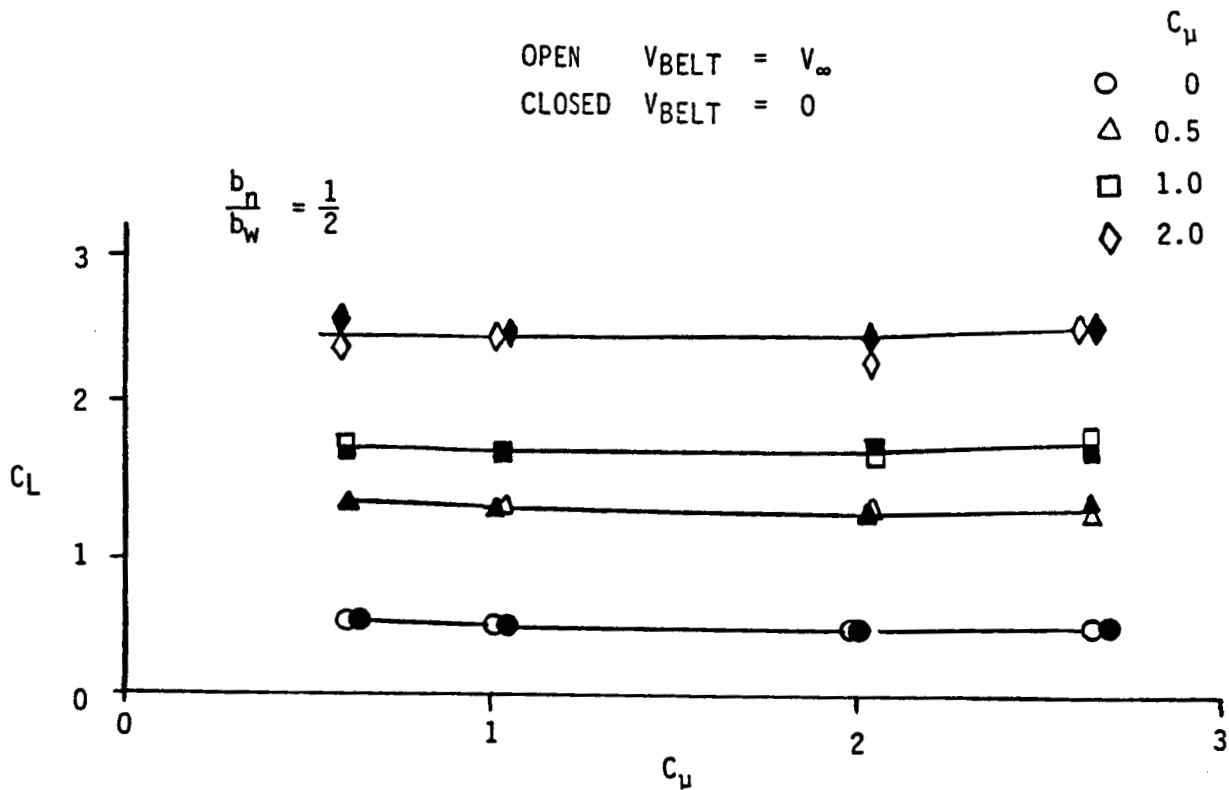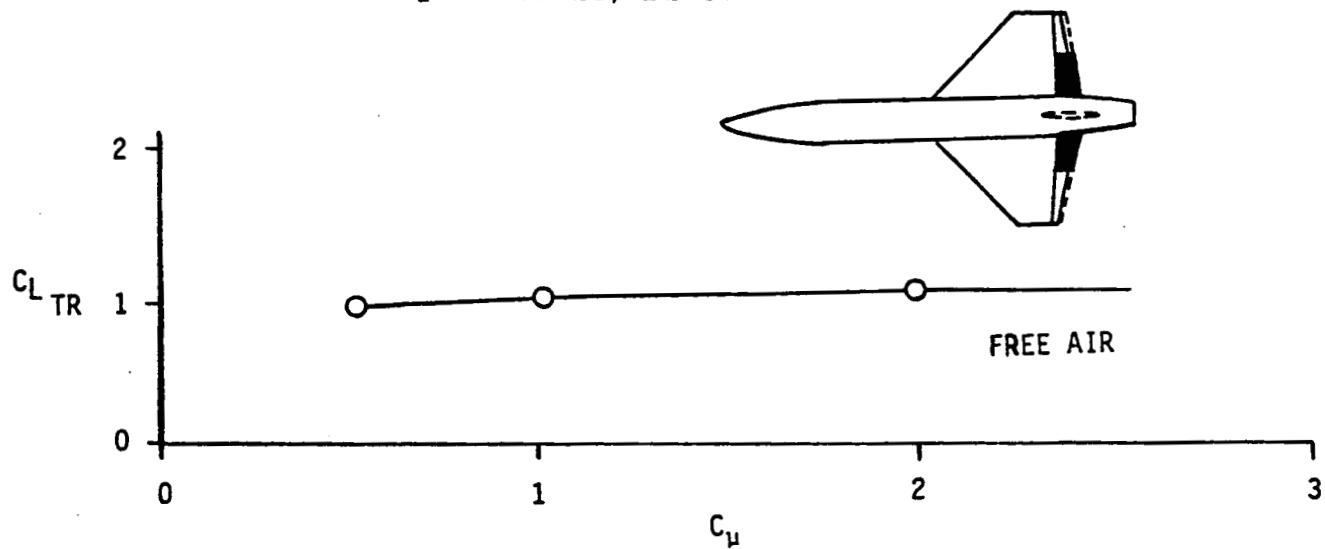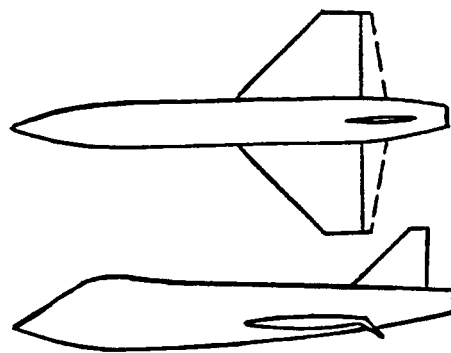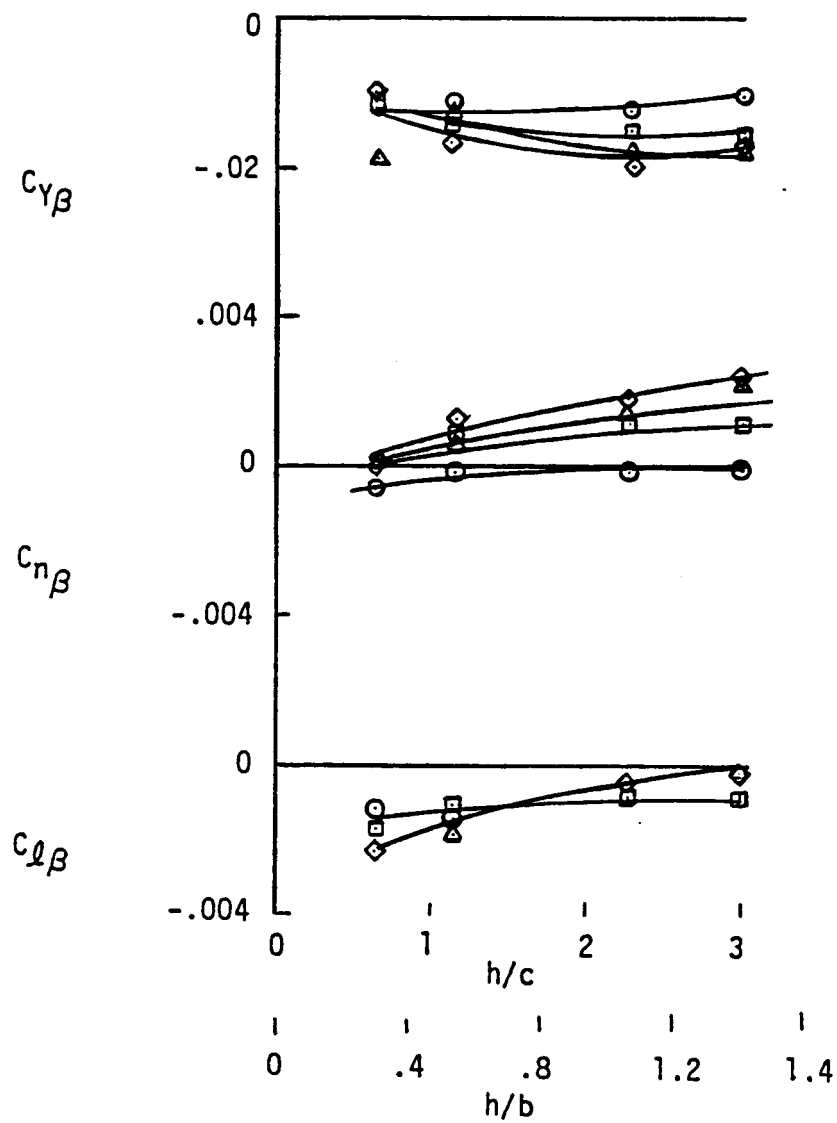
77

Figure 49. Effect of Ground Proximity on the Lateral/Directional Parameters

Previous investigations indicate that this lift coefficient is too low to have incurred a negative ground effect lift increment.

Figure 49 presents the effect of ground proximity on the lateral/directional characteristics of the wing-body configuration. These data show that the ground has a small destabilizing effect at the higher blowing coefficients, but that the blowing-on parameters in ground effect are still slightly more stable than the unblown wing-body configuration.

The lateral/directional stability of the total configuration (wing-canard-body) was not tested at yawed conditions. The only significant difference expected would be a decrease in the canard effect on the dihedral parameter shown in Figure 40 and discussed in paragraph 3.2.1. As the wing-canard-body configuration approaches the ground the canard downwash will be significantly reduced and, therefore, the change to C_{ℓ_β} due to the canard can be expected to be reduced accordingly.

3.4   Flow Field Characteristics

The flow field of the propulsive wing model was investigated behind both the wing and the canard. The measurements behind the wing were made with the rake mounted vertically as shown in Figure 10. These data were taken concurrent with the wing pressure coefficient data except for the ground effect studies when the rake was removed to prevent accidental contact with the moving belt. The rake data consists of the local velocity and flow angles at the probe locations. When mounted in the fixed vertical position behind the propulsive wing a slice of the downwash characteristics was measured.

The location of the jet path is a major consideration in determining the optimum placement of lifting surfaces for any configuration. Figure 50 shows the relative placement of the downwash rake and the calculated wing jet path for several flap deflections. The jet path is computed by (see Reference 9):

$$\frac{x}{t_o} = \frac{0.25\, C_x}{\sin \alpha_o}\left(\frac{q_\infty}{q_j}\right)\left(\frac{z}{t_o}\right)^2 + \left(\frac{z}{t_o}\right) \cot \alpha_o$$

where

$$C_x = 1 + 0.5\left(\frac{V_j}{V_\infty}\right)$$

α_o = jet deflection angle

t_o = nozzle gap

Figure 51 shows the probe velocity for the flap deflections tested. The
data are referenced to the calculated jet sheet location shown in Figure
50. These results indicate that the calculation method from Reference 9
is quite accurate for locating the jet path. The jet center appears to be
within one inch of the predicted location at a point twenty-one inches
downstream of the nozzle. The flap chord aft of the nozzle may account for
this discrepancy. It may be possible to account for the effect of the flap
chord by a modification to the jet sheet equation if a more precise jet
location is required.

The flow field behind the canard was surveyed for several combinations of
flap deflection and blowing coefficient, and at several longitudinal
positions behind the canard. These surveys were made with the wing
removed. The canard flow field survey information and the complete downwash
probe data are presented in Appendix C of Volume II. Figure 52 presents the
flow field vectors at one location downstream of the canard with the canard
flap deflected 45 degrees. Figure 53 shows the locations of the canard
surveys relative to the canard and the wing even though the surveys were
made with the wing off. The effect of wing circulation on the canard wake
is not known. At these very slow speeds the wing circulation will likely
have some effect on the canard wake. The flow survey shown in Figure 52 is
located in front of the wing leading edge. Superimposing the wing location
on Figure 52 shows that the canard tip vortex with the jet blowing is
displaced well below the canard plane and well inboard of the canard tip.
The canard vortex is centered on the wing plane directly ahead of the wing
leading edge for this flap deflection and blowing combination. The canard
jet flow is displaced inboard and under the wing leading edge resulting in
the relative large negative interference discussed in Section 3.2. The view
depicted in the figure presents the velocity vector projection into a YZ
plane at a longitudinal location just ahead of the wing. The large vectors
located from $0 > Z > -18$ show the canard jet velocities and the downwash
angles associated with the jet. The very small vectors located well away
from the canard and the canard jet depict flows which are nearly parallel to
the free stream. Section 3.2 contains a discussion of the same flow
conditions and Figure 24 shows the jet velocities and downwash angles
projected in the XZ plane. Note that the vectors located well away from the
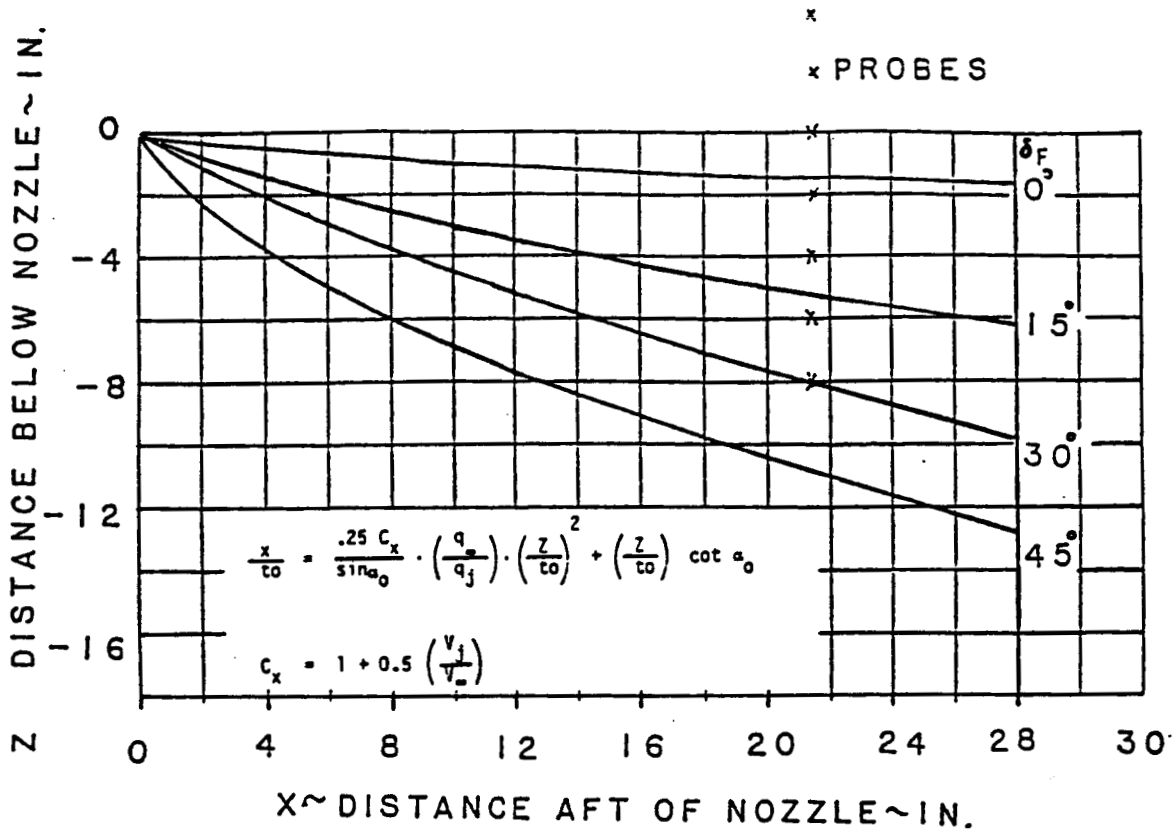jet tend to represent free stream conditions.

x PROBES

Figure 50. Wing Jet Sheet Path, $C_\mu = 1.0$

$$\frac{x}{to} = \frac{.25\ C_x}{\sin a_o} \cdot \left(\frac{q_\infty}{q_j}\right) \cdot \left(\frac{z}{to}\right)^2 + \left(\frac{z}{to}\right)\cot a_o$$

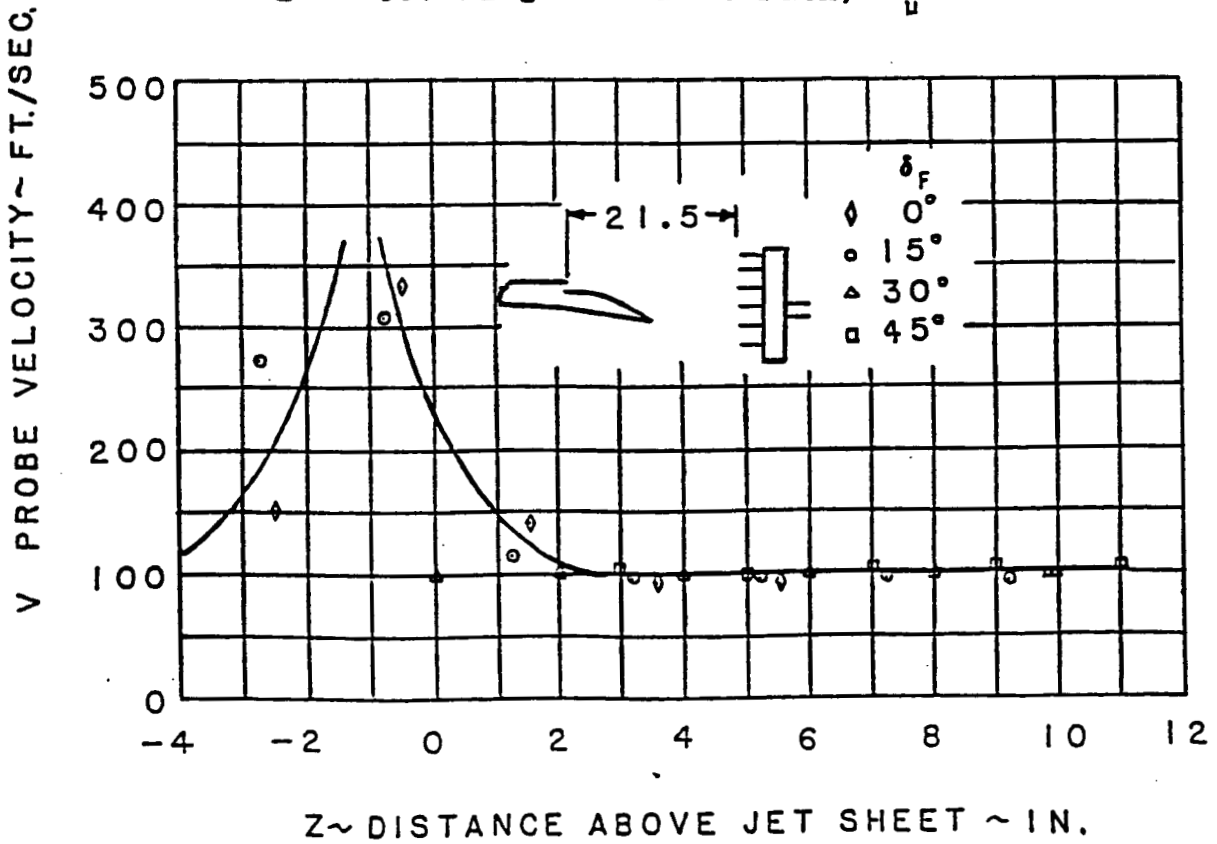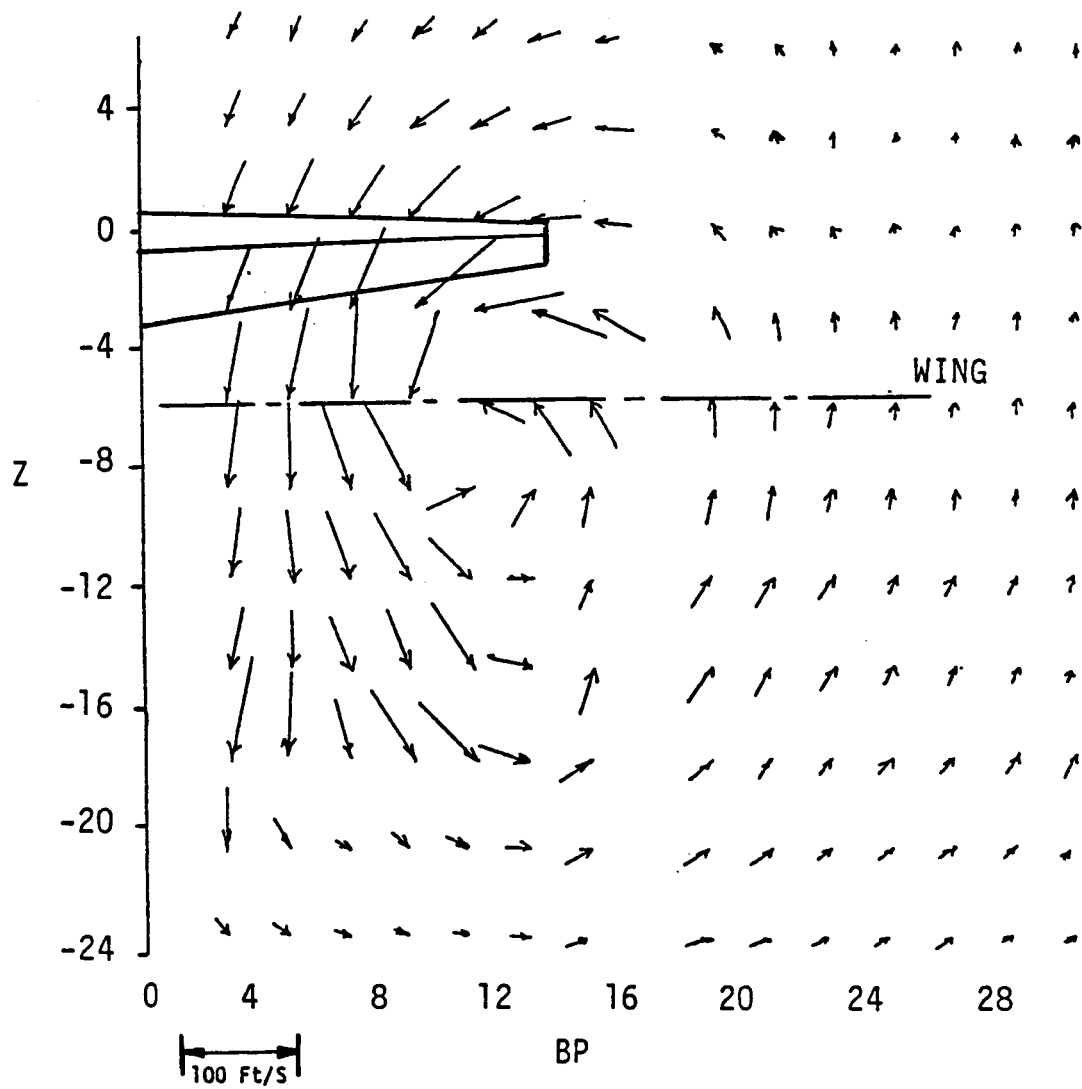$$C_x = 1 + 0.5 \left(\frac{V_j}{V_\infty}\right)$$

Figure 51   Wing Jet Sheet Velocity, $C_\mu = 1.0$

POSITION A

Figure 52   Canard Flow Pattern, $\delta_F = 45°,$ $C_\mu = 0.5$
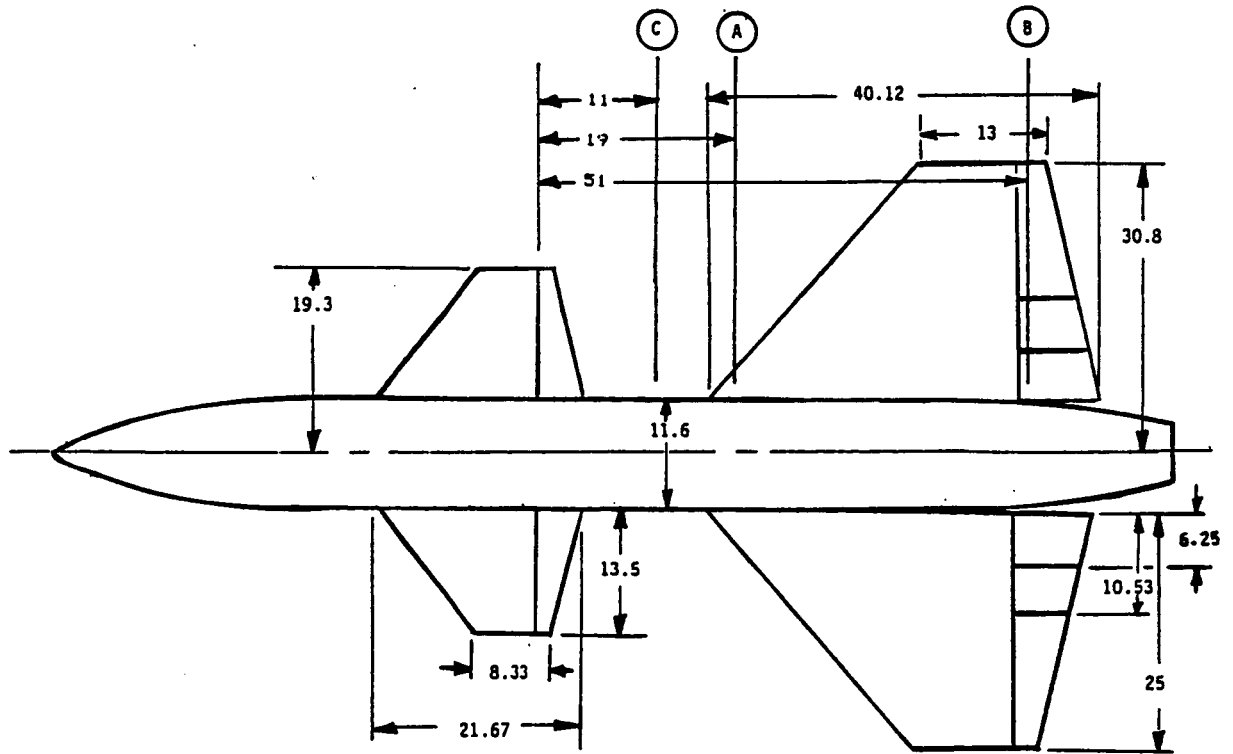
Figure 53. Canard Rake Survey Positions

SECTION 4.0

CONCLUSIONS

Wind tunnel tests of a propulsive wing/canard concept at STOL conditions have investigated the use of jet flaps on the wing and on the canard for several flap configurations. The model was tested in free air and in ground effect at various pitch and yaw angles. The data show the following results:

1. The wing/canard concept produces sufficient lift to fly at speeds as low as approximately 40 knots at 12 degrees angle of attack.

2. The canard imparts a significant downward load on the wing. This downward loading is particularly noticeable at 45 degrees of canard flap deflection.

3. Canard blowing acts as an upper surface blowing jet to the wing at low canard flap angles, but the jet impinges on the wing at the higher angles of flap deflection.

4. A canard positioned low relative to the wing is preferred for STOL landings while a high canard is desired for take-off and other cruise modes which might utilize the beneficial aspects of blowing. The data suggest that the high canard/low wing relationship is preferred as the best compromise for overall performance.

5. The results of canard interference investigations suggest that a three-surface configuration has potential for STOL fighter applications.

6. Ground proximity tests show that a significant lift loss is experienced with the wing alone.

7. The large negative lift increment induced by ground proximity for the wing-alone configuration at large blowing coefficients occurs at a lower value than would have been expected based on available higher aspect ratio data. The lift loss may be caused by a ground vortex which could be influenced by the stationary belt used for these tests. Comparison of stationary and moving belt test results show no effect of belt speed. However, these tests were performed with a half-span jet nozzle which produced very low circulation lift coefficients.

8. Ground proximity tests of the wing and canard demonstrate a significant lift increase at low model heights and large flap deflections. These characteristics may result from the reduction of canard downwash onto the wing.

9. Canard flow field surveys indicate that the canard tip vortex intersects the model wing plane for the condition of large flap deflections and blowing.

SECTION 5.0

RECOMMENDATIONS

1. A three-surface propulsive wing concept (canard, wing, horizontal tail) should be investigated experimentally.

2. The low aspect ratio jet flap wing should be tested in ground effect at maximum lift coefficient and with a moving ground belt to determine the applicability of the Turner criteria for a moving belt.

3. The low and high speed data from the propulsive wing/canard concept should be analyzed more completely.

SECTION 6.0

REFERENCES

1. Stewart, V. R., "Aerodynamic Characteristics of a Propulsive Wing/Canard at STOL Speeds", NASA CR-177982, November 1985.

2. Stewart, V. R., "An Investigation of the Use of a Propulsive Wing/Canard Concept for Improved Maneuvering", AIAA Paper 81-2622, December 1981.

3. Stewart, V. R., Paulson, J. W. Jr., "The Aerodynamic Characteristics of a Propulsive Wing/Canard Concept in STOL", AIAA Paper 84-2396, October 1984.

4. Stewart, V. R., "Evaluation of a Propulsive Wing/Canard Concept at Subsonic and Supersonic Speeds", Rockwell Report NR82H-85, February 1983.

5. Smeltzer, D. B., Stewart, V. R., Durston, D. A., "Wing and Canard Jet Flap Effects", AIAA Paper 83-0081, January 1983.

6. Stewart, V. R., "Pre-Test Report for the Full Span Propulsive Wing/Canard Model Test in the NASA Langley 4 x 7 Meter Low Speed Wind Tunnel Second Series Test", Rockwell Report NA-86-0015, April 1986.

7. Stewart, V. R. and Kuhn, R. E., "A Method for Estimating the Propulsion Induced Aerodynamic Characteristics of STOL Aircraft in Ground Effect", NAVAIRDEVCEN Report No. NADC 80226-60, August, 1983.

8. Turner, T. R., "A Moving Belt Ground Plane for Wind Tunnel Ground Simulation and Results for 2 Jet-Flap Configurations", NASA TN D-4228, 1967.

9. Petit, J. E., Schuley, M. B., "STOL Transport Thrust Reverser Vectoring Program", AFAPL TR-72-109, February 1973.

10. Lowry, J. G., Vogler, R. D., "Wind Tunnel Investigation at Low Speeds to Determine the Effect of Aspect Ratio and End Plates on a Rectangular Wing with Jet Flaps Deflected to 85 Degrees," NACA TN 3863, December 1956.

16. Abstract

A propulsive wing/canard model has been tested at STOL operating conditions in the NASA Langley Research Center 4 x 7 meter wind tunnel. Longitudinal and lateral/directional aerodynamic characteristics were measured for various flap deflections, angles of attack and sideslip, and blowing coefficients. Testing was conducted for several model heights to determine ground proximity effects on the aerodynamic characteristics. Flow field surveys of local flow angles and velocities were performed behind both the canard and the wing.

This report consists of two volumes. Volume I (NASA CR-178348) describes the model, instrumentation, and test procedures; and includes an analysis of the data. Volume II (NASA CR-178349) contains all of the test data in three appendices. Appendix A presents tabulated six component force and moment data, Appendix B presents tabulated wing pressure coefficients, and Appendix C presents the flow field data.